MODIFICATION OF MAGNETIC PROPERTIES OF SIDERITE BY THERMAL TREATMENT

A THESIS SUBMITTED TO
THE GRADUATE SCHOOL OF NATURAL AND APPLIED SCIENCES
OF
MIDDLE EAST TECHNICAL UNIVERSITY

BY
DİLEK ALKAÇ

IN PARTIAL FULFILLMENT OF THE REQUIREMENTS
FOR
THE DEGREE OF MASTER OF SCIENCE
IN
MINING ENGINEERING

SEPTEMBER 2007

Approval of the thesis:

MODIFICATION OF MAGNETIC PROPERTIES OF SIDERITE BY THERMAL TREATMENT

submitted by **DİLEK ALKAÇ** in partial fulfillment of the requirements for the degree of **Master of Science in Mining Engineering Department, Middle East Technical University** by,

Prof. Dr. Canan Özgen _____
Dean, **Graduate School of Natural and Applied Sciences**

Prof. Dr. Celal Karpuz _____
Head of Deparment, **Mining Engineering**

Prof. Dr. M. Ümit Atalay _____
Supervisor, **Mining Engineering Department, METU**

Examining Committee Members:

Prof. Dr. Gülhan Özbayoglu _____
Mining Engineering Department, METU

Prof. Dr. Mustafa Ümit Atalay _____
Mining Engineering Department, METU

Prof. Dr. Ali İhsan Arol _____
Mining Engineering Department, METU

Prof. Dr. Çetin Hoşten _____
Mining Engineering Department, METU

Dr. Cevdet Öztin _____
Chemical Engineering Department, METU

Date: 14. 09. 2007

I hereby declare that all information in this document has been obtained and presented in accordance with academic rules and ethical conduct. I also declare that, as required by these rules and conduct, I have fully cited and referenced all material and results that are not original to this work.

Name, Last name: Dilek Alkaç

Signature:

ABSTRACT

MODIFICATION OF MAGNETIC PROPERTIES OF SIDERITE BY THERMAL TREATMENT

Alkaç, Dilek

M. Sc, Department of Mining Engineering

Supervisor: M. Ümit Atalay

September 2007, 113 pages

Obtaining high magnetic susceptibility phases from Hekimhan–Deveci siderite ore via preliminary thermal treatment has been the basic target of the thesis study. Thermal decomposition characteristics of samples, determined by thermogravimetric analysis (TGA), differential thermal analysis (DTA), and differential scanning calorimetry (DSC), were referenced in advancement of the study. Heat treatment experiments, particularly roasting, were carried out by conventional heating and microwave heating. Results showed that roasting of Hekimhan–Deveci siderite samples could not be achieved by microwave energy whilst conventional heating experiments recorded success. Subsequent low–intensity magnetic separation of roasted samples gave recovery above 90%, where low–intensity magnetic separation of run–of–mine sample had failed. Formation of high magnetic susceptibility phases was verified by magnetic susceptibility balance and x–ray diffraction analysis (XRD), on roasted samples.

Statistical modeling was applied to determine the optimum conditions of roasting in conventional heating system; based on heating temperature, time of heating, particle size as factors.

It was concluded that roasting at T= 560 ºC, for t= 45 minutes was adequate to obtain desired results. Particle size was noted to be not much effective on the process as other factors at the studied size range.

Kinetics (*E*, *n*) and reaction mechanism for the thermal decomposition in conventional heating system were evaluated with different solid–state reaction models by interpretation of the model graphs.

Three–dimensional diffusion reaction models reported to characterize the thermal decomposition well, with values of activation energy (E), E= 85.53 kJ/mol (Jander); E= 85.49 kJ/mol, (Ginstling–Brounshtein).

Keywords: Siderite, Roasting, Magnetic Susceptibility, Statistical Modeling, Three–Dimensional Diffusion Reaction Models.

ÖZ

SİDERİTİN MANYETİK ÖZELLİKLERİNİN ISISAL İŞLEM İLE İYİLEŞTİRİLMESİ

Alkaç, Dilek

Yüksek Lisans, Maden Mühendisliği Bölümü

Tez Yöneticisi: M.Ümit Atalay

Eylül 2007, 113 sayfa

Hekimhan–Deveci siderit cevherinin ısıl işleme tabi tutulması yoluyla manyetik fazların elde edilmesi tez çalışmasının temelini oluşturmuştur. Numunelerin, termogravimetrik analiz (TGA), türevsel termal analiz (DTA), ve türevsel taramalı kalorimetre (DSC) yöntemleriyle, belirlenen ısıl özellikleri çalışmanın yönlendirilmesinde kullanılmıştır. Isıl işlem deneyleri, kavurma işlemi, hem mikrodalga enerjisi hem de geleneksel yöntemlerle gerçekleştirilmiştir. Sonuçlar incelendiğinde geleneksel ısıtma yöntemiyle kavurma işlemi gerçekleşirken mikrodalga ile işlemin gerçekleşmediği görülmüştür. Bunu izleyen düşük alan şiddetli manyetik ayırım yöntemi % 90' nın üzerinde verimle sonuçlanmıştır; tüvenan cevherin aynı alan şiddetinde manyetik ayırımı gerçekleşmemiştir. X ışını kırınımı (XRD) analizleri ve manyetik duyarlılık terazisi yardımıyla manyetik duyarlılığı yüksek fazların oluştuğu ayrıca gösterilmiştir.

Koşulların saptanması amacıyla istatistiksel modelleme uygulanmıştır; ısıtma sıcaklığı, ısıtma süresi, parça boyutu incelenen faktörler olmuştur.

Modelleme çalışmaları, kavurma deneyleri T= 560 ºC sıcaklıkta, t= 45 dakika süreyle gerçekleştirildiğinde istenen sonuçların elde edilmesi için yeterli olduğunu kaydetmiştir. Parça boyutunun, çalışılan parça boyutu aralığında, işlem üzerinde diğer faktörler kadar etkili olmadığı görülmüştür.

Isıl çözünme kinetiği (E, n) ve reaksiyon mekanizması geleneksel ısıtma sisteminde asıl veri noktalarına uygun grafik modellerinin yorumlandığı farklı katı hal reaksiyon modelleri ile incelenmiştir. Üç boyutlu difüzyon reaksiyon modelleri deney verilerini kinetik açıdan en iyi şekilde temsil etmiş, aktivasyon enerjileri (E), sırasıyla = 85.53 kJ/mol (Jander); E= 85.49 kJ/mol, (Ginstling–Brounshtein) olarak bulunmuştur.

Anahtar Kelimeler: Siderit, Kavurma, Manyetik Duyarlılık, İstatistiksel Modelleme, Üç Boyutlu Difüzyon Reaksiyon Modelleri.

To My Family

ACKNOWLEDGEMENTS

I want to express my deepest gratitude to my supervisor Prof. Dr. M. Ümit Atatalay for his supervision, criticism, advice, insight and encouragements throughout thesis study. I wish to extend my thanks to Prof. Dr. Pınar Çalık for her valuable comments and suggestions on kinetics study.

Prof. Dr. Cemal Göncüoğlu is acknowledged for his guidance and comments in mineralogical analyses of samples.

I would also like to thank to Eren Caner Orhan for his assistance in magnetic susceptibility analyses.

The technical assistance of department staff is gratefully appreciated.

Finally, my sincerest thank goes to my family for always being by my side through the study. Spiritual support of them has made anything more meaningful, helping me on my way to success.

TABLE OF CONTENTS

LIST OF TABLES

TABLES

LIST OF FIGURES

FIGURES

CHAPTER 1

INTRODUCTION

Iron is one of the common metals used in industry, as well as being the fundamental raw material used in iron–steel industry; products are wide spread even in daily uses. The total iron ore reserves of the world have been estimated as 370 billion tones; 160 billion tones is classified as economical, while 210 billion tones as potentially economical [Yıldız Necati, 2007]. Classification is based on extractability of the ore at the initial stage; however extractability of the metal value is the predominant criteria sought on the following stages. Extractive metallurgy has been utilized in obtaining the metal value, particularly pyrometallurgy. Pyrometallurgy consists of thermal treatment of minerals and metallurgical ores to enable recovery of valuable metals.

Qualifying for use in industry necessitates high iron grade moreover the concentration of silica, sulphur, titanium, phosphate, manganese and alkaline content is required to be at low level. Qualified iron ore reserves in Turkey are noted in Sivas, Kayseri, Adana, Balıkesir, Malatya, and Ankara. In addition there exist iron ore reserves (19–54% Fe) which may be rendered qualified upon preliminary processing; specifically in Malatya, Sivas, Erzincan, Bingöl, Kayseri, Kahramanmaraş, Balıkesir, Aydın.

Of the qualified iron ore reserves in Turkey, the highest iron metal content is intensified in Divriği basin, the following table (Table 1.1) lists the reserve values on basis of location;

Table 1.1- Iron Ore Reserves in Turkey [Yıldız Necati, 2007]

	RESERVE (1000 TONS)				GRADE
LOCATION	**Proven**	**Probable**	**Total**	**Workable**	**(%Fe)**
Sivas- Divriği A Kafa	41,000	-	41,000	41,000	54
Sivas-Divriği B Kafa	10,000	-	10,000	10,000	56
Sivas-Divriği Dumluca	200	-	200	200	57
Sivas-Divriği Purunsur	100	1,800	1,900	100	55
Sivas-Divriği Taşlıktepe	60	300	360	60	62
Sivas-Divriği Otlukilise	1,420	1,000	2,420	1,300	54
Sivas-Kangal Çetinkaya	3,500	-	3,500	3,000	54
Adana-Feke Attepe	10,000	-	10,000	10,000	57
Kayseri-Karamadazı	800	1,000	1,800	300	51
Ankara-Bala-Kesikköprü	2,000	1,000	3,000	2,000	54
Balıkesir-Büyükeymir	3,690	5,400	9,090	340	53
Balıkesir-Samlı-Şamlı	684	257	941	543	58
Kayseri-Pınarbaşı-Tacın	70	100	170	70	51
Kayseri–Yahyalı-Karaçatı	9,480	15,000	24,480	2,500	54
Kayseri-Koruyeri	7,000	-	7,000	7,000	52
Adana-Yenigireği	40	100	140	40	57
Adana-Elmadağ	1,000	400	1,400	1,000	53
Kayseri-Ayıgediği	590	300	890	590	54
Adana-Uyuzpınar	236	-	236	236	58
Malatya-Hekimhan-Deveci	48,000	-	48,000	48,000	38
Sivas-Divriği-Ekinbaşı	9,700	2,300	12,000	8,000	55
TOTAL	**149,845**	**28,957**	**178,802**	**137,540**	**54**

It has been reported that, yearly iron ore production is approximately 5 million tones in Turkey. Ore produced is processed in iron–steel plants; Karabük, İskenderun, Ereğli iron–steel works respectively [Anonim, 2001]. Availability of high grade iron ores is limited to 75 million tones with iron grade 51–62%. As a matter of fact, scarcity of qualified iron ore is, unfortunately, notified as the potential risk that may come up in a while. Therefore studies have recently been concentrated on upgrading of low grade iron ore reserves.

The iron ore reserve in Malatya-Hekimhan-Deveci, Siderite ($FeCO_3$) ore deposit, is considered to be one of the potential areas of research, both due to tonnage and the average iron grade, Fe%. Thermal decomposition characteristics of the ore under controlled heating conditions yield minerals which may be readily concentrated by magnetic separation.

At present, Hekimhan–Deveci siderite ore (38% Fe, 4–5% Mn) from Malatya is produced 500 thousand tons on yearly basis. The ore is blended with the blast furnace feed, 20%, in İsdemir iron–steel works [Anonim, 2001]. In conjunction with development strategies of utilization of siderite ore, significant reduction in import of iron and scrap is foreseen.

The aim of present study is enhancement of concentration of Hekimhan–Deveci siderite ore by low–intensity magnetic separation, as a result of which direct use of ore in blast furnaces or blending at a greater concentration may become possible.

The increase in iron content, Fe%, is specific of heat treatment of siderite; hematite (α–Fe_2O_3) which is paramagnetic at room temperature or magnetite (Fe_3O_4) and maghemite (γ– Fe_2O_3) which are ferromagnetic may be obtained as end products of thermal treatment.

Low-intensity magnetic separation offers advantages such as low operational cost, ease of operation, better control etc.; in light of data of thermal decomposition characteristics of siderite, low-intensity magnetic separation is expected to be the method of concentration for the ore upon being heated under controlled conditions.

Roasting, encompassing the conversion to oxide forms prior to smelting, in air is the fundamental heat treatment applied in the study. The roasting experiments were both carried out in microwave heating system and conventional heating system; comparison of the methods has been given with respect to percent weight loss obtained. Statistical modeling was made use of in determining the optimum conditions yielding phases of high magnetic susceptibility. Furthermore kinetic analysis of thermal decomposition was conducted, proposing the reaction mechanism and the activation energy for the reaction.

Respective chapters of thesis are *introduction, literature survey, materials and methods, results and discussion, conclusions and recommendations*. Information on siderite, thermal characteristics, and microwave heating is covered in chapter II following the introduction, chapter I. Detailed data with respect to mineral, analyses conducted through out the study is given in chapter III.

Chapter IV is composed of results of analyses of which the details have been given in chapter III. Finally, the conclusions of the study are stated in chapter V along with recommendations for further studies.

CHAPTER 2

LITERATURE SURVEY

2.1. Siderite

Siderite ($FeCO_3$, iron carbonate) is authigenic carbonate mineral, it is commonly found in hydrothermal veins and may also be deposited by sedimentary processes. In sedimentary rocks, siderite often forms at shallow burial depths and its elemental composition is related to the depositional environment of the enclosing sediments. Siderite theoretically consists of 62.1% FeO (48.3% Fe) and 37.9% CO_2. Being a member of calcite group together with calcite ($CaCO_3$), dolomite ($CaMg(CO_3)_2$), magnesite ($MgCO_3$), and rhodochrosite ($MnCO_3$), Fe may be fully or partially substituted by Mn, Mg, and Ca in siderite, forming a partial solid solution series. As all members of calcite group, siderite crystallizes in trigonal system which is the subdivision of hexoganal system; crystals are rhombohedral or of distorted rhombohedral aspect.

Siderite is noted to be paramagnetic at room temperature, having mass magnetic susceptibility of $32–270*10^{-8}$ m^3/kg [Hunt et al., 1995], however due to both compositional instability and susceptibility to oxidation, the mineral can acquire remnant magnetization in oxidation process. Siderite disintegrates into strongly magnetic magnetite and/or maghemite and weakly magnetic hematite upon being heated in air [Freederichs et al., 2003; Pan et al., 2000, 2002]. Pan et al. showed that magnetite might form by decomposition of siderite directly, or be produced as results of oxidation reaction; it was also shown that magnetite was transformed to maghemite and hematite and that maghemite phase was relatively stable upon further thermal treatment.

Moreover, metamagnetism was reported to be magnetic property of siderite, gradually transforming into a ferromagnetic lattice when exposed to strong magnetic fields of 12–14 T [Freederichs et al., 2003].

Defined as super linear increase in magnetization over a range of magnetic field, metamagnetism gives indications of spin–flip transitions antiferromagnetic and paramagnetic materials as transforming to paramagnetic or ferrimagnetic, ferromagnetic phases respectively.

At low temperatures siderite is antiferromagnetic, that is the magnetic moments oriented antiparallely in neighboring atoms, with a *Neel temperature (T_N)* of about 38 K derived from magnetization data [Mookherji et al., 1965; Freederichs et al., 2003; Pan et al., 2000].

Siderite is mainly used as minor ore of iron for use in blast furnaces, besides owing to thermal decomposition characteristics it is utilized in paleomagnetic studies; identification of siderite in bulk rocks and detailed knowledge of its oxidation at elevated temperatures are said to be essential for studying reliability of recorded geomagnetic fluctuations through geological time and variations in paleoenvorienments [Pan et al., 2000, 2002; Frederichs et al., 2003]. In addition, since roasting of siderite yields high pore volume and high surface area species, the end products are also used in capture of sulphur dioxide (SO_2) in a wide temperature range [Jagtap et al., 1992; Böhm et al., 2006].

Low grade siderite ore is treated in rotary furnaces, yielding products high in iron grade in Turkey. The products are of quality that may be directly fed to the blast furnaces, via which iron is obtained in metal form as a result of smelting process. On the other hand, the practical application is that calcined siderite is blended with materials low in iron grade, such as hematite (α-Fe_2O_3), in preparation of feed to blast furnace for smelting process [Atesok et al., 2000].

2.2. Concentration Techniques Applied to Iron Ores

The important iron minerals are magnetite (Fe_3O_4), hematite (α–Fe_2O_3), limonite ($FeO(OH).nH_2O$), goethite ($FeO(OH)$), siderite ($FeCO_3$), pyrite (FeS_2) and laterite (hydrated oxide of iron or aluminum). Iron ores are almost entirely used in the manufacture of pig iron and steel.

Nonmetallurgical uses are very few; spathic iron ore, also known as siderite, is used for the production of the hydrogen by the steam–iron process. Micaceous iron ore, a variety of hematite, is used as a coating material in the preparation of welding rods.

Pig iron ore (Fe_3OH_6) is used as a purifying and desulphurizing material. Magnetite is used for the preparation of heavy media in coal washing plants. Iron fines are also used in pipe coating.

Concentration of iron ores is performed in two stages, physical concentration referred to as beneficiation and processing by means of thermal treatment to extract the metal value. Beneficiation involves removal of gangue material as well as the regulation of product size, or other steps such as agglomeration to improve its chemical or physical characteristics prior to processing.

Iron ore beneficiation is fulfilled by milling (crushing and grinding); washing; filtration; sorting; sizing; gravity concentration; magnetic separation; flotation; and agglomeration (pelletizing, sintering, briquetting, or nodulizing). Milling operations are designed to produce uniform size particles by crushing, grinding, and wet or dry classification. Magnetic separation which may be performed dry or wet is most commonly used; low intensity magnetic field separation is widely applied for concentration of ferromagnetic ores. Iron-bearing metallic mineral flotation operations are of two main types: anionic and cationic. In anionic flotation, fine-sized crystalline iron oxides, such as hematite or siderite, are floated away from siliceous gangue material such as quartz or chert.

In cationic flotation, the silica material is floated and the value-bearing minerals are removed as underflow. Gravity concentration is used to suspend and transport lighter gangue (nonmetallic or nonvaluable rock) away from the heavier valuable mineral.

Three gravity separation methods have historically been used for iron ore: washers, jigs, and heavy-media separators. Following the preliminary beneficiation activities, the iron concentrate is balled in drums and heated to create hardened agglomerate. Agglomerates may be in the form of pellets, sinter, briquettes, or nodules. The purpose of agglomerating iron ore is to improve the permeability of blast furnace feed leading to faster gas-solid contact in the furnace. Smelting in blast furnaces is the principal pyrometallurgical application utilized in extracting the metal.

Siderite is concentrated by high–intensity magnetic separation; specifically there exists a new technology for magnetic separation of siderite [Xiong et al., 1998]. In the study, pulsating high gradient magnetic separation (PHGMS) is applied to beneficiate siderite, reporting the recovery of fine siderite at desired metallurgical grade.

Due to the fact that siderite oxidizes to magnetite (Fe_3O_4) or maghemite (γ–Fe_2O_3), when exposed to air, low grade siderite ore is treated in rotary furnaces to obtain products high in iron grade. The products are fed to the blast furnaces to yield iron (Fe) as result of smelting process.

2.3. Thermal Decomposition Characteristics of Siderite

Factors affecting thermal decomposition of siderite reported in literature are cited as *heating temperature, gaseous atmosphere, crystallinity, porosity*, *particle size of the ore, quantity of sample,* and *availability of* O_2 [Pan et al., 2000; Dhupe et al., 1990]. The process has been carried out in number of atmospheres, i.e. He, N_2, CO_2, inert and under vacuum.

The studies on influence of experimental conditions have indicated that siderite decomposition yields hematite (α-Fe_2O_3) in oxidizing environment, magnetite (Fe_3O_4) in carbon dioxide atmosphere, while magnetite (Fe_3O_4) and wüstite (FeO) in inert atmosphere or in vacuum [Gotor et al., 2000; Gokarn et al., 1990].

Considering different mechanisms of decomposition proposed, it has also been noted that alteration of siderite with temperature depends on its starting chemistry [Pan et al., 2002].

The theoretical data on the mineral points out that *siderite* has a characteristic thermal curve with an *endothermic effect* due to *dissociation of $FeCO_3$ at 475–540 ºC* and subsequent *exothermic effect at 600–890 ºC*, corresponding to oxidation of FeO [Teodorovich, 1961; Pan et al., 2000].

It has been stated that siderite decomposes into strongly magnetic magnetite and/or maghemite and weakly magnetic hematite, upon being heated in air, by the following reactions [Pan et al., 2002].

$$3\ FeCO_3 \rightarrow Fe_3O_4 + 2CO_2 + CO$$

$$4Fe_3O_4 + O_2 \rightarrow 3\gamma\text{-}Fe_2O_3 + 3\alpha\text{-}Fe_2O_3$$

$$3\gamma\text{-}Fe_2O_3 + 3\alpha\text{-}Fe_2O_3 + 2CO \rightarrow 4Fe_3O_4 + 2CO_2$$

$$\gamma\text{-}Fe_2O_3 \rightarrow \alpha\text{-}Fe_2O_3$$

$$3FeCO_3 + 0.5O_2 \rightarrow Fe_3O_4 + 3CO_2 \qquad (2.1)$$

$$\gamma\text{-}Fe_2O_3 \rightarrow \alpha\text{-}Fe_2O_3 \qquad (2.2)$$

Detailed analyses has proven that susceptibility of siderite increases between 400 °C and 530 ºC, indicating formation of ferrimagnetic phases carrying natural remnance, of which the vector sum of magnetic moments is oriented in a specific direction parallely.

Upon continued heating, it has been observed that the ferrimagnetic minerals convert to hematite (α-Fe_2O_3) around 700 ºC [Pan et al., 2000].

Beneficiation of artificial magnetite processed from an iron mineral containing siderite ($FeCO_3$) and ankerite ($CaFe(CO_3)_2$) has been carried out on industrial scale. Using the scheme of treating 0–30 mm Siderite & Ankerite iron ores with magnetizing roasting at 800 ºC, followed by wet grinding and low-intensity wet magnetic separation respectively. The recovery has been reported as 80 % with Fe content of 35 % [Morar et al., 1999].

Calcination of Hekimhan-Deveci siderite samples has been studied, using rotary furnace [Atesok et al., 2000]. It has been found that Fe% of calcined samples varies between 56.02 % and 59 % in relation to particle size fed to the furnace.

A study conducted on siderite ore for improvement of process conditions, namely the process duration, has resulted that the modification of the magnetic properties of mineral components in siderite ores by microwave heating results in increasing the efficiency of their magnetic separation [Znamenackova et al., 2005].

In that study pretreatment in a microwave oven with maximum power of 900 W on weakly paramagnetic ore (25.1% Fe, 9.6% SiO_2) of particle size 0.5–1mm for 10 min has been applied. Conclusion has been in the way that 10 min heating yielded essential change in the magnetic properties of the ore samples, and after 15 min, a rapid increase of magnetic susceptibility value was observed, suggesting the following mechanism for reactions;

$$FeCO_3 \rightarrow FeO + CO_2$$
$$6FeO + O_2 \rightarrow 2Fe_3O_4$$
$$4FeO + O_2 \rightarrow 2Fe_2O_3$$
$$6Fe_2O_3 \rightarrow 4Fe_3O_4 + O_2$$

$$6FeCO_3 + O_2 \rightarrow 2Fe_3O_4 + 6CO_2 \qquad (2.3)$$

The decomposition kinetics of various siderite have been of interest, both due to the complexity of process and practical use of products obtained by controlled heating conditions [Gotor et al., 2000; Jagtap et al., 1992; Gokarn et al., 1990]. The mechanism of thermal decomposition has been investigated, determining the kinetic model [Gotor et al., 2000]. The conditions in air atmosphere have been investigated, specifically the kinetics, proposing the following mechanism for the reactions [Gokarn et al., 1990].

$$FeCO_3 \rightarrow FeO + CO_2$$
$$4FeO \rightarrow Fe_3O_4 + Fe$$
$$3FeO + CO_2 \rightarrow Fe_3O_4 + CO$$
$$2FeO + CO_2 \rightarrow Fe_2O_3 + CO$$
$$2Fe_3O_4 + CO_2 \rightarrow 3Fe_2O_3 + CO$$
$$3FeO + H_2O \rightarrow 4Fe_3O_4 + O_2$$

$$2FeCO_3 + 0.5O_2 \rightarrow Fe_2O_3 + 2CO_2 \qquad (2.4)$$

2.4. Fundamental Applications of Microwave Heating in Mineral Processing

Referencing the advantages offered by selective and volumetric heating of minerals by microwaves, there have been a number of studies, as means of microwave treatment of minerals, investigating the methods of utilization.

Particularly comminution studies have received much attention, upon obtaining significant reductions in ore strength as result of microwave treatment.

The applications on coal cover the desulphurization studies, enhancement of flow characteristics in coal-water slurries and coal grindability. For leaching practises, microwave treatment has also been made use of in improving extraction efficiency as well as reduction in required leaching time. Microwave heating has been applied in environmental engineering; especially remediation of soil, waste processing, and activated carbon generation are fields that have been studied.

Dry comminution and liberation characteristics of various minerals have been investigated [Kingman et al., 2004]. The results have shown that the particle size has a significant effect on microwave heating behavior and grindability of preheated material. Carbonate minerals have been noted as insensitive to microwave while copper ore associated with sulphide has been found microwave sensitive. Whereas, microwave treatment of copper ore from Çayeli Copper deposit has been shown not effective on grindability characteristics, relating the results to the ore composition; the effect of microwave treatment on chromite ore from Kef Chromite deposit has also been investigated in the same study. There has been noted no significant change in grindability characteristics of chromite ore either, suggesting that water quenching may enhance the formation of cracks if used as the cooling method following microwave treatment [Güngör, 1998]. The influence of high electric field strength microwave energy has been examined, with the aim of investigating the comminution behavior of ore treated at high microwave power but for short residence times [Jackson et al., 2004].

Preliminary tests in a single-mode microwave cavity gave strength reductions of 50% at 10 kW of microwave power with a residence time of only 0.1 s, indicating that high electric field strength is important in the failure of ore.

Using a multimode microwave cavity, the effect of power level and type of applicator have been studied, treating lead–zinc ore with 15 kW of microwave power for 0.5 s [Wang et al., 2005]. Drop weight tests were used to quantify the change in strength in terms of reduction in required comminution energy. Reductions of up to 40% were achieved for particles of mean size.

There have been several attempts to minimize sulphur content in coal using microwave energy to assist coal desulphurization [Kingman et al., 1998; Huang et al., 2001]. Comparing the dielectric heating behavior of minerals in a microwave field, it is found that most of sulphide minerals have a strong ability to absorb microwave energy and can be preferentially and rapidly heated to elevated temperatures, whereas most of gangue minerals are transparent to microwaves.

Amenability of lignite to desulphurization by magnetic separation following microwave heating has been studied, using microwave oven at 850 W, 2.45 GHz with subsequent high intensity dry magnetic separation [Atalay et al., 2003].

Facilitator addition to enhance microwave heating has been practiced [Marland et al., 1998; Uslu et al., 2003]. Heating could not be achieved at initial attempts, therefore magnetite, as an excellent microwave absorber, was added to systems to obtain phases susceptible to magnetic separation.

Coal grindability has been one of fields of microwave applications in terms of coal [Lester et al., 2004; Özbayoğlu et al., 2006; Marland et al., 1998]. It has been shown that microwave pretreatment reduces the viscosity and the pumping cost and opens a new outlook for pipeline transport. Attempts have been made to quantify the improvement of rheological characteristics due to microwave pretreatment [Meikap et al., 2005; Marland et al., 1998].

Microwave assisted operations in extractive metallurgy have involved consideration of the applications of microwave energy for pyrometallurgy and hydrometallurgy.

Reduction of metal oxides has been studied; emphasizing on the advantage of volumetric heating, offered by microwave applications [Kingman et al., 1998]. Effect of microwaves on the leaching kinetics of sphalerite in a solution of 1.0 M $FeCl_3$ and 0.1 M HCl at 95 ºC has been investigated [Al-Harahsheh et al., 2004]. It was observed that the total zinc extracted after 1h microwave treatment, 650 W at 2.45 GHz, reached 90% whereas under conventional leaching conditions, the maximum zinc recovery was about 52%.

Microwave heating applications in environmental engineering encompasses many areas, including contaminated soil remediation, waste processing, and activated carbon regeneration.

Many soils and bodies of water throughout the world are heavily contaminated, heavy metal ions, including radio nuclides, are major contaminants of soil and ground water. It has been said that decontamination of soils polluted with heavy metal ions is one of the most difficult problems of clean-up technology. In one study, preliminary investigation has been reported on the in situ remediation of soils contaminated with toxic metal ions: Cd(II), Mn(II), Th(IV), Cr(III) and mainly Cr(VI), by immobilization of the ions [Xia et al., 2000]. In situ remediation of toxic metal ions in soil using microwave energy has been found viable, and eventually economical (short heating times) method for immobilizing metals in contaminated soils, making them virtually unleachable, yet representing only one type of soil.

Microwaves are being investigated as a possible treatment for many mixed wastes including process sludge, incinerator ash, and miscellaneous wastes; scrap tyre processing, plastic waste processing, treatment of sewage sludge, sterilization of hospital wastes, and also packaging of wastes have found utilization by microwave processing. Microwave heating has been applied in production-regeneration of activated carbon, and treatment of compounds adsorbed onto the carbon matrix in environmental engineering applications [Jones et al., 2002].

CHAPTER 3

MATERIAL AND METHODS

3.1. Siderite Samples

Siderite samples from Malatya–Hekimhan–Deveci were used in the study; particularly being subjected to heat treatment. The chemical analysis of samples has been obtained by X–Ray Fluorescence (XRF). The analysis was carried out on powder samples (-75 μm), which were pelletized using wax material as binder; measurements were done with XRF device, SPECTRO iQ (Fig. 3.1).

Fig.3.1– Spectro iQ X–Ray Flourescence Device

3.2. Characterization of the Sample

The compositional and surface characterizations of samples were accomplished using X-Ray Diffraction (XRD) analysis, and mineralogical analysis under microscope.

Mineralogical analysis was carried out, under optical microscope, on thin–polished sections of samples that were identified to differ macroscopically; microscopic analysis thus was conducted on three different samples. The samples were analyzed in Geological Engineering Department at METU.

For XRD analysis, representative siderite samples were ground to -75 μm size. Samples prepared were sent to Department of Chemistry at METU for analysis. Interpretation of X-Ray results has been made by the software designed for that purpose; the outcome has also been checked by using mineral cards, showing d-spacing values of minerals. The governing equation, *Bragg's Law*, is utilized for interpretation of results;

$$n\lambda = 2d \sin\theta \qquad (3.1)$$

n=1, λ= 1.54051 Aº for the device used; the left side of equation is constant, therefore for any angle d-spacing is the changing parameter, hence the characteristic of treated mineral on the basis of relative intensity of rays (I/I_0).

Mass of sample reserved for experiments was divided representatively; 3 portions–mass sized down to -20 mm (1/2), mass crushed to -9.53 mm (1/4), while (1/4) of whole mass sized down to -2.36 mm for analysis. Particle size distribution of samples was determined by dry & wet sieve analyses on samples sized down to -2.36 mm. Iron grade distribution on particle size was additionally analyzed with the same sieve set. Combination of methods [E 1028/ASTM, E 246/ASTM, TS 1455; *see Appendix C*], referred by standard procedures in total iron determination have been applied.

3.3. Thermal Characterization of the Sample

Thermal decomposition characteristics of ore samples were initially determined by thermogravimetric analysis (TGA), recording the change in mass of sample with respect to temperature. Representative samples of ore were sized down to -75 μm, and sent to central laboratory at METU for analysis.

Differential Thermal Analysis (DTA) was requested from central laboratory to confirm the results of TGA and to be utilized in kinetics interpretation. DTA enabled understanding of heating profile in detail; endothermic and exothermic parts of thermal decomposition of siderite in air have been verified by the results.

Originally siderite ($FeCO_3$) and hematite (α-Fe_2O_3) *are* paramagnetic at room temperature, while phases obtained after heat treatment, wüstite (F*eO), magnetite* (Fe_3O_4)*, and maghemite* (γ-Fe_2O_3) are ferromagnetic. Stability of magnetic phases relies on the fact that heat treatment is performed under controlled conditions. Therefore the temperature range for the analyses has been set by using the results of TGA analysis and curie temperatures, which are the temperatures above which the species do not have magnetic properties, Tc(magnetite)= 580 ºC, Tc(maghemite)= 600 ºC, Tc(hematite)= 675 ºC, Tc(iron)= 770 ºC.

3.4. Heating Experiments

Siderite samples were crushed down to - 20 mm and sized with the sieve set, + 19 mm, 19+12.7 mm, 12.7+9.53 mm, 9.53+6.35 mm, 6.35+4.76 mm, 4.76+3.35 mm, - 3.35 mm, for heating experiments.

Microwave heating experiments involved treatment in microwave oven for t= 2, 4, 6 minutes at power level P= 900 W, f= 2.45 GHz.

Conventional heating experiments were initiated, upon receiving results of TGA from central laboratory. Based on the results, working range has been decided to be started at 465 ºC, with the largest particle size fraction, +19 mm, available in muffle furnace. The analysis was carried out on samples, at increments of 35 ºC, up to 605 ºC. The percent weight loss of samples, heated in air, against time has been interpreted in terms of graphics.

Additionally heating experiments were carried out at temperatures where significant weight loss of the sample occured within 45 minutes. T= 550 ºC, T= 560 ºC, T= 570 ºC were the temperatures of heat treatment in this respect in addition to the range studied, T= 465 ºC– 605 ºC.

3.5. Magnetic Susceptibility Analysis

Magnetic susceptibility determination has been accomplished through magnetic susceptibility balance (SHERWOOD SCIENTIFIC, Fig. 3.2). The system is based on use of two pairs of magnets placed at opposite ends, creating the magnetic field; introduction of the sample into the magnetic field attempts to deflect the beam and the movement is optically detected.

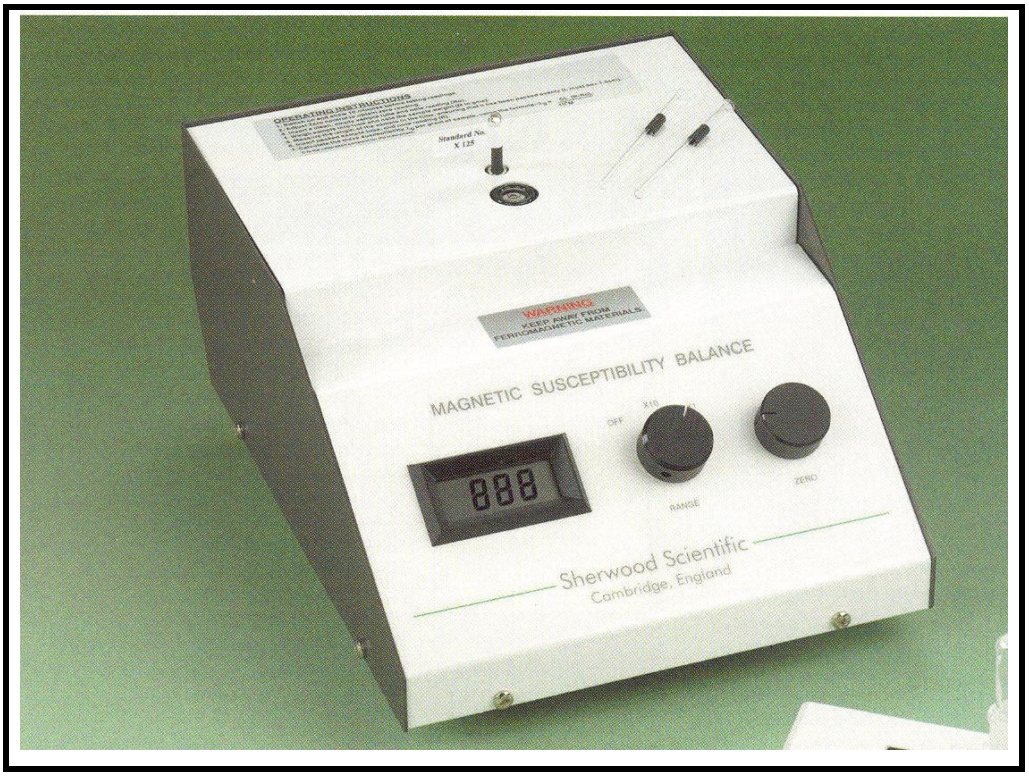

Fig.3.2– Sherwood Magnetic Susceptibility Balance

There are two kinds of magnetic susceptibility, which is the ratio of the intensity of magnetism induced in a substance to the magnetizing force or intensity of the field it is subjected, measures; namely volume magnetic susceptibility (χ_v) and mass magnetic susceptibility (χ_g).

$(\chi_v) = I/H$, I= Intensity of magnetism produced in a substance

H= Intensity of magnetic field applied externally

$(\chi_g) = \chi_v/d$, d= density of the substance.

Magnetic susceptibility balance (MSB) utilized gives the mass magnetic susceptibility of the samples, (χ_g). The calculation of (χ_g) from the readings of magnetic susceptibility is;

$$(\chi_g) = \frac{C \times L \times (R - R_0)}{10^9 \times m} \quad (3.2),$$

C= Calibration constant of the balance

L= Length of sample in tube (cm)

m= Mass of sample (gram)

R= Reading on MSB of the sample in the tube

R_0= Reading of empty tube

Magnetic susceptibility measurements were conducted on samples heated at various temperatures for different time periods; run-of-mine sample (T= 25 ºC), first set (T= 510 ºC, T= 560 ºC, T= 605 ºC at t=30 minutes), second set (T= 465 ºC, T= 510 ºC, T=560 ºC at t=60 minutes) respectively.

Presence of magnetic phases has also been verified by XRD analysis conducted on roasted samples. Heated samples were ground down to -75 μm, both for magnetic susceptibility measurement and XRD analysis.

3.6. Magnetic Separation

Assessment of applicability of magnetic concentration to final products has been made by laboratory scale experiments; by wet low intensity magnetic separation with DAVIS TUBE (Fig. 3.3).

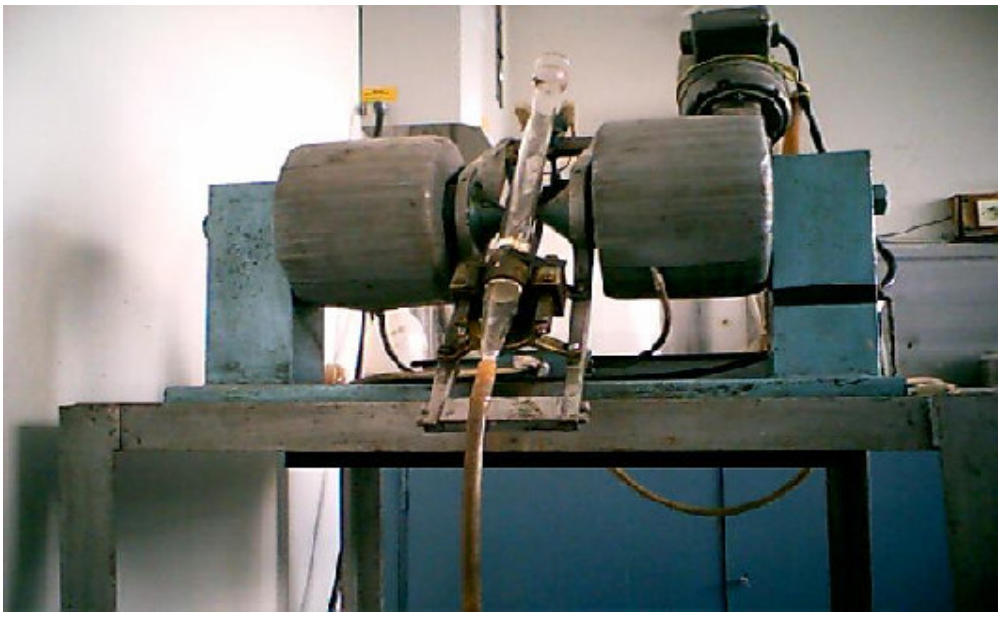

Fig.3.3– Davis Tube Magnetic Separation Device

Samples, roasted at T= 560 ºC for t= 45 minutes, were prepared in 833+589 μm size fraction. There groups of 10 g were taken to be treated at different currents (I); I= 0.1 A, I=0.25 A, I= 0.5 A, corresponding to magnetic field intensities of 0.046 T, 0.1037 T, 0.195 T respectively.

Magnetic fractions obtained were collected, dried, and weighed. Recoveries on mass basis have been reported. In addition magnetic separation of run-of-mine siderite sample was performed at the highest current level, I= 0.5 A (0.195 T).

3.7. Statistical Modeling

Experimental methods have found increasing use in terms of optimization of the process; specifically, the goal of these methods is to identify the optimum settings for the different factors that affect the process. By analysis of experimental data with use of statistical techniques "empirical models" are designed. Empirical models represent the relation defined by the data around the system studied.

Common method applied is one with all input factors set at two levels each. These levels are called `high' and `low' or `+1' and `-1', respectively. A design with all possible high/low combinations of all the input factors is called a full factorial design in two levels. If there are k factors, each at 2 levels, a full factorial design has 2^k runs.

Design procedure includes planned steps for determination of the empirical model in terms of regression analysis. Algebraic calculation of regression coefficients of interest is made by *Analysis of Variance (ANOVA)* technique. The empirical model that results is as shown below;

$$Y = \beta_0 + \beta_1 x_1 + \beta_2 x_2 + \beta_3 x_3 + \beta_{12} x_1 * x_2 + \beta_{23} x_2 * x_3 + \beta_{13} x_1 * x_3 + \beta_{123} x_1 * x_2 * x_3 \qquad (3.3)$$

Y= Response (Parameter of interest of the model)

x_i= Coded Factors

β_i= Regression Coefficients

$$\text{Coded x} = \frac{(design level\ of\ \ factor) - (s\tan dard\ level\ of\ \ factor)}{(dis\tan ce\ of\ high(low)\ level\ \ from\ s\tan dard\ level)} \qquad (3.4)$$

In the models designed for "determination of optimum conditions for roasting of siderite ore, yielding phases of high magnetic susceptibility", the response items are "weight loss of siderite ore (R_1, %)" and "Iron (Fe) content of roasted product (R_2, %)".

The model for R_1 has comprised of temperature, time, and particle size as factors meanwhile computations for R_2 have involved two level factorial design for two factors (2^2), temperature and time;

a- Temperature (℃), (X_1)

b- Time (minutes), (X_2)

c- Particle Size (mm), (X_3)

The data for modeling R_1 has been collected by following the standard order in two level factorial design for three factors (2^3) (Table 3.1); experiments have been conducted in the order shown in Table 3.1 and the runs have been replicated for three times (3 replicates).

Table 3.1 - 2^3 two-level full factorial design table showing runs in Standard Order

	X_1	X_2	X_3
RUN			
1	-1	-1	-1
2	1	-1	-1
3	-1	1	-1
4	1	1	-1
5	-1	-1	1
6	1	-1	1
7	-1	1	1
8	1	1	1

Determination of relation among temperature, time and iron (Fe) content of roasted products has been conducted through use of results of experiments with respect to iron percentage. Table 3.2 gives the standard order for two level factorial design for two factors (2^2).

Table 3.2– 2^2 two-level full factorial design table showing runs in Standard Order

	X_1	X_2
RUN		
1	-1	-1
2	1	-1
3	-1	1
4	1	1

The design levels for each factor have been set as follows;

T_{low}= 465 ℃ t_{low}= 30 minutes (Particle Size)$_{low}$ =-4.76+3.35 mm

T_{high}= 560 ℃ t_{high}= 60 minutes (Particle Size)$_{high}$=-22.23+19.05 mm

$T_{standard}$= 512.5 ℃ $t_{standard}$= 45 minutes (Particle Size)$_{standard}$=-13.50+11.20 mm

3.8. Kinetic Analysis

Kinetic parameter determined in this study is activation energy along with the reaction mechanism.

In isothermal experiments, run-of-mine (r.o.m.) ore sized down to -20 mm was used while -75 μm was used in non-isothermal runs for TGA; heat treatment of different sizes did not influence the kinetic parameters, in agreement with the results of previous studies [Jagtap et al., 1992]. Samples have been prepared under same conditions and heating experiments were conducted in identical experimental conditions. Calculations on isothermal runs are based on the following equation;

$$f(x) = k(T) * t \qquad (3.5)$$

x= fractional conversion; t= time (minutes); T= temperature (Kelvin, K)

Expressions for f(x), reaction model, comprise of the particular fractional conversion and related mechanism in terms of mathematical equations; once the fractional conversion with respect to time, x vs. t, data is obtained by isothermal experiments the calculation of f(x) values for given conversions is straight forward. The linearity of line of data plotted, f(x) vs. t, is indicator of the degree of fit; the slope gives the value of rate constant, k, at temperature of interest.

Kinetic parameters determination in nonisothermal runs has been through;

$$\ln[f(x)] - 2In(T) \cong \ln(\frac{AR}{E\beta}) - \frac{E}{RT} \qquad (3.6)$$

E= Activation Energy, kJ/mol

T= temperature (Kelvin, K)

As defined by the equation, the value of $\left(E/R\right)$ is obtained by the slope of line of -ln [f(x)] vs. (1/T); the degree of linearity of the line also verifies the consistency of the model in representing the data. Eventually activation energy, E, is calculated by multiplication of the value of slope with *universal gas constant, R* [R= 8.314 $J/mol \times K$].

In addition, conventional method of calculation of E is by use of Arrhenius equation.

$$k(T) = k_0 \times \exp(-E/RT) \qquad (3.7)$$

k= Rate Constant; k_0= Pre–exponentional Factor; E= Activation Energy

Rearrangement of the equation in exponentional form yields;

$$\ln(k) = \ln(k_0) - E/RT \qquad (3.8)$$

The slope of the plot -lnk vs. (1/T) gives $\left(E/R\right)$, thus comparison of values obtained both in isothermal and non–isothermal runs for the reaction model of interest becomes possible, reporting to be a good method of checking the consistency. On calculations, k values have been obtained by the slopes of plots (f*(x) vs. t*) in isothermal runs; taking the natural logarithm of k values gotten for constant temperature of concern, the data for evaluation by Arrhenius equation is gained.

CHAPTER 4

RESULTS AND DISCUSSION

4.1. Chemical Analysis of Siderite Samples

Results of chemical analysis have shown that, iron (Fe) is the predominant element within ore matrix, besides magnesium (Mg), aluminum (Al), silicon (Si), calcium (Ca), and manganese (Mn) have significant concentrations. The loss of ignition of the sample is comparatively high, as characteristic of carbonate minerals. Table 4.1 lists notable values obtained in analysis.

Table 4.1- Chemical Analysis of Hekimhan–Deveci Siderite Samples

Component	**Concentration, %**
MgO	*2.86*
Al_2O_3	*1.36*
SiO_2	*5.67*
CaO	*1.39*
MnO	*5.54*
Fe_2O_3 (Fe %= 37.69)	*53.89*
Loss on Ignition	***28.87***

4.2. Characterization of Siderite Samples

4.2.1. X–Ray Diffraction Analysis

XRD profile of sample used in thesis study points out the presence of carbonate minerals, namely siderite, ankerite, dolomite, and calcite along with hematite, and quartz. Fig. 4.1 gives the results of analysis on graph drawn intensity vs. 2θ.

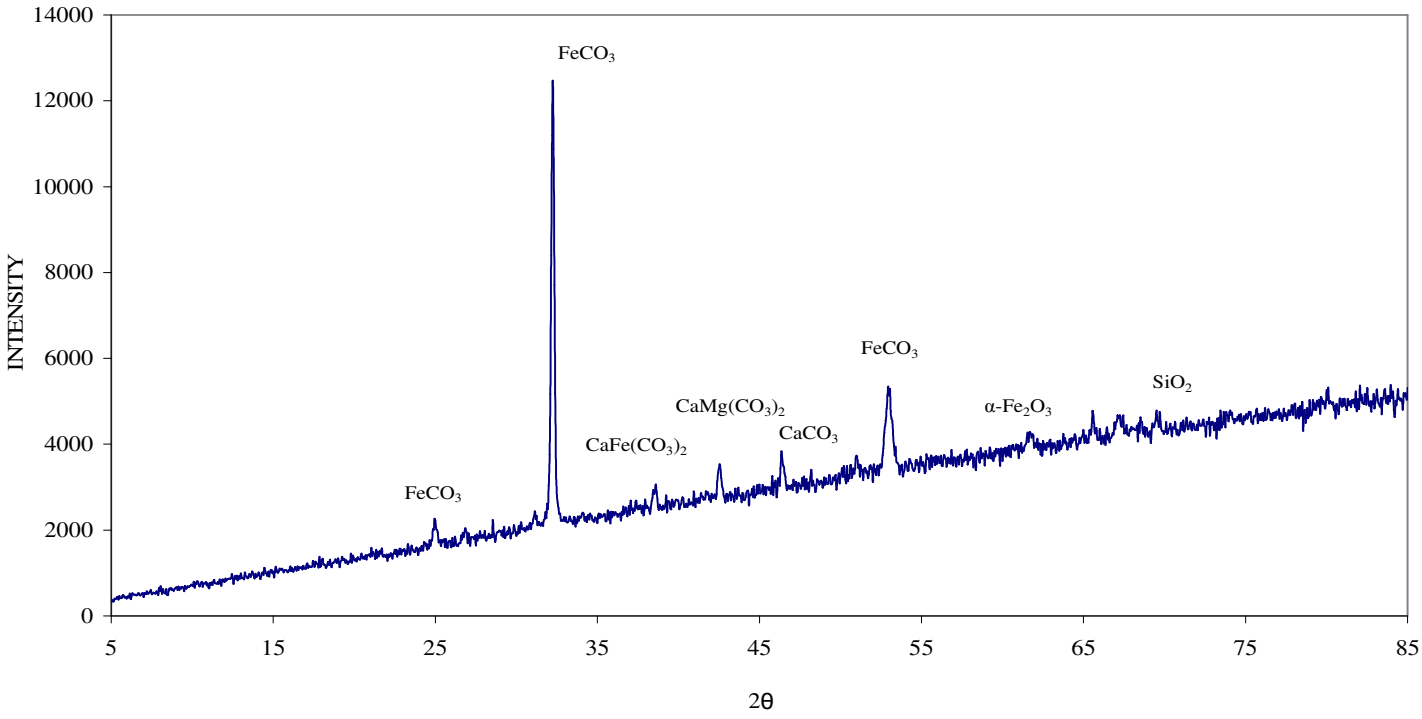

Fig.4.1– XRD Analysis of run-of-mine Sample, T= 25 °C

4.2.2. Mineralogical Analysis

Mineralogical analysis, conducted on three different samples, verifies the following;

Sample: S–1

Subhedral calcite ($CaCO_3$), with fine–average grain size, occurs as the predominant carbonate mineral. Siderite ($FeCO_3$) is noted as lamellar, iron oxide stained, subhedral crystals with perfect cleavage. Sample consists of ankerite ($CaFe(CO_3)_2$) and dolomite ($CaMg(CO_3)_2$) euhedral crystals in form of rhombohedrons. Approximately 1cm in thickness, silicate formations (mainly thin–cryptocrystalline quartz, SiO_2 & rare phyllosilicate forms) are observed in the sample (Fig. 4.2, Fig. 4.3).

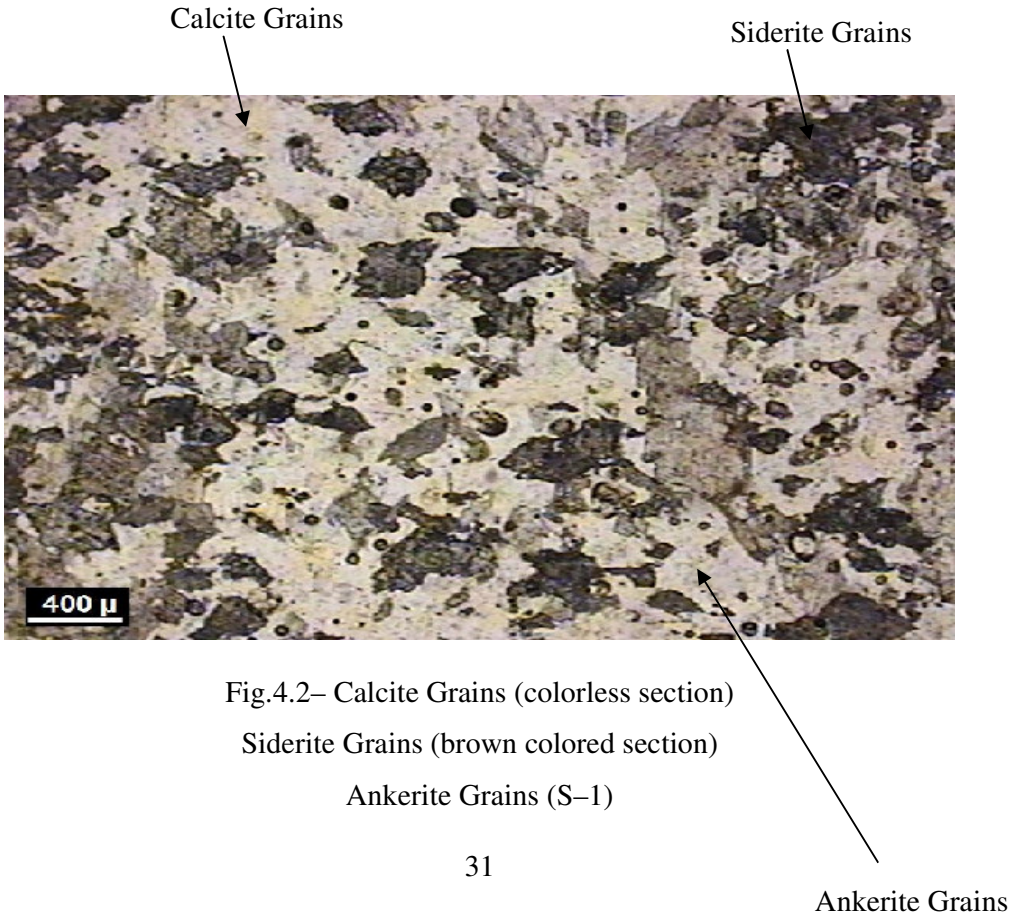

Fig.4.2– Calcite Grains (colorless section)
Siderite Grains (brown colored section)
Ankerite Grains (S–1)

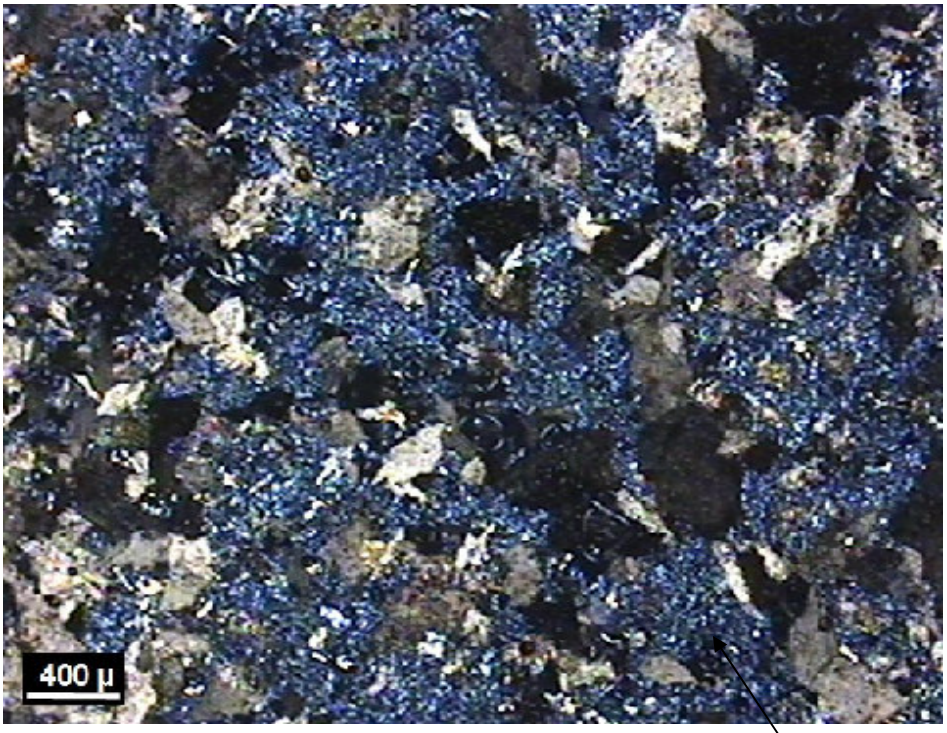

Fig.4.3– Silicate Formations (S–1)

Sample: S–2

Sample is mainly made up of subhedral siderite, euhedral dolomite, ankerite crystals microscopically (Fig. 4.4). Cracks filled up with coarse grained calcite grains are noticed. Remarking the occurrence of alterations, there exist irregular limonite ($FeO(OH).nH_2O$) traces.

Fig.4.4– Siderite Grains (brown colored section)
Dolomite Grains (S–2)

Sample: S-3

Limonite traced parts are observed within breccia textured sample; there exist rare subhedral ankerite and dolomite grains. Calcite is seen in two locations within the sample. The sample consists of silicate formations; particularly cryptocrystalline quartz is observed along the cracks. Furthermore there exist rare autigenic quartz and phyllosilicate minerals (Fig. 4.5).

Ankerite Grains

Siderite Grains

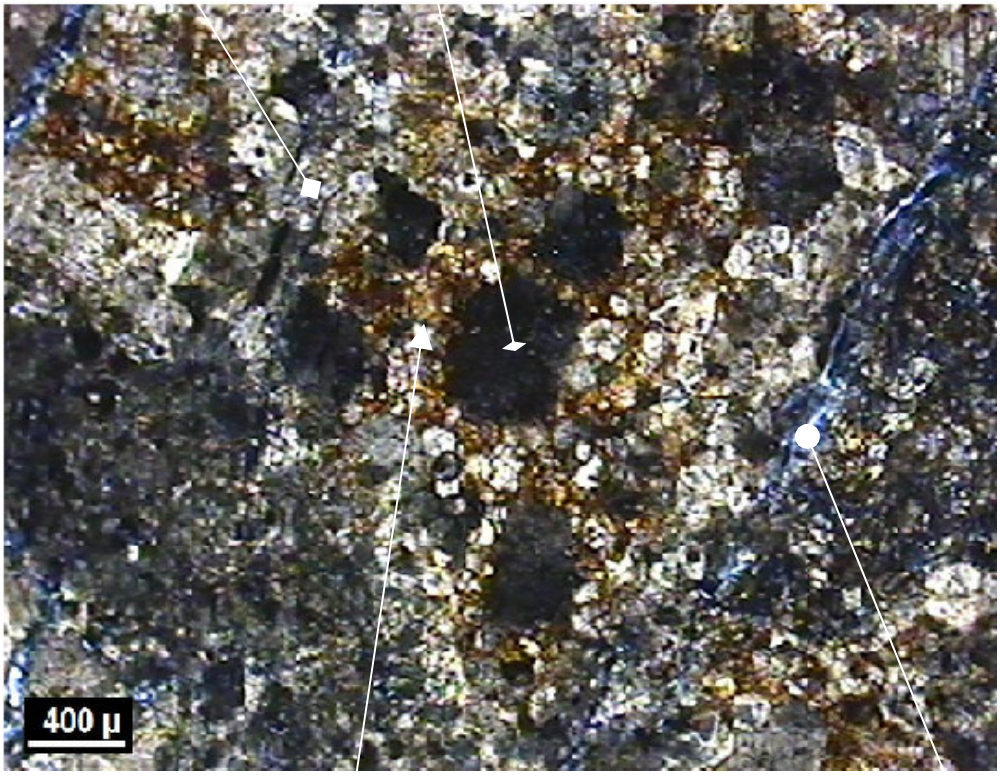

Limonite

Quartz

Fig.4.5– Siderite & Ankerite Grains in breccia textured formations traced with Limonite & Quartz filled cracks (S–3)

4.2.3. Particle Size Analysis

The results of the dry & wet particle size analyses are tabulated in following tables (Table 4.2; Table 4.3). Fig. 4.6 gives the comparison of analyses, on a graph drawn cumulative undersize, % vs. nominal particle size, μm.

Table 4.2– Results of Dry Particle Size Analysis

Sieve Size Range (μm)	Nominal Aperture Size (μm)	Weight Percent, %	Cumulative Undersize, %
+2400	2400	3.51	96.49
2400+1615	1615	21.42	75.07
1615+1168	1168	12.23	62.84
1168+833	833	11.31	51.53
833+589	589	10.82	40.71
589+417	417	10.60	30.11
417+250	250	8.72	21.39
250+150	150	6.93	14.46
150+106	106	4.54	9.92
106+75	75	5.25	4.67
-75		4.67	

Table 4.3– Results of Wet Particle Size Analysis

Sieve Size Range (μm)	Nominal Aperture Size (μm)	Weight Percent, %	Cumulative Undersize, %
+2400	2400	2.72	97.28
2400+1615	1615	21.37	75.92
1615+1168	1168	19.36	56.56
1168+833	833	14.58	41.98
833+589	589	9.33	32.65
589+417	417	7.42	25.23
417+250	250	5.42	19.80
250+150	150	3.75	16.06
150+106	106	1.76	14.30
106+75	75	1.26	13.04
-75		13.04	

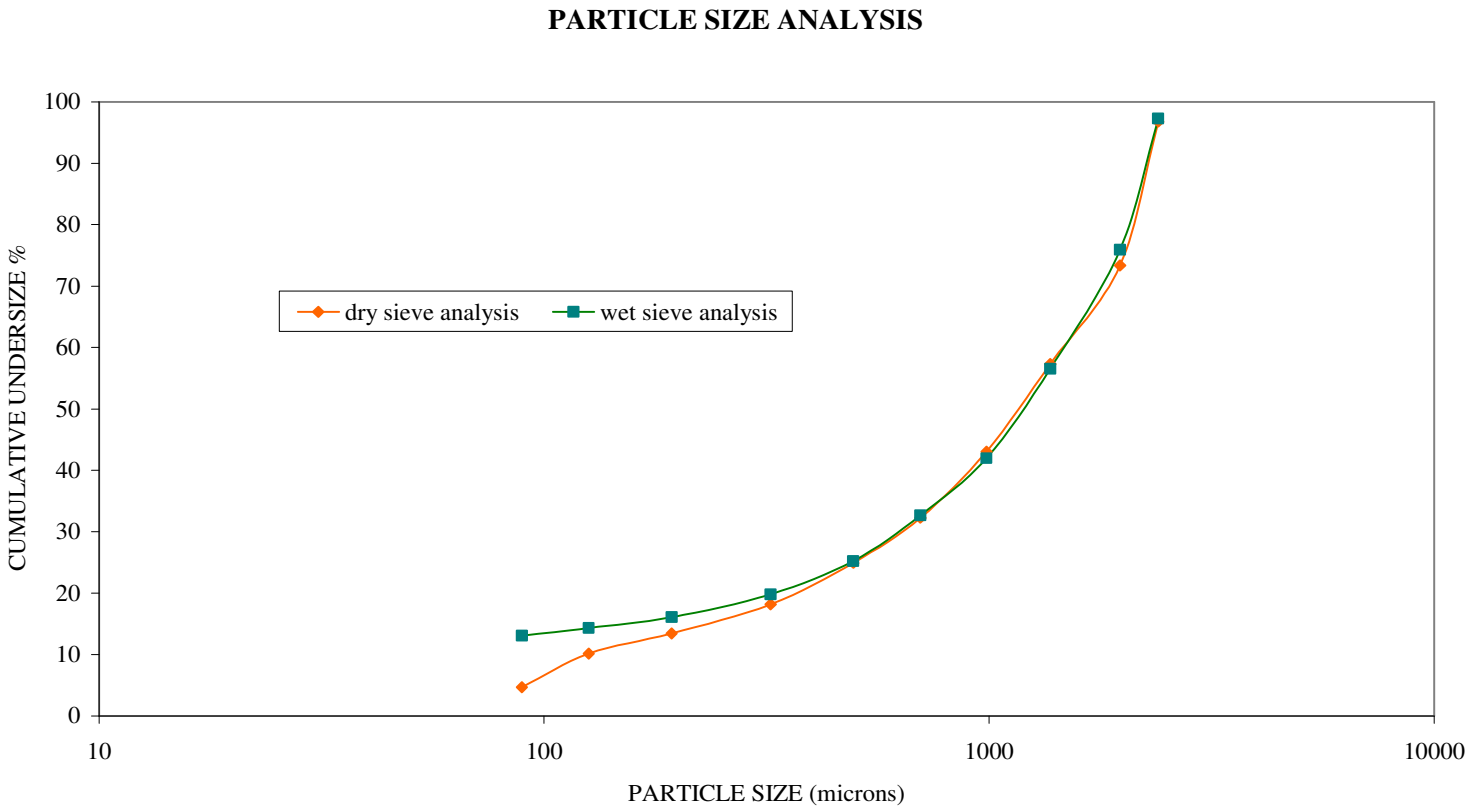

Fig. 4.6– Comparison of Dry Particle Size Analysis and Wet Particle Size Analysis

Given by Table 4.4, there is uniform distribution of iron grade on particle size, except for the range where particle size is between 1168 μm and 833 μm and for the range where particle size is finer than 75 μm. The value obtained for overal iron grade as result of analysis conducted along with dry particle size analysis verifies the consistency of distribution (Table 4.4), being in close agreement with the value obtained by chemical analysis of sample (Fe %= 37.69).

Table 4.4– Results of Iron Grade Analysis on Dry Particle Size Analysis Samples

Sieve Size Range (μm)	Nominal Aperture Size (μm)	Weight Percent, %	Iron Grade, %	Iron Grade Distribution, %
+2400	2400	3.51	35.58	3.36
2400+1615	1615	21.42	37.2	21.42
1615+1168	1168	12.23	40.11	13.19
1168+833	833	11.31	40.45	12.30
833+589	589	10.82	38.2	11.11
589+417	417	10.60	36.11	10.29
417+250	250	8.72	37.11	8.70
250+150	150	6.93	36.22	6.75
150+106	106	4.54	38.29	4.67
106+75	75	5.25	38.15	5.38
-75		4.67	25.2	3.16
Feed		100.00	37.32	100.00

4.3. Thermal Characterization of Siderite Samples

Thermal analyses, Thermogravimetric Analysis (TGA); Differential Thermal Analysis (DTA), and X–Ray Fluorescence (XRF) analysis have shed light to thesis study in gathering the required data to initialize the experiments. Thereafter, X–Ray Diffraction (XRD) analysis and magnetic susceptibility analysis were used in identification of the phases obtained.

4.3.1. Thermogravimetric Analysis

TGA demonstrates that the thermal decomposition of the sample starts at around T= 465 °C, up to T= 650 °C significant weight loss of the sample is observed. Thus, according to the analytical findings, energy flow in form of heat to the system is continuous at temperature range T= 465 °C– 650 °C. Rate of weight loss due to the heat flow to the system is most intensive at temperatures between T= 515 ºC and T= 550 ºC, indicative of endothermic reactions. Hence endothermic and exothermic parts of thermal decomposition reactions are somehow determined by TGA, relying on DTA for further details of reactions.

Being mainly composed of carbonate minerals, TGA of Hekimhan–Deveci siderite sample demonstrates the weight loss of sample is approximately 30 %, reaching steady state at around T= 700 °C. As seen on the figure there is no significant change beyond T= 650 °C (Fig. 4.7). Temperature range of thermal decomposition reactions is thereby determined based on TGA,

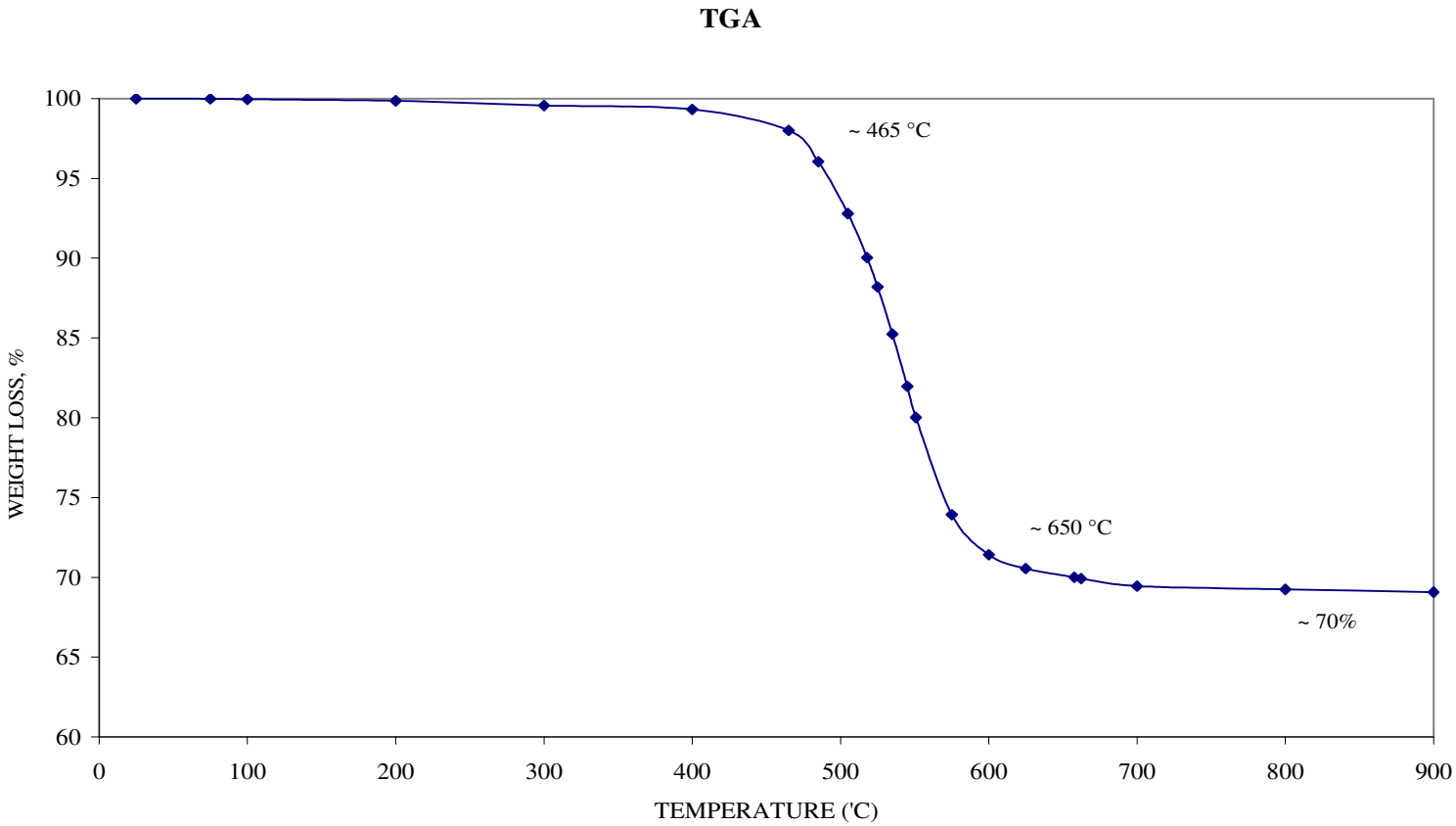

Fig.4.7– TGA of run-of-mine Sample, in air, heated from 25 °C to 900 °C at 10 °C/min

4.3.2. Differential Thermal Analysis

DTA has detailed the results obtained by TGA, explaining the nature of reactions in course of thermal decomposition. Weight loss due to thermal treatment is most intensive at around T= 550 ℃; that is the reaction is endothermic up to T= 560 ℃, where exothermic reactions are detected by heat flow curve (Fig. 4.8). There is slight weight loss noticed at temperatures T= 650 °C–750 °C, indicated by both heat flow curve and dTG curve.

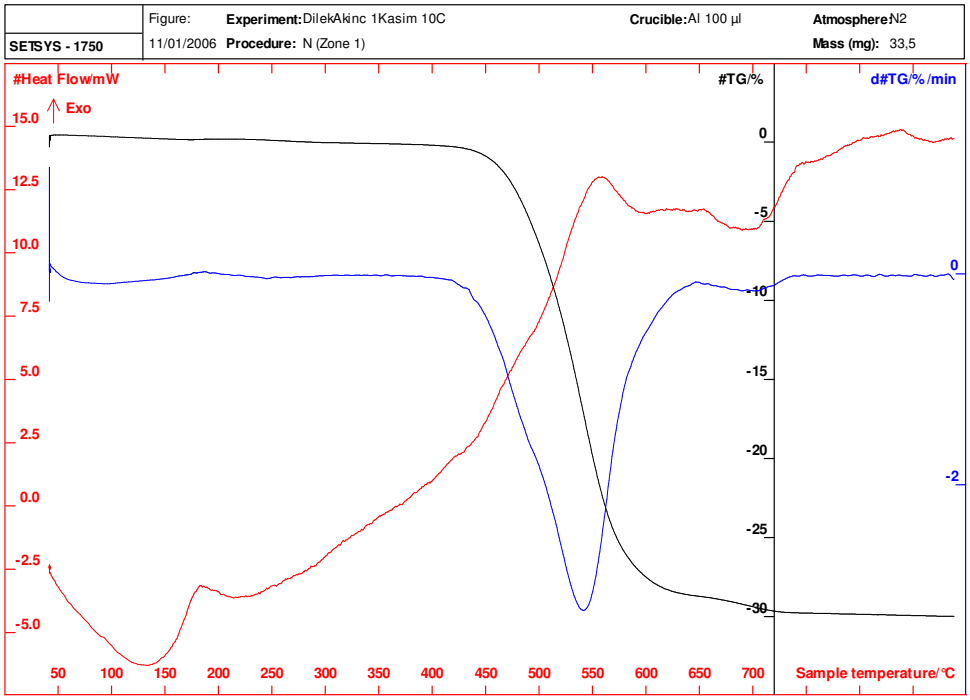

Fig.4.8– DTA of run-of-mine Sample, in air, heated from 25 °C to 900 °C at 10 °C/min

4.4. Heating Experiments

4.4.1. Microwave Heating

Microwave heating of samples did not yield successful results with respect to roasting, samples were not heated even at exposure to microwave energy for t= 30 minutes. Weight loss obtained was not significant even tough time of treatment was successively increased (Fig. 4.9).

There were no attempts in respect of microwave heating for longer periods since conventional heating experiments were parallely carried out, recording significant weight loss at t= 30 minutes. Considering that molecular interaction of microwaves with siderite sample could be achieved by use of facilitator, fine magnetite was added to the system. However, heating could not be enhanced.

Separately, the following figure (Fig. 4.10) demonstrates the weight loss of sample heated by microwave oven for t= 6 minutes on prepared size fractions.

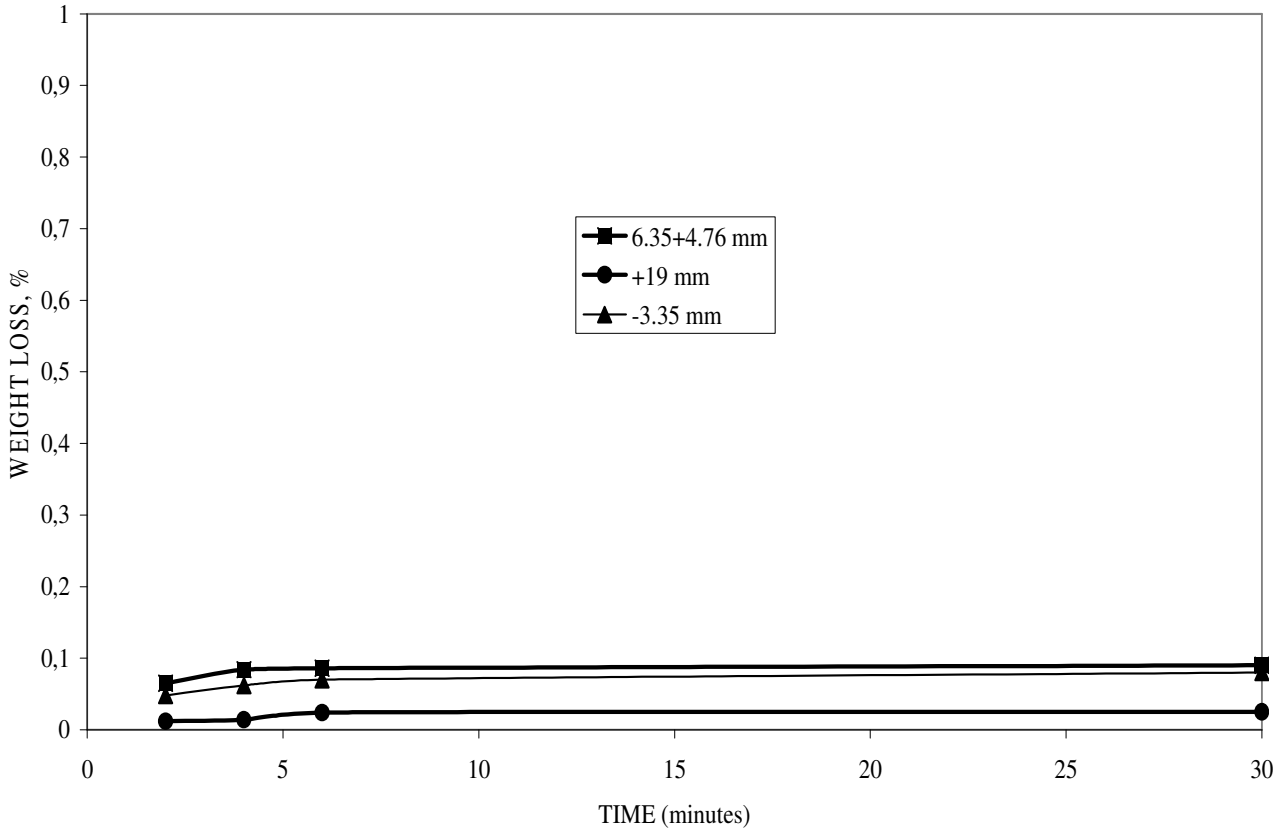

Fig.4.9– Weight Loss of Sample against Time, by Microwave Heating

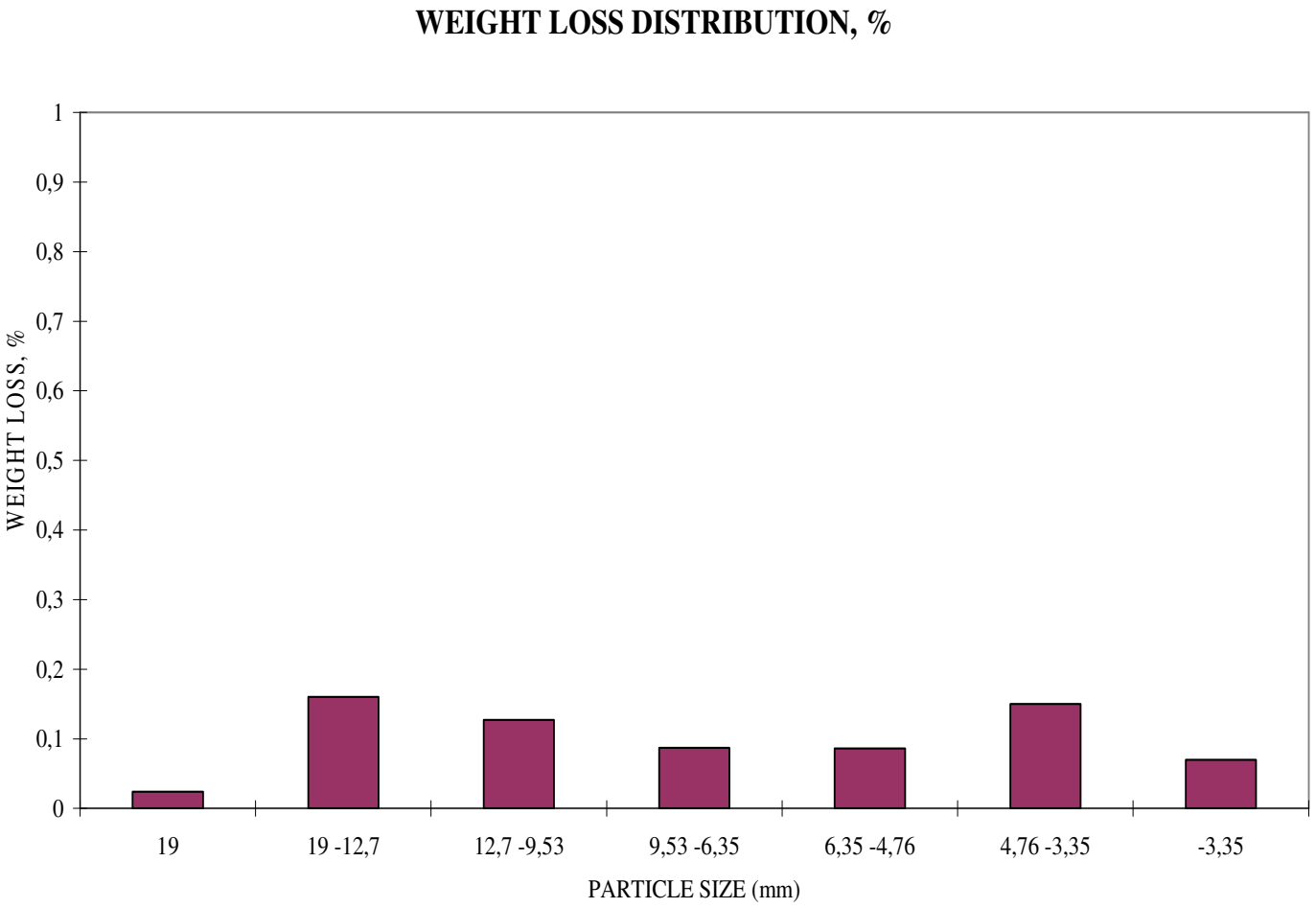

Fig.4.10– Weight Loss of Sample by Microwave Heating, recorded in t= 6 minutes, P= 900 W, f= 2.45 GHz

4.4.2. Conventional Heating

Heating temperature and heating time have been the parameters analyzed in conventional heating runs. Roasting was not achieved at T= 465 ℃; at temperatures T= 500 ℃, T= 535 ℃, in t= 45 minutes, roasting did occur, relatively at a slower rate though. Enhancement of completion of weight loss has been achieved at T= 550 ℃, T= 560 ℃, T= 570 ℃ within 45 minutes. Heating experiments has verified the analytical findings of thermal analysis (TGA, DTA). It has been shown that heating at high temperatures ensures obtaining desired changes in course of roasting process at shorter times of treatment.

Fig. 4.11 gives the graphical representation of results experiments performed in the range, T= 465 ℃–605 ℃ while fig. 4.12 demonstrates the results obtained at T= 550 ℃, T= 560 ℃, and T= 570 ℃. Data related to results obtained at T= 605 ℃ indicated that weight loss of samples reached to completion within 30 minutes. However, further analysis of samples, i.e. magnetic susceptibility and iron grade analysis, has proven that it is not essential operate at high temperatures as T= 605 ℃.

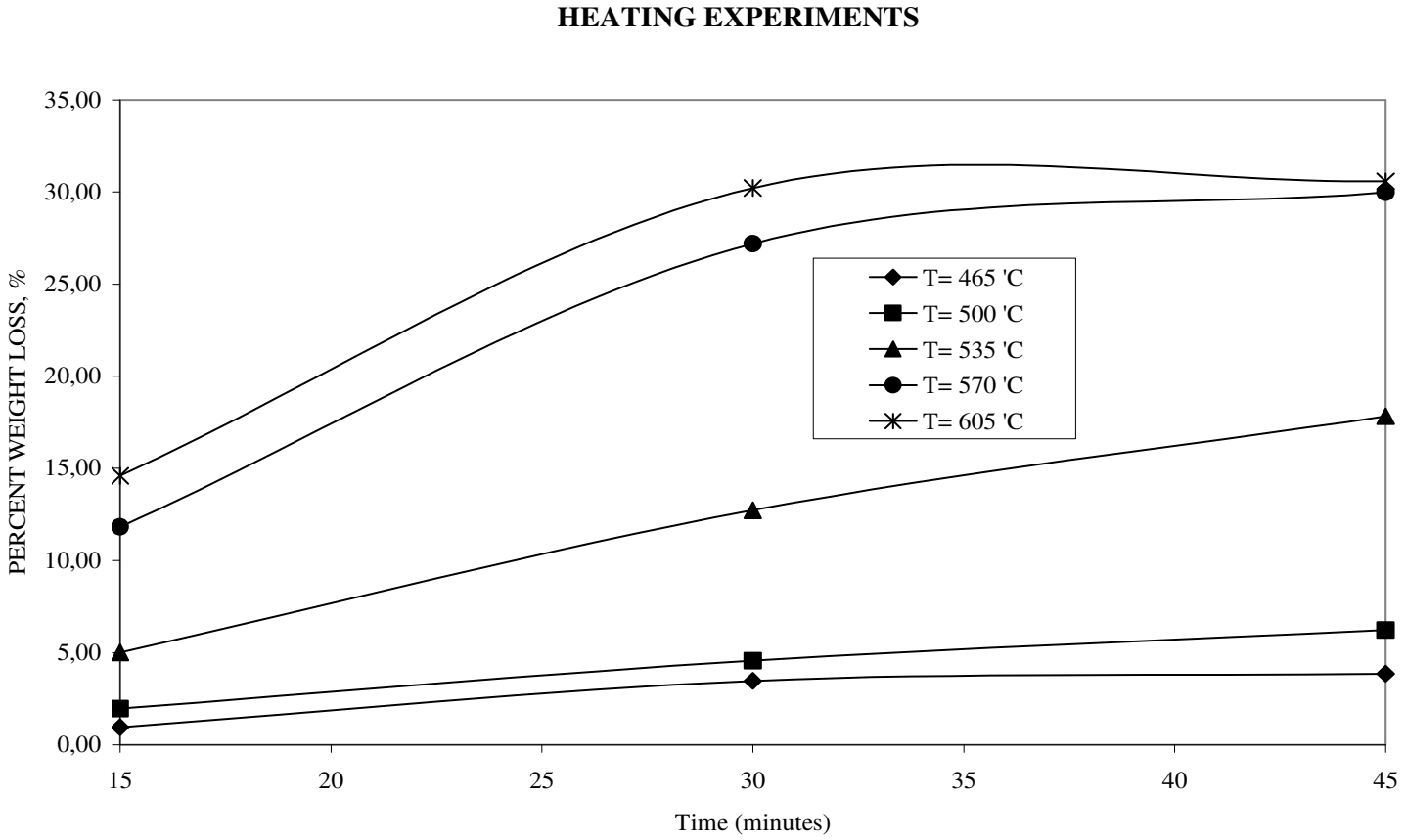

Fig.4.11–Weight Loss of Samples on Time Basis, by Conventional Heating

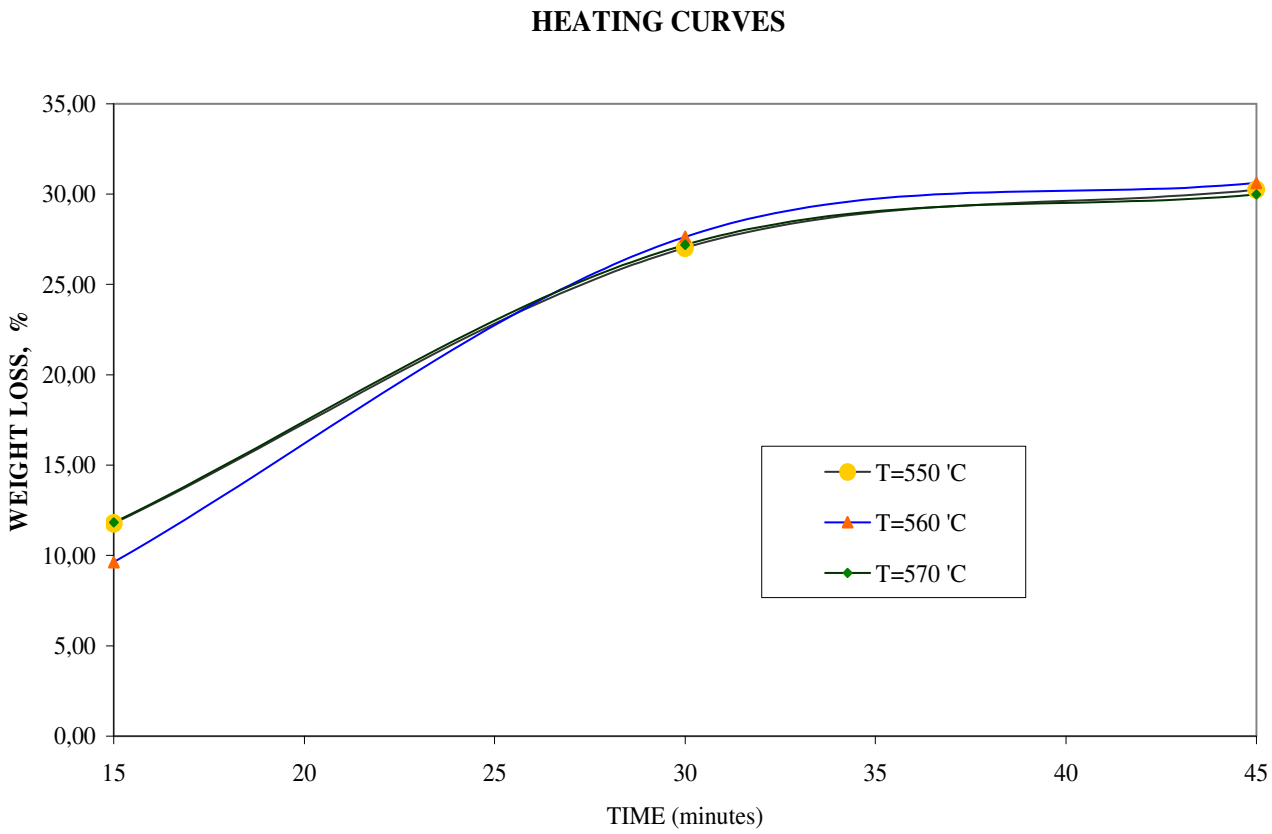

Fig.4.12– Weight Loss of Samples on Temperature Basis, by Conventional Heating

4.4.3. Comparison of Microwave Heating and Conventional Heating

Hekimhan–Deveci siderite samples have not responded to microwave energy, whereas conventional heating runs have yielded expected results. Comparison of microwave heating to conventional heating is given below (Table 4.5, Fig. 4.13).

Table 4.5– Results of Microwave Heating & Conventional Heating Experiments

	MICROWAVE HEATING			CONVENTIONAL HEATING
	PERCENT WEIGHT LOSS, %			
Size (mm)	2’	4’	6’	T= 560 °C, t= 30'
+19	0.012	0.014	0.024	24.07
19 -12.7	0.05	0.12	0.16	25.68
12.7 -9.53	0.016	0.041	0.127	28.05
9.53 -6.35	0.036	0.035	0.087	28.72
6.35 -4.76	0.065	0.085	0.086	28.93
4.76 -3.35	0.065	0.073	0.15	29.40
-3.35	0.048	0.062	0.07	28.98

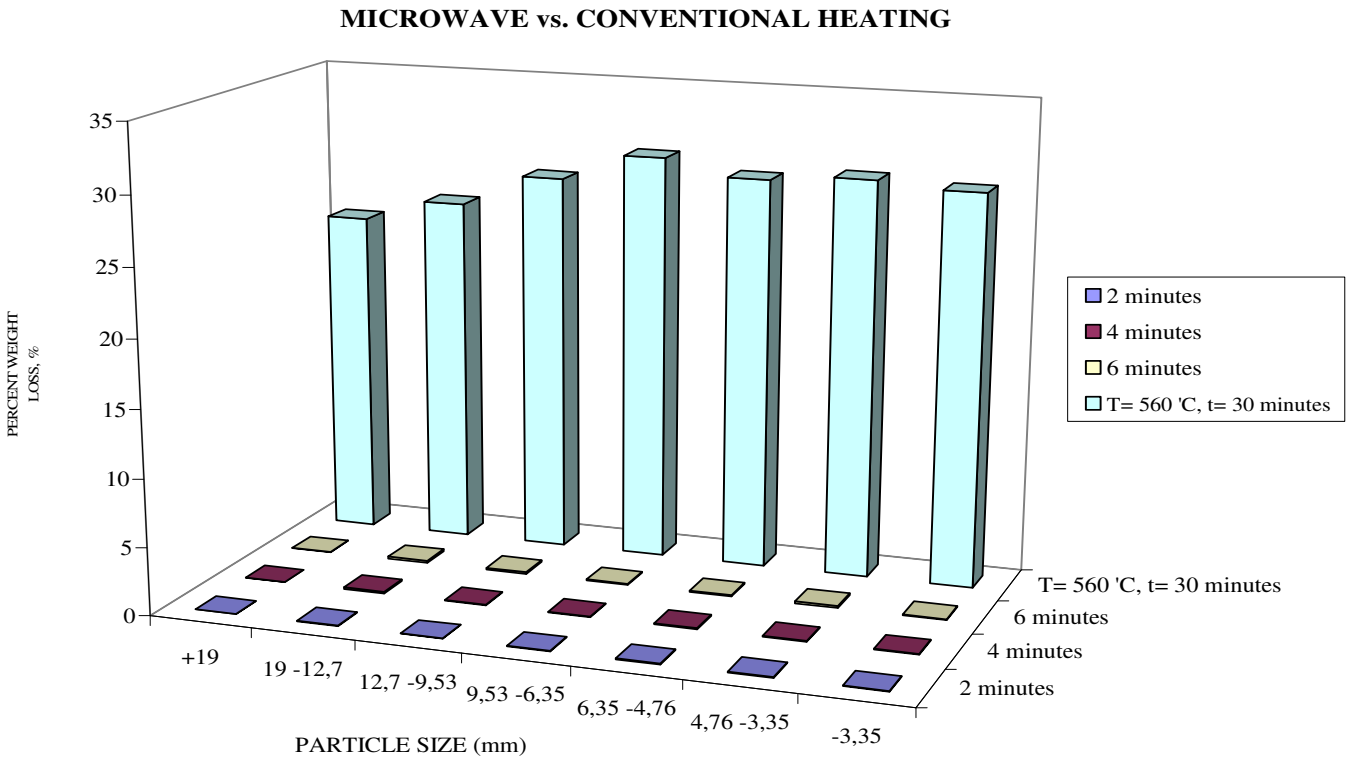

Fig.4.13– Comparison of Microwave Heating to Conventional Heating

4.5. Magnetic Susceptibility Analysis

4.5.1. Magnetic Susceptibility Balance

Having mass magnetic susceptibility of 32–270*10^{-8} m^3/kg, siderite is classified paramagnetic at room temperature. The value of mass magnetic susceptibility has been found as 92*10^{-8} m^3/kg in analysis carried out on Hekimhan–Deveci siderite samples at T= 25 °C. The results of magnetic susceptibility measurements verified the increase in magnetic susceptibility at high orders upon being heated at indicated temperatures against time. It has been concluded that, heating for t= 30 minutes may result in increase of magnetic susceptibility provided that samples are heated at high temperatures (T= 560 °C; T= 605 °C). Increase in magnetic susceptibility is reported to increase against longer time of heating. On the other hand, there has been noted no significant change on samples, which were analyzed referencing the TGA results, heated at T= 465 °C for t= 60 minutes.

Table 4.6 lists the results of analyses in detail, grouped on basis of time. Summary of the results is seen on fig. 4.14 graphically.

Table 4.6– Results of Magnetic Susceptibility Measurements

Sample	**Heating Temperature (°C)**	**Heating Time (minutes)**	**Mass Magnetic Susceptibility (m^3/kg)*10^{-8}**
1	25	-	92.0
2	510	30	3721.4
3	560	30	18253.3
4	605	30	20758.1
5	465	60	84.6
6	510	60	5017.1
7	560	60	20530.0

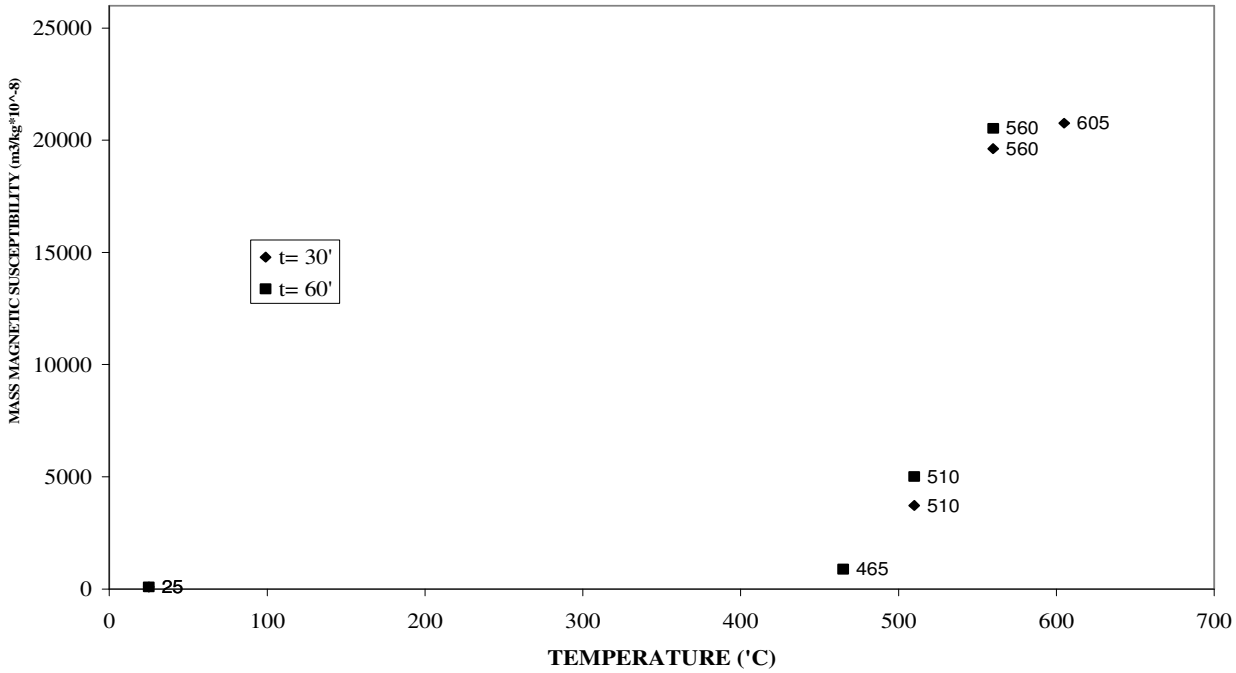

Fig.4.14– Variations in Magnetic Susceptibility of samples upon heat treatment

4.5.2. XRD Analysis

Variations in magnetic susceptibility of heated samples have been checked in terms of new phases formed by XRD analysis. Analysis was done on four sets of heated samples.

1. T= 465 °C, t= 210 minutes; 2. T= 560 °C, t= 45 minutes;
3. T= 605 °C, t= 45 minutes; 4. T= 700 °C, t= 45 minutes.

Tough it is so verified by TGA, there has been noted no distinct variations of XRD profile of the sample heated at T= 465 °C for long time period. Phases observed are identical to run-of-mine sample at T= 25 °C despite the fact that it was subjected to the longest time interval of heat treatment among all. XRD analysis was also performed on samples heated at T= 700 °C to check the consistency of results with respect to new phases. XRD analysis has shown that siderite ($FeCO_3$), ankerite ($CaFe(CO_3)_2$), dolomite ($CaMg(CO_3)_2$), calcite ($CaCO_3$), quartz (SiO_2) along with hematite (α–Fe_2O_3) are present in run-of-mine sample (Fig. 4.1). Newly formed phases, as results of thermal treatment, are noted to be magnetite (Fe_3O_4), maghemite (γ– Fe_2O_3) (Fig. 4.15–Fig. 4.18). Hence increase in magnetic susceptibility has been proved by identification of ferromagnetic phases in heated samples in comparison to phases that are paramagnetic at room temperature.

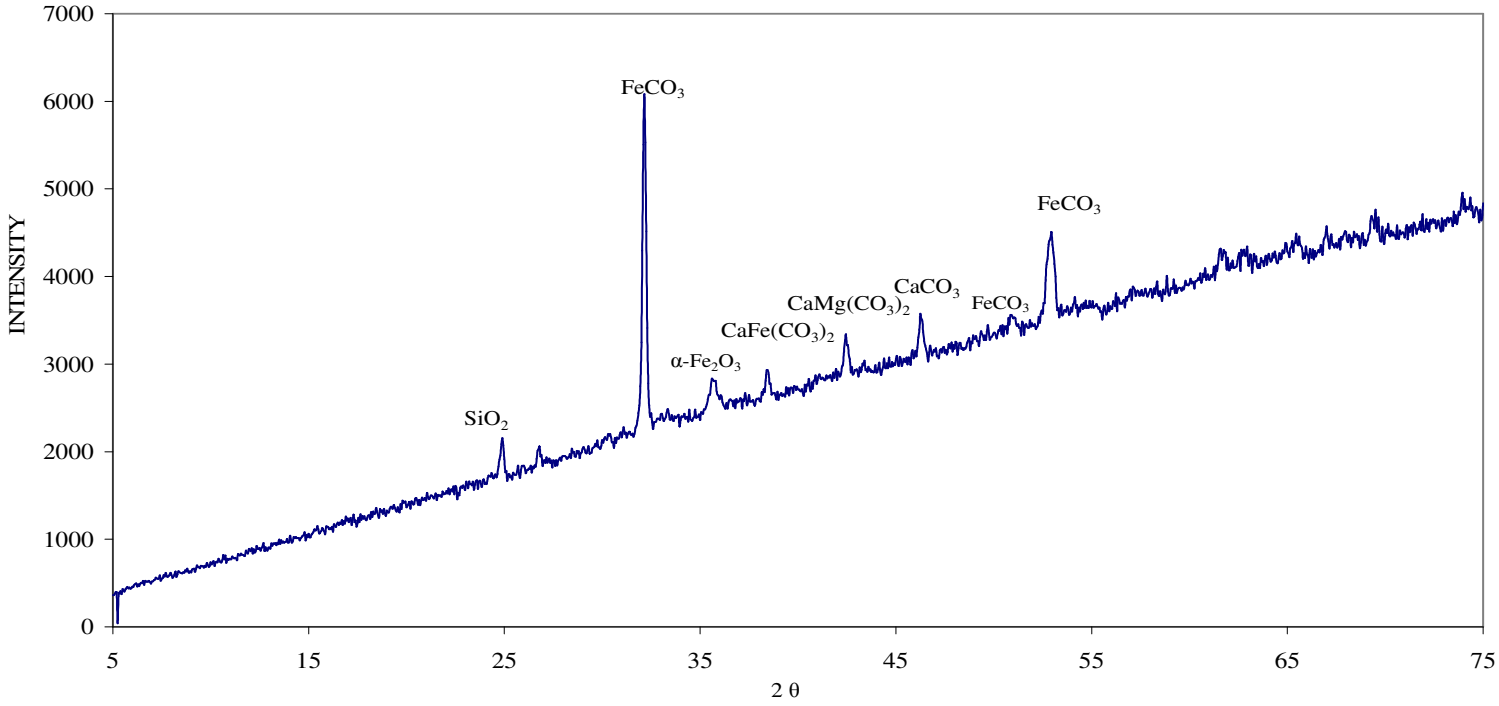

Fig.4.15– XRD Analysis of Heated Samples, T= 465 °C

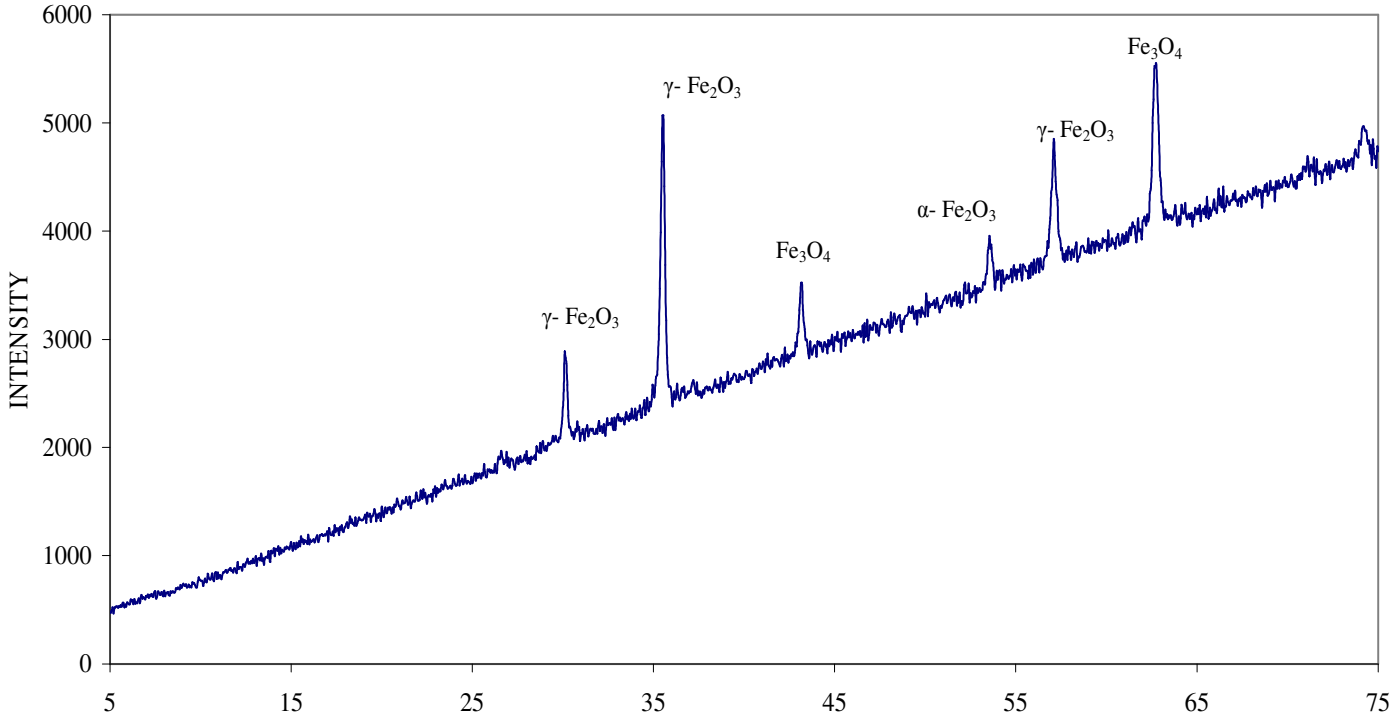

Fig.4.16– XRD Analysis of Heated Samples, T= 560 °C

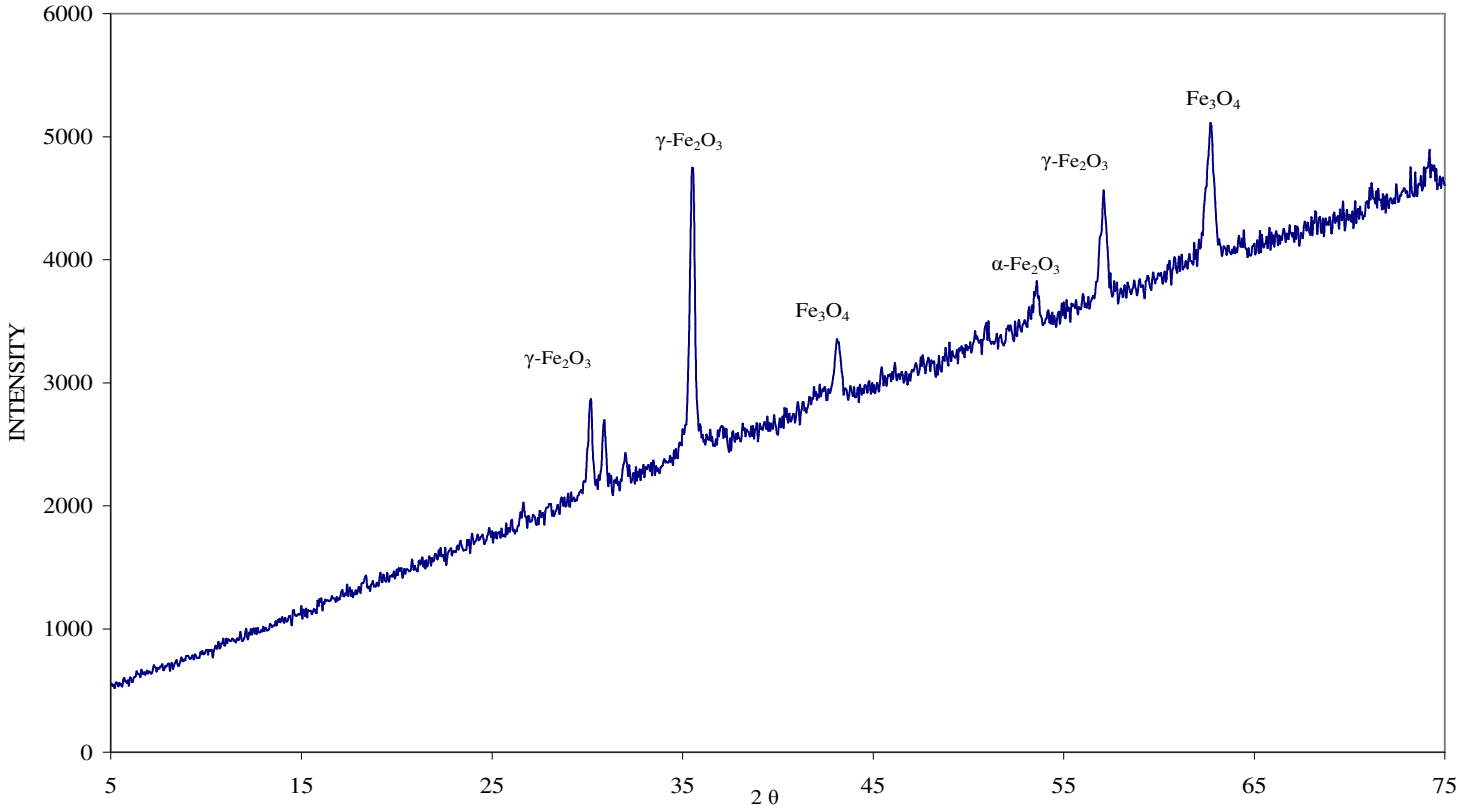

Fig.4.17– XRD Analysis of Heated Samples, T= 605 °C

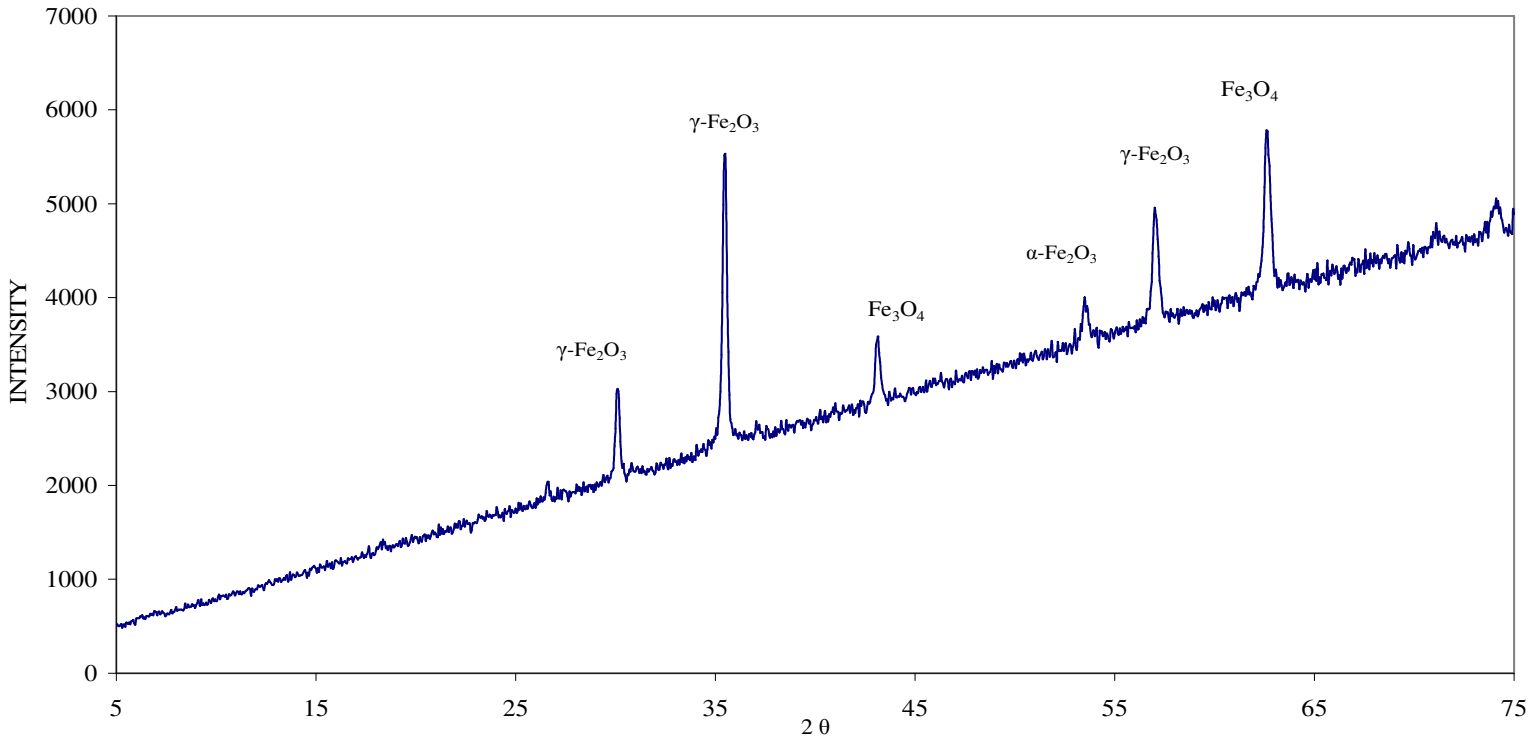

Fig.4.18– XRD Analysis of Heated Samples, T= 700 °C °C/min

4.6. Magnetic Separation

Wet low intensity magnetic separation experiments on heated samples yielded high recovery. Magnetic recovery reported of increase against increasing of applied current (Fig. 4.19). The values of recovery for I= 0.1 A (0.046 T), I=0.25 A (0.1037 T), I= 0.5 A (0.195 T) were respectively 6.0%, 98.46%, and 99.50%. On magnetic separation of run-of-mine sample with Davis tube at field intensity of 0.195 T, all reported to nonmagnetic fraction, resulting in no separation.

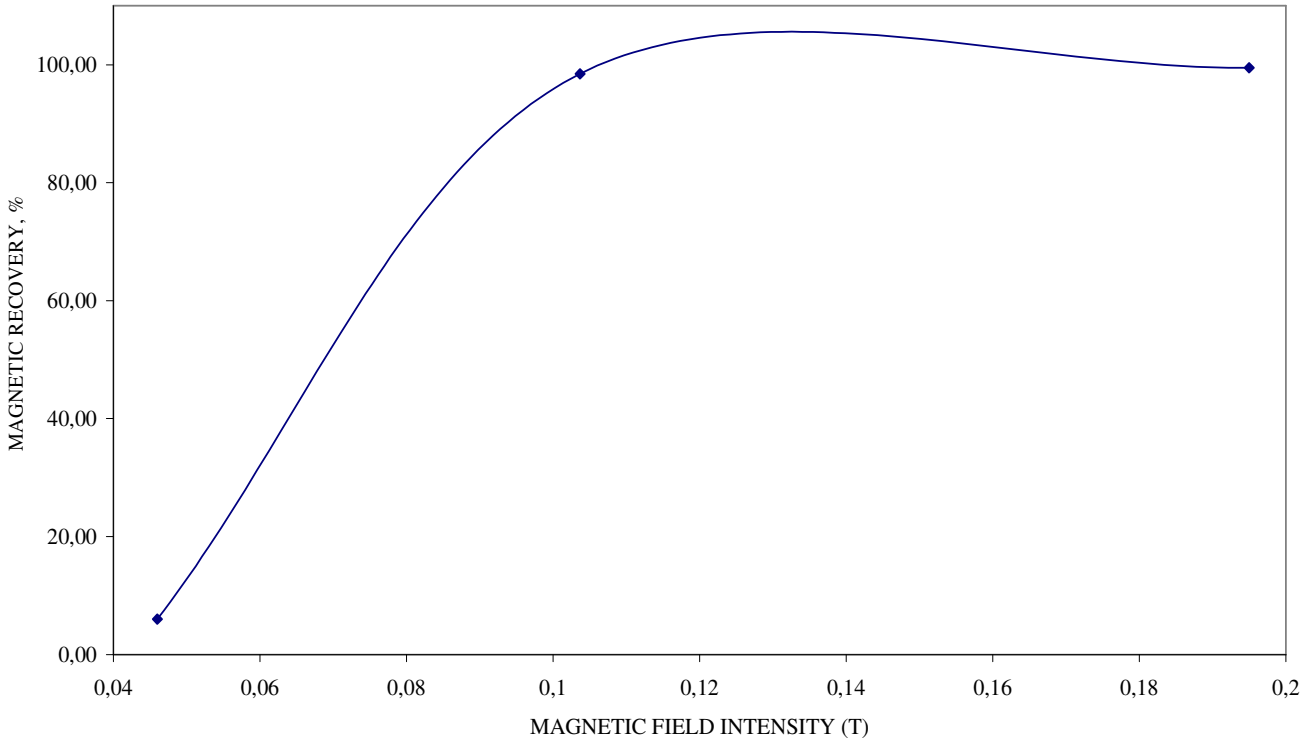

Fig.4.19– Recovery recorded by Wet Low Intensity Magnetic Separation on Heated Samples

4.7. Statistical Modeling

Regression analysis has been made by both using *"Design-Expert 7.1.1"* program and *"Excel worksheets"*, same values have been obtained by two methods in terms of ANOVA; below follows the results of analysis in terms of mathematical equations and related graphs. Table 4.7 gives the summary of order of input parameters (R_1) for each run; then comes the results of program for R_1 (weight loss of siderite ore, %) (Table 4.9).

Table 4.7- Input Parameters for Design Model in indicated order [3 replicates]

RUN	$FACTOR_1$ (TEMPERATURE) A:A ('C)	$FACTOR_2$ (TIME) B:B (minutes)	$FACTOR_3$ (PARTICLE SIZE) C:C (mm)	R_1
1	1	-1	-1	27.91
2	1	1	1	30.2
3	1	-1	-1	27
4	-1	1	1	3.32
5	1	-1	1	21.16
6	1	-1	1	22.45
7	-1	1	-1	7
8	-1	1	1	3.49
9	-1	1	1	3.23
10	1	1	-1	29.82
11	-1	-1	-1	2.5
12	-1	1	-1	7.15
13	1	1	-1	30.1
14	-1	1	-1	6.9
15	1	1	-1	30.5
16	-1	-1	-1	2.93
17	1	-1	-1	26.85
18	1	1	1	30.33
19	1	-1	1	21.51
20	-1	-1	1	1.49
21	-1	-1	1	1.39
22	-1	-1	1	1.62
23	1	1	1	30.27
24	-1	-1	-1	2.85

Calculations comprising the ANOVA table are based on sum of results of runs (y_i) multiplied by respective sign as indicated by the design procedure (Table 4.8).

Table 4.8- Algebraic signs for calculating effects in 2^3 designs

T	**t**	**T*t**	**P**	**T*P**	**t*P**	**T*t*P**
-	-	+	-	+	+	-
+	-	-	-	-	+	+
-	+	-	-	+	-	+
+	+	+	-	-	-	-
-	-	+	+	-	-	+
+	-	-	+	+	-	-
-	+	-	+	-	+	-
+	+	+	+	+	+	+

The values ($contrast_x$) obtained in that manner are made use of in preparation of ANOVA table;

$(\text{Main Effect})_x = \frac{(contrast)_x}{n(2^{k-1})}$, Coefficient of Estimate$= \frac{(Main\ Effect)_x}{2}$

n: number of replicates; N: total number of runs

k: number of factors

$SS_x = \frac{(Contrast)_x^2}{n2^k}$, Mean Square$= \left(SS_x / df \right)$, $df_{model} = 2^k - 1$, $df_{total} = N - 1$, $df_E = df_{total} - df_{model}$

$$\text{F value} = \left(MS_x / MS_E \right)$$

$SS_T = \sum_{i=1}^{j} (y)_i^2 - \frac{\left(\sum_{i=1}^{j} y_i \right)^2}{n2^k}$, $SS_T = SS_E + SS_{model}$

	$(\text{Contrast})_x$
Temperature (T)	284.23
Time (t)	52.65
T*t	16.03
Particle Size (P)	-31.05
T*P	-1.47
t*P	9.79
T*P*t	24.25

Table 4.9- Analysis of Variance (ANOVA) for R_1

Response		R_1				
ANOVA for selected factorial model						
Analysis of variance table [Partial sum of squares - Type III]						
	Sum of				p-value	
Source	Squares	df	Mean Square	F Value	Prob > F	
Model	3561.077	7	508.725	4094.506	< 0.0001	significant
A-A	3366.112	1	3366.112	27092.355	< 0.0001	
B-B	115.500	1	115.500	929.616	< 0.0001	
C-C	40.171	1	40.171	323.318	< 0.0001	
AB	10.707	1	10.707	86.173	< 0.0001	
AC	0.0900	1	0.090	0.725	0.4072	not significant
BC	3.993	1	3.993	32.142	< 0.0001	
ABC	24.503	1	24.503	197.210	< 0.0001	
Pure Error	1.988	16	0.124			
Cor Total	3563.065	23				

The Model F-value of 4094.506 implies the model is significant. In respect of fact that values of –Prob > F– less than 0.0500 implies significant model terms, A (x_1), B (x_2), C (x_3), AB (x_1*x_2), BC (x_2*x_3), ABC ($x_1*x_2*x_3$) report to be important model terms while AC is insignificant, having a value of 0.4072. Therefore AC term (x_1*x_3) may be omitted from the model equation to improve the model.

Table 4.10– Statistical Parameters of the model for R_1

Std. Dev.	0.352	R-Squared	0.999
Mean	15.499	Adj R-Squared	0.999
C.V. %	2.274	Pred R-Squared	0.998
PRESS	4.473	Adeq Precision	141.354

The "Pred R-Squared" of 0.998 is in reasonable agreement with the "Adj R-Squared" of 0.999. "Adeq Precision" measures the signal to noise ratio; considering that a ratio greater than 4 is desirable, ratio of 141.354 indicates an adequate signal for the model.

Thus, the coefficients of model parameters equation are as represented below (Table 4.11);

Table 4.11–Coefficients of factors in design model for R_1

	Coefficient		Standard	95% CI	95% CI
Factor	Estimate	df	Error	Low	High
Intercept	15.500	1	0.072	15.346	15.651
A-A	11.843	1	0.072	11.690	11.995
B-B	2.194	1	0.072	2.041	2.346
C-C	-1.294	1	0.072	-1.446	-1.141
AB	0.668	1	0.072	0.515	0.820
AC	-0.061	1	0.072	-0.214	0.0912
BC	0.408	1	0.072	0.255	0.560
ABC	1.010	1	0.072	0.858	1.163

$$R_1 = 15.50 + 11.84x_1 + 2.19x_2 - 1.29x_3 + 0.67x_1x_2 + 0.41x_2x_3 + 1.01x_1x_2x_3 \qquad (4.1)$$

Referencing the model equation, it is seen that temperature (x_1), time (x_2) affect the weight loss process positively while particle size (x_3) affects negatively; that is increasing the temperature and time of operation, in the studied range, increases the percent weight loss obtained. However decrease in particle size is necessitated to get better results, though particle size is not as much influencing the process as temperature or time.

Graphical summaries for case statistics have been given by the following figures; the first figure, normal probability plot, verifies that the residuals in design for R_1 follow a normal distribution (Fig. 4.20).

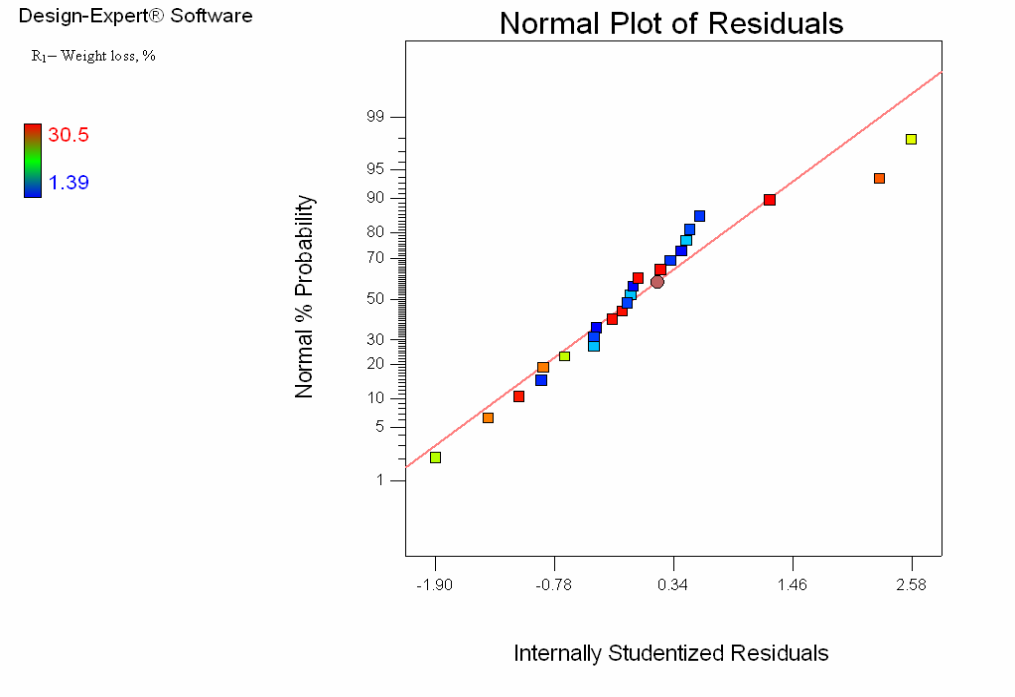

Fig.4.20– Normality Plot of Residuals in Model for Weight Loss (R_1)

The degree of consistency of model on basis of actual vs. predicted values has been checked on the following graph (Fig. 4.21).

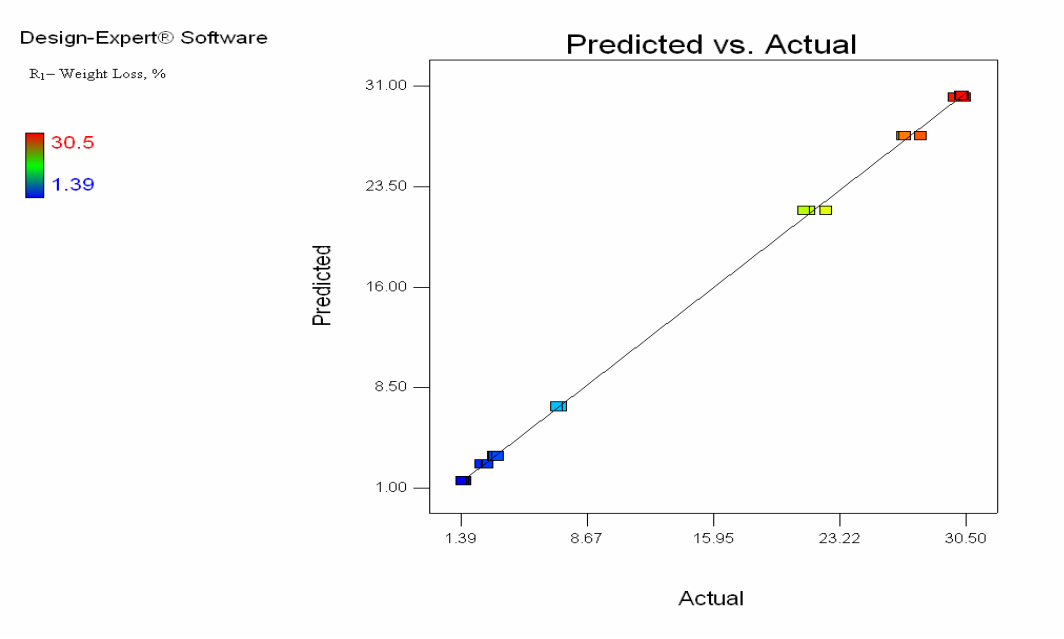

Fig.4.21– Comparison of model results with Actual data in design for (R_1)

Interactions of factors in model equation are represented (Fig. 4.22, Fig. 4.23, Fig. 4.24, Fig. 4.25, and Fig. 4.26);

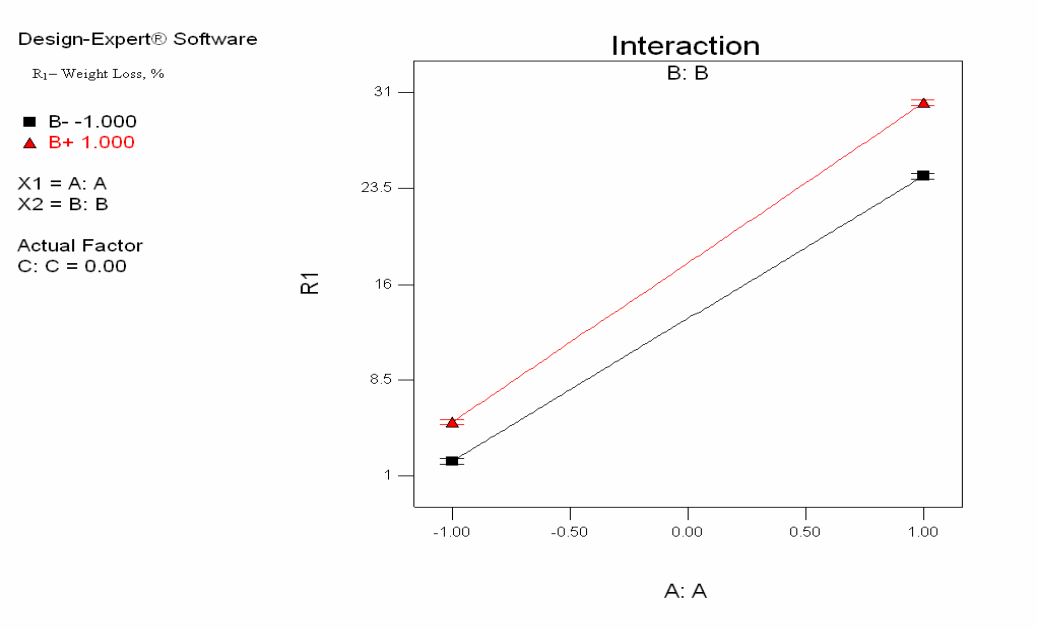

Fig.4.22– Interaction of temperature (x_1) and time (x_2) in model (R_1)

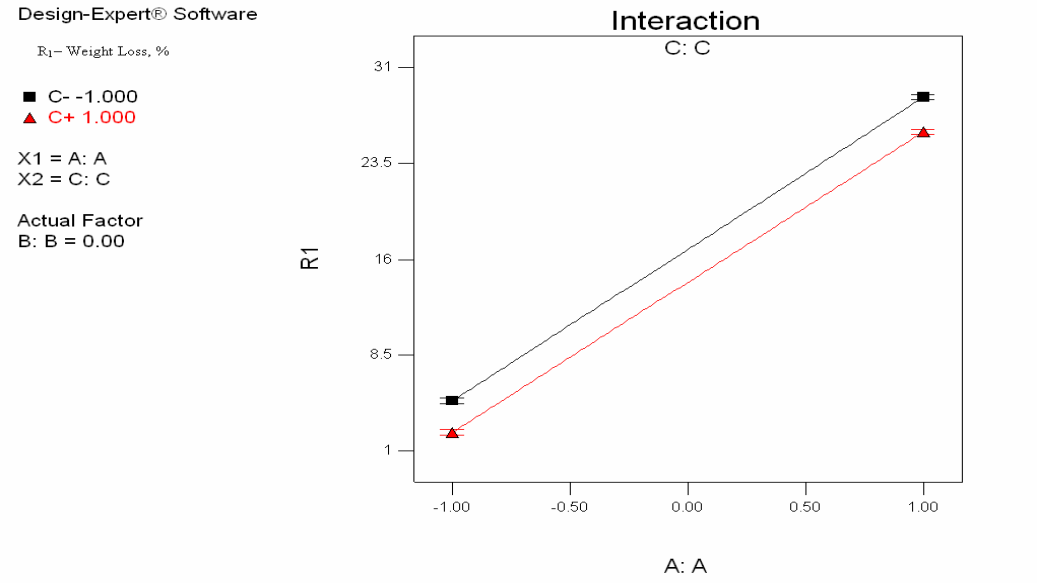

Fig.4.23– Interaction of temperature (x_1) and particle size (x_3) in model (R_1)

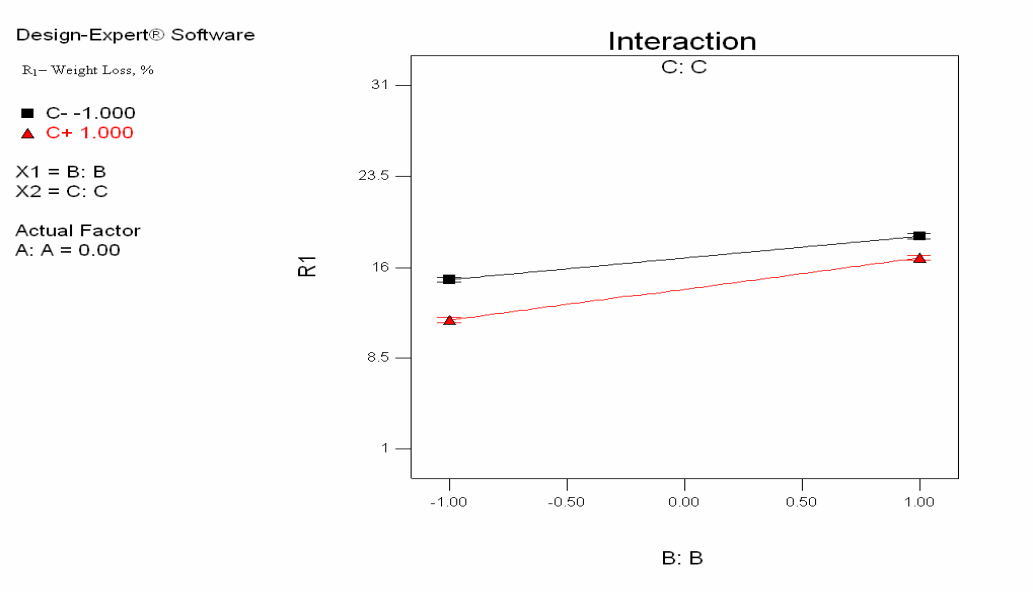

Fig.4.24– Interaction of time (x_2) and particle size (x_3) in model (R_1)

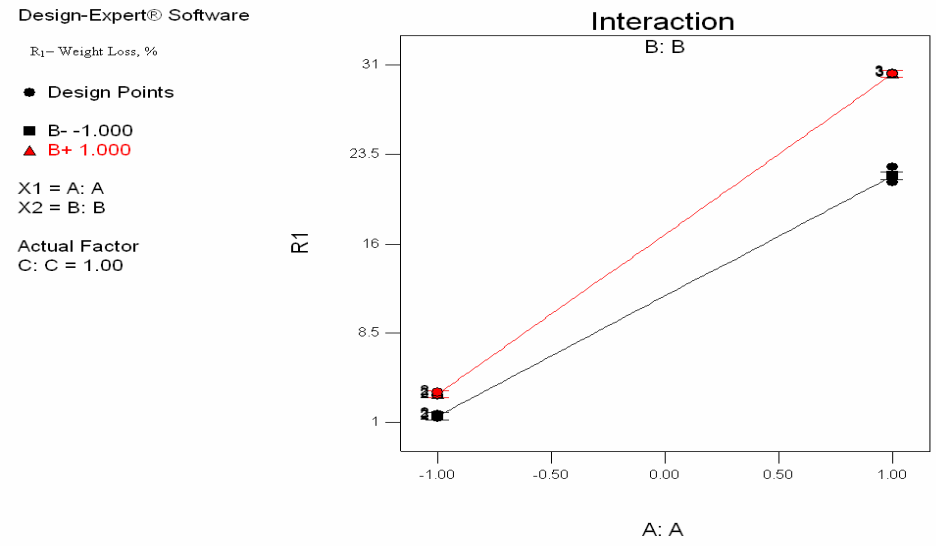

Fig.4.25– Interaction of temperature (x_1), time(x_2), and particle size (x_3) in model (R_1)

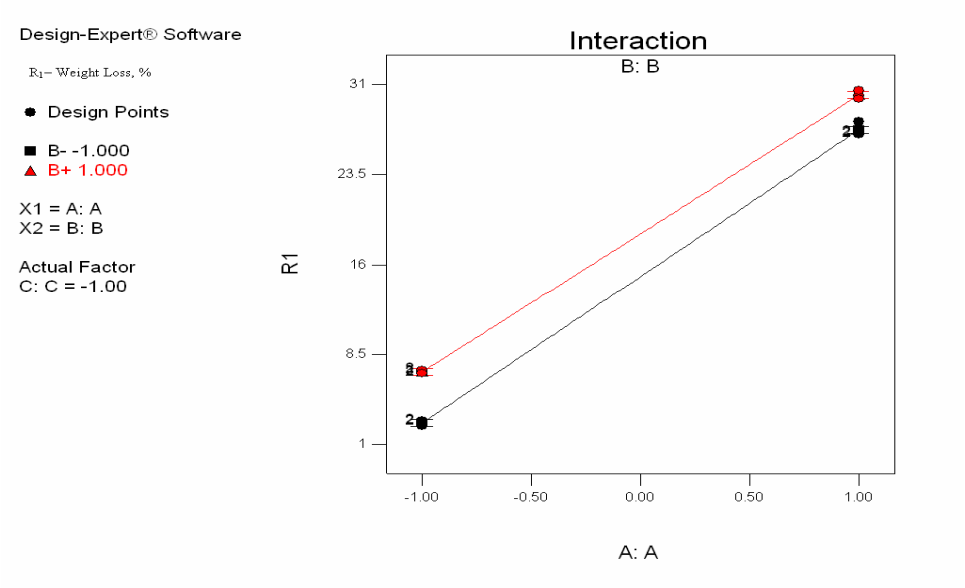

Fig.4.26– Interaction of temperature (x_1), time(x_2), and particle size (x_3) in model (R_1)

ANOVA has once more been utilized in interpretation of data for design of R_2 (Iron (Fe) content of roasted product, %); table 4.12 gives the input parameters for two level factorial design for two factors.

Table 4.12- Input Parameters for Design Model in indicated order [3 replicates]

RUN	FACTOR (TEMPERATURE) A:A (°C)	FACTOR (TIME) B:B (minutes)	R_2
1	-1	-1	38.86
2	-1	1	38.45
3	1	1	51
4	-1	1	36.94
5	1	-1	37.2
6	1	1	56
7	1	1	55
8	-1	-1	37.19
9	1	-1	38.42
10	-1	1	41.32
11	1	-1	42.38
12	-1	-1	36.55

Table 4.13- 2^2 two-level, full factorial design table showing runs in Standard Order & Algebraic signs for calculating effects in 2^2 designs

	X_1	X_2	X_3
RUN			
1	-1	-1	-1
2	1	-1	-1
3	-1	1	-1
4	1	1	-1
T	**t**	**T*t**	
-	-	+	
+	-	-	
-	+	-	
+	+	+	

	$(Contrast)_x$
Temperature (T)	52.23
Time (T)	49.65
T*t	41.43

The results of analysis is presented in table 4.14.

Table 4.14- Analysis of Variance (ANOVA) for R_2

Response		R_2				
ANOVA for selected factorial model						
Analysis of variance table [Partial sum of squares - Type III]						
	Sum of				p-value	
Source	Squares	df	Mean Square	F Value	Prob > F	
Model	539.605	3	179.868	34.746	< 0.0001	significant
A-A	214.123	1	214.123	41.364	0.0002	
B-B	192.881	1	192.881	37.260	0.0003	
AB	132.601	1	132.601	25.615	0.001	
Pure Error	41.413	8	5.170			
Cor Total	581.018	11				

The Model F-value of 34.746 implies that the model is significant. All factors in the model are counted significant with respect to *"Prob > F"* values; therefore A (x_1), B (x_2), AB (x_1*x_2) are significant model terms.

Table 4.15– Statistical Parameters of the model for R_2

Std. Dev.	2.2752	R-Squared	0.929
Mean	42.442	Adj R-Squared	0.902
C.V. %	5.360	Pred R-Squared	0.839
PRESS	93.178	Adeq Precision	12.535

Adequacy of the model designed has been verified both by F–statistics in ANOVA and by the values of R–squared.

Table 4.16–Coefficients of factors in design model for R_2

	Coefficient		Standard	95% CI	95% CI
Factor	Estimate	df	Error	Low	High
Intercept	42.442	1	0.657	40.928	43.957
A-A	4.224	1	0.657	2.709	5.738
B-B	4.009	1	0.657	2.495	5.523
AB	3.324	1	0.657	1.809	4.838

Final model equation (4.2) is thereby;

$$R_2 = 42.44 + 4.22x_1 + 4.01x_2 + 3.32x_1x_2 \qquad (4.2)$$

All factors, temperature, time, have approximately equal influence on the response, R_2. In contrast to the model for R_1, the interactions have a marked effect; samples treated at higher temperature for longer durations prove to yield better results in the studied range. Normal probability plot of residuals in design for R_2 has been presented in the figure below (Fig. 4.27).

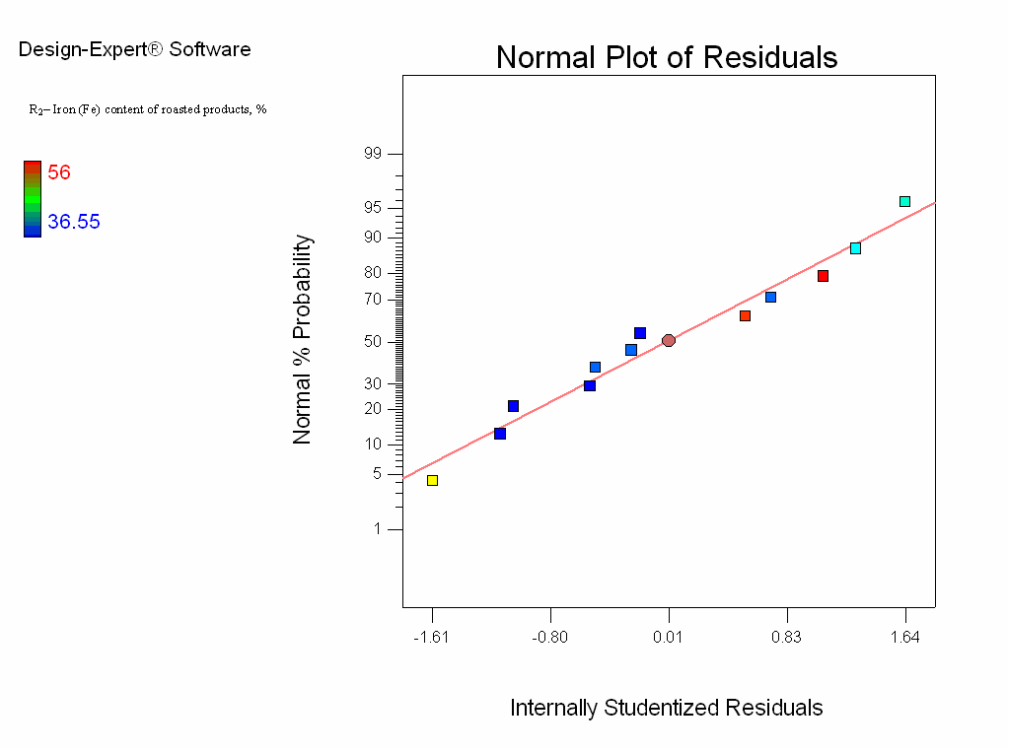

Fig.4.27– Normality Plot of Residuals in Model for (R_2)

Model validity in defining the Fe content of roasted products has been confirmed by plot of the values predicted by the model against the actual data (Fig. 4.28).

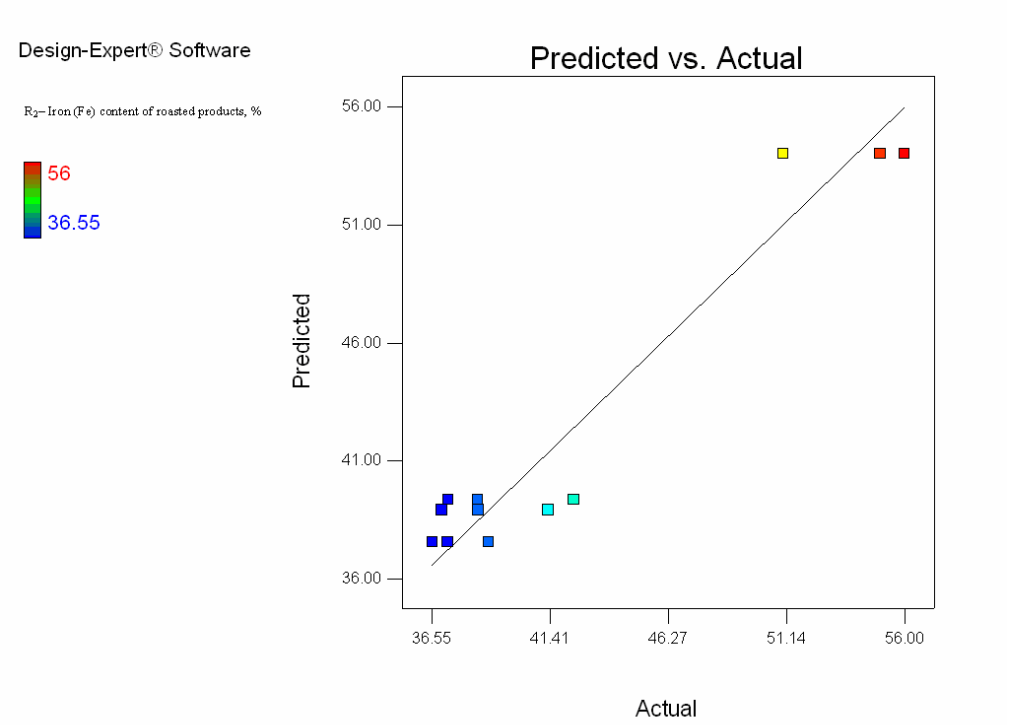

Fig.4.28– Comparison of model results with Actual data in design for (R_2)

Interaction of factors in model equation is represented (Fig. 4.29);

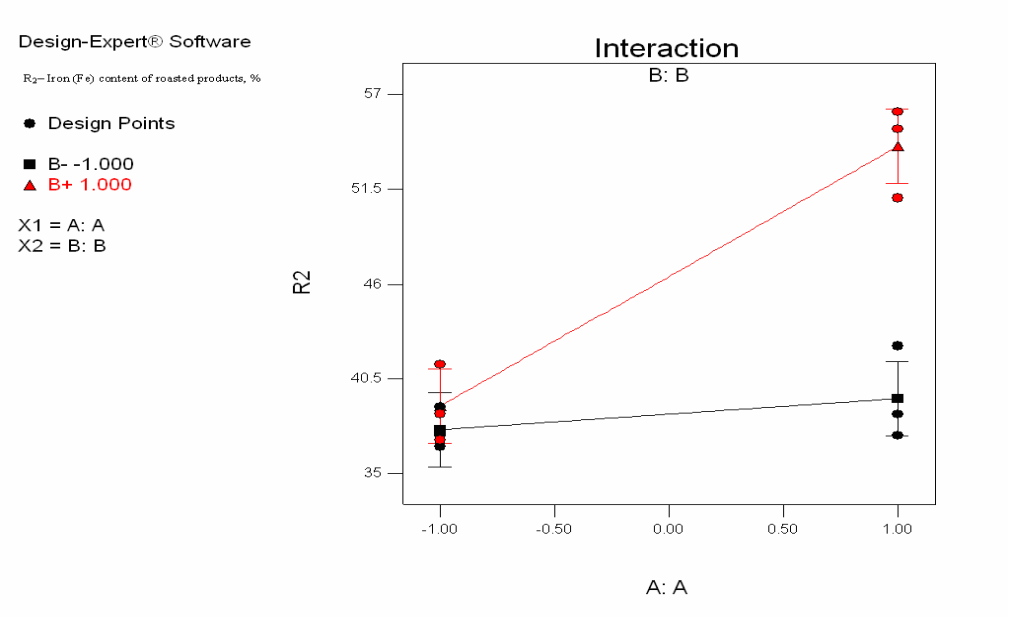

Fig.4.29– Interaction of temperature (x_1) and time (x_2) in model (R_2)

Two response items, namely weight loss of siderite ore and Fe content of roasted products, have been shown to differently defined based on results of factorial design, the weight of factors on the processes or intensity of each factor. Emphasizing on the fact that direct inference by the results of two models is not proper, it may be said that increasing all three factors as limiting the particle size in a range defined by replicates of experiments gives the optimum conditions in treatment of siderite ore. Nonetheless, verified by magnetic susceptibility analysis and XRD analysis as well, heating temperature is more influential on roasting process for the study. The fact has also been pointed out statistically. Relying on the results of modeling work and set of analyses it is concluded that the optimum conditions for the process is ensured at T= 560 ºC for t= 45 minutes.

4.8. Kinetics of Thermal Decomposition of Hekimhan–Deveci Siderite

Resulting characteristic TGA curve indicates that thermal decomposition of Hekimhan–Deveci siderite starts at around T= 465 ºC; the temperature range of thermal decomposition is T= 465 ºC– 550 ºC. Range of process of interest has been demonstrated by differential scanning calorimetry (DSC) [Fig. B.1] curve as well, the endothermic peak, maximum heat flow to the system, is confirmed to be at around T= 550 ºC.

Decomposing according to the reaction, Hekimhan–Deveci siderite ore undergoes oxidation reactions commencing at T= 560 ºC up to T= 650 ºC.

$$FeCO_3 \rightarrow FeO + CO_2 \qquad (4.3)$$

Subsequent to completion of intense decomposition of iron carbonate at around T= 550 °C, oxidation reactions take place in the system, under presence of air; possible set of reactions is as given below,

$$4FeO + O_2 \rightarrow 2\gamma\text{-}Fe_2O_3 \qquad (4.4)$$

$$6FeO + O_2 \rightarrow 2Fe_3O_4 \qquad (4.5)$$

$$4FeO + O_2 \rightarrow 2\alpha\text{-}Fe_2O_3 \qquad (4.6)$$

Kinetic models for solid state reactions (Table 4.17) have been tested for ore of interest by consideration of all factors stated. The criterion, in assessing the model validity with respect to recorded data, has been the consistency of graphical representation of data both for isothermal and nonisothermal runs. Thereby, *Avrami Erofe'ev*, *Power law*, and *Diffusion (2)* reaction models have been found to represent the thermal decomposition data obtained by experiments.

Results of kinetic parameter analyses by all four methods are given (Fig. 4.30–Fig. 4.36), examining data from isothermal and non-isothermal runs as discussed. Summary of parameter values obtained through analyses are included on the table (Table 4.17) for indicated reaction models.

Table 4.17– Kinetic Models for Solid State Reactions

Reaction Model	**f(x)**	**n** **(reaction order)**	**E (kJ/mol)**	**R^2**
1. Power Law	$(x)^{1/n}$			
		n= 1.0051	32.58	0.792
		n= 1.0437	30.85	0.787
		n=1.1911	25.30	0.763
2. Exponentional Law	In(x)			
3. Avrami Erofe'ev	$[-\ln(1-x)]^{1/n}$ n>1			
		n= 1.086	35.25	0.811
		n= 1.1215	33.71	0.807
		n= 1.2603	28.45	0.790
4. Prout-Tompkins	ln[x/(1-x)]			
5. One-dimensional Diffusion	x^2			
6. Two-dimensional Diffusion	(1-x)In(1-x)+x			
7. Jander Three-dimensional Diffusion	$[1-(1-x)^{1/3}]^2$		85.53	0.860
8. Ginstling-Brounshtein Three-dimensional Diffusion	$[1-(2x/3)]- (1-x)^{2/3}$		85.49	0.858
9. Geometric Models (contracting area)	$2[1-(1-x)^{1/2}]$			
10. Geometric Models (contracting volume)	$3[1-(1-x)^{1/3}]$			
11. Order of Reaction Models (n=1)	-ln(1-x)			
12. Order of Reaction Models (n=2)	$(1-x)^{-1}$			
13. Order of Reaction Models (n=3)	$(1-x)^{-2}$			

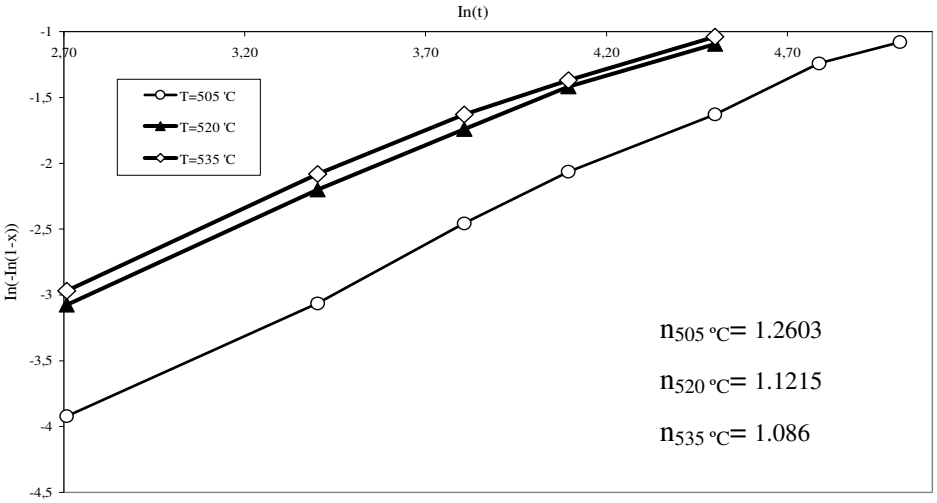

Fig.4.30- Fractional Conversion data evaluated by Avrami Erofe'ev Reaction Model vs. ln(t) for determination of Reaction Order (n) Values

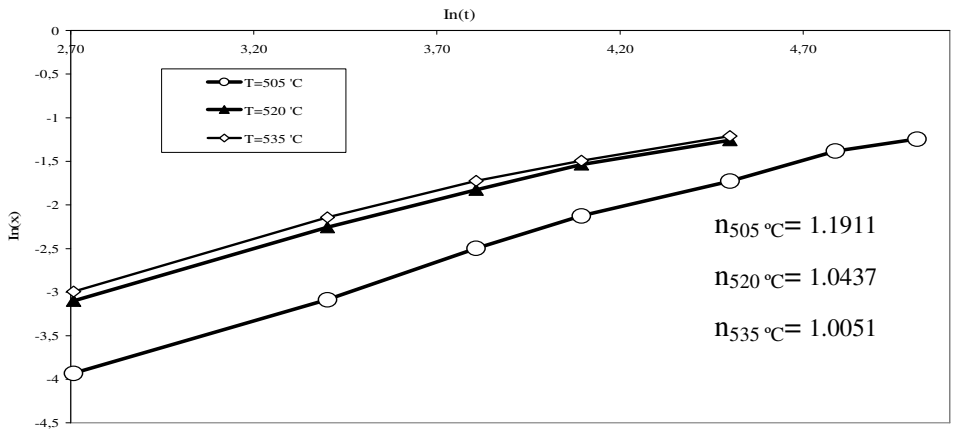

Fig.4.31 - Fractional Conversion data evaluated by Power Law Reaction Model vs. ln(t) for determination of Reaction Order (n)

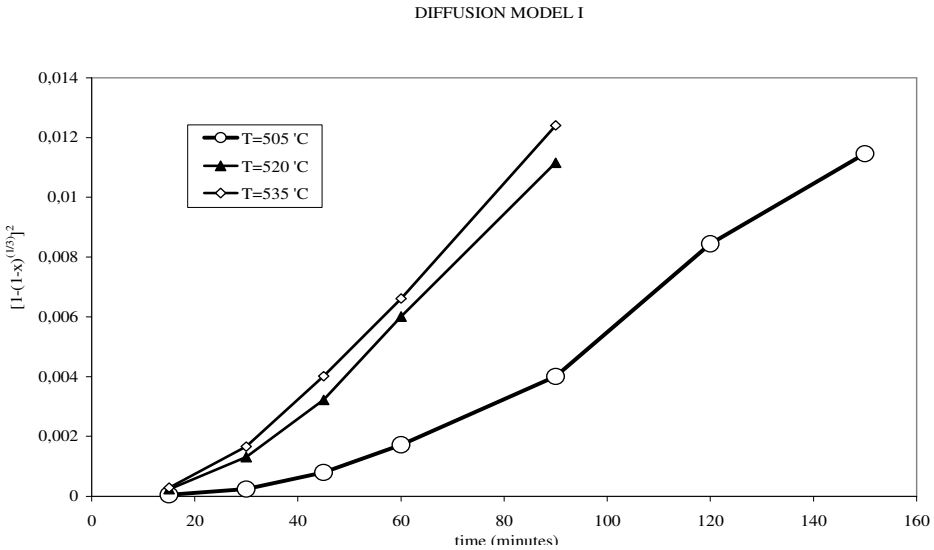

Fig.4.32 - Jander Three–dimensional Diffusion Model (Diffusion Model I) evaluated on basis of fractional conversion values *(x)* at different temperatures

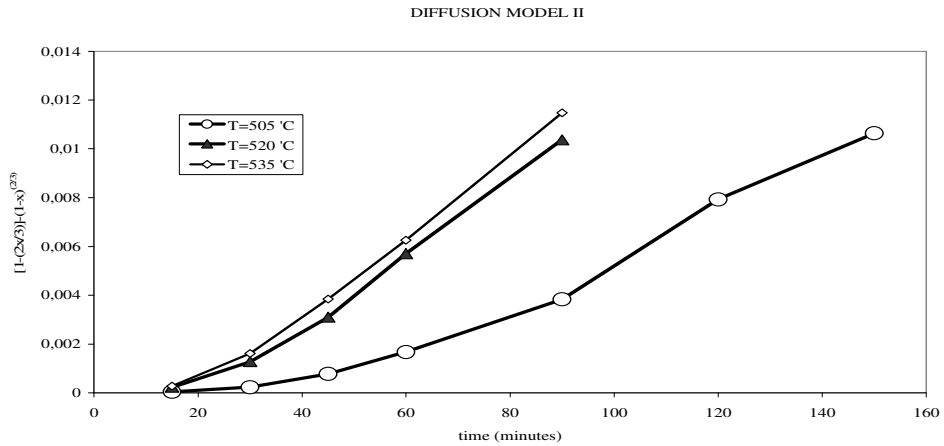

Fig.4.33- Ginstling– Brounshtein Three–dimensional Diffusion Model (Diffusion Model II) evaluated on basis of fractional conversion values *(x)* at different temperatures vs. Time [8th reaction model in table 4.17]

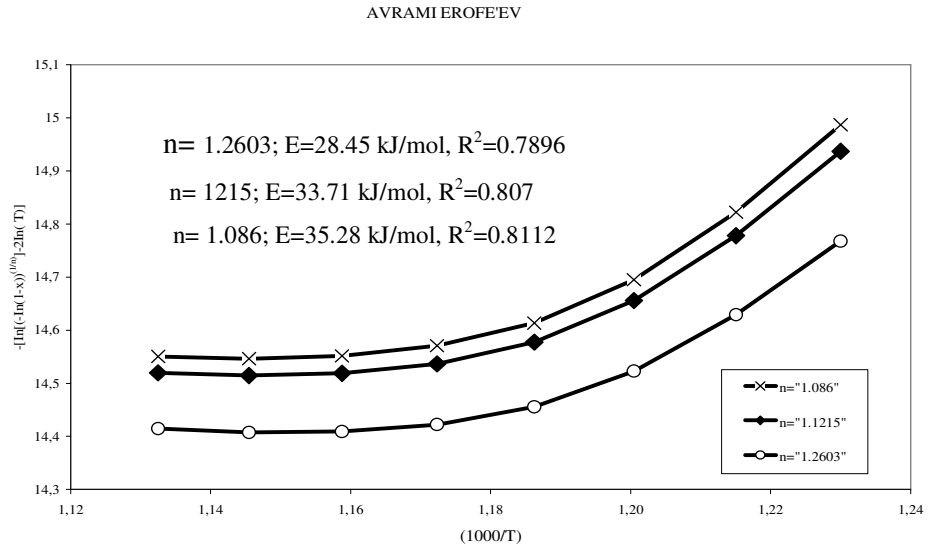

Fig.4.34 - Avrami Erofe'ev Reaction Model evaluated at different conversion values *(x)* at respective orders indicated vs. (1000/T)

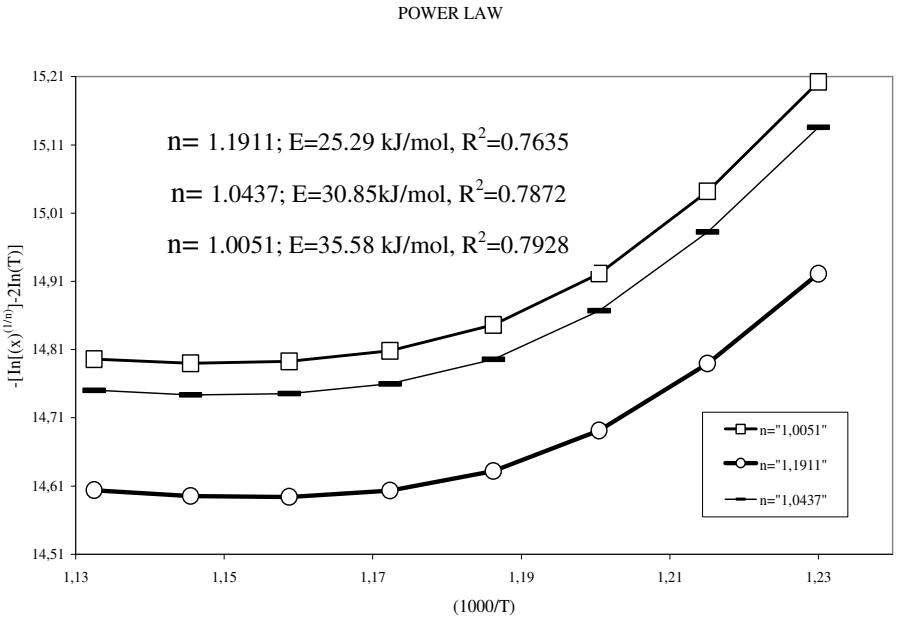

Fig.4.35 - Power Law Reaction Model evaluated at different conversion values *(x)* at respective orders indicated vs. (1000/T)

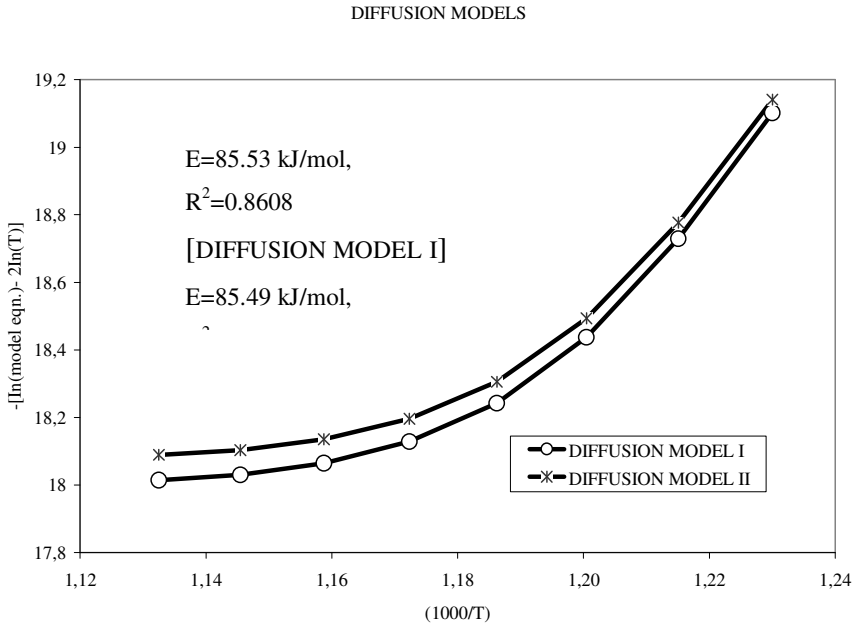

Fig.4.36– Diffusion Reaction Models evaluated at different conversion values *(x)* vs. (1000/T)

By use of Arrhenius equation in evaluating the data for isothermal runs, activation energy (E) values have been determined on basis of 7^{th} and 8^{th} reaction models in table 4.17. The figure (Fig. 4.37) below shows the determination of E by Arrhenius relation in terms of graphical representation.

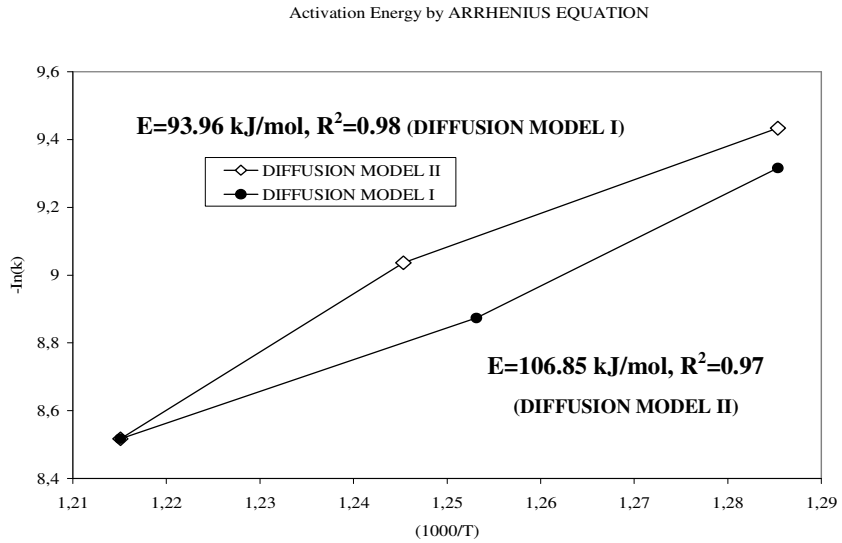

Fig.4.37 - Evaluation of results of heating experiments, using *Ink* values obtained by graphs of diffusion reaction models (Fig. 4.32; Fig. 4.33), by Arrhenius Relation

The reaction models being in origin sigmoid rate equation (3rd reaction model; table 4.17), acceleratory rate equation (1st reaction model; table 4.17), and deceleratory rate equations (7th& 8th reaction models; table 4.17) respectively diffusion reaction models have better fit. Therefore, diffusion reaction models, specifically 3–D, are concluded to be models defining the thermal decomposition kinetics among all solid state reaction models.

In agreement with the outcome of the isothermal runs, adequacy of the diffusion reaction models in representing the data has been confirmed by non–isothermal runs. The best degree of fit value (R^2) belongs to 3–D diffusion reaction models.

Examination of results in terms of degree of fit brings about the conclusion that three–dimensional diffusion models are the reaction models representing the thermal decomposition kinetics of Hekimhan–Deveci siderite ore. In contrast to the study [Gokarn et al., 1990], the experimental data obtained on Hekimhan–Deveci siderite ore proves to have a better fit to *3–D diffusion models* rather than *Avrami–Erofe'ev model*.

Type of ore treated reports to be the reason explaining the difference in results; furthermore consistency of diffusion models in describing the kinetics have also been verified by influence of parameters such as chemical composition or temperature range operated.

Reaction models determined for the process are;

Jander Three–dimensional Diffusion Model (Diffusion Model I): $f(x) = [1-(1-x)^{1/3}]^2$

Ginstling– Brounshtein Three–dimensional Diffusion Model (Diffusion Model II):

$$f(x) = [1-(2x/3)]-(1-x)^{2/3}$$

Evaluation of model equations via *Arrhenius relation* gives comparable results for activation energy, indicative of the fact that the reaction is diffusion controlled in set conditions (Table 4.18).

Table 4.18– Kinetic Parameters of Diffusion Reaction Models

	ISOTHERMAL RUNS	NON–ISOTHERMAL RUNS
	ACTIVATION ENERGY (E) (kJ/mol)	
DIFFUSION MODEL I	85.53	93.96
DIFFUSION MODEL II	85.49	106.85

Consequently it is seen that not only the results are precise within identical runs, i.*e. isothermal or non–isothermal runs*, but also consistency is observed among different runs, as expected. Anyhow, under any circumstances, influence of experimental conditions and of the studied range as well as the characteristics of material must be accounted in analyzing the results.

Hekimhan–Deveci siderite ore has a characteristic thermal curve, on which intense heat flow to the system, corresponding parts of endothermic reactions, is required in the first place. Exothermic reactions take place following the thermal decomposition, generating heat through the system. In accordance to the solid state reaction models which are classified into subclasses, with respect to the mechanism, that either the rate is acceleratory or deceleratory, the present study has concluded that thermal decomposition is represented by diffusion reaction models, particularly three–dimensional diffusion models.

Models of three–dimensional diffusion both give identical results by different methods; reliability of findings is thereby verified. On the other hand, it is noteworthy to emphasize that the decomposition of siderite is influenced by conditions of treatment, and also by the substitutions in chemical composition.

CHAPTER 5

CONCLUSIONS AND RECOMMENDATIONS

Thermal characteristics of the Hekimhan–Deveci siderite ore have been studied in detail as well as the physical characteristics. The following conclusions can be drawn on basis of thesis study, with remarks for further studies;

- Investigation of heating characteristics of materials may be the key point in success of probable concentration methods. The sample studied did not respond to microwave heating; however,g conventional heating experiments yielded phases which could be concentrated by magnetic separation, particularly by low–intensity magnetic separation.

- Heating temperature, time of heating, and particle size have been identified as the factors effective on heat treatment of the ore. Heating temperature is the dominant factor on the weight loss of sample by heating, influencing process positively. In addition, the results of heating experiments have shown that increase of temperature, i.e T= 605 °C, resulted in attaining the expected weight loss of sample in shorter time period. Checking the results on magnetic susceptibility basis, there noted slight difference between the values, χ_g (T= 605 °C, t= 30 minutes) = 20758.13 m^3/kg, χ_g (T= 560 °C, t= 45 minutes) = 20530.02 m^3/kg.

Therefore it has been concluded that operating at T= 605 °C is not essential, considering the economics on one hand as well. The optimum experimental conditions for roasting, resulting in formation of high magnetic susceptibility phases, have been found 560 °C, 45 minutes as heating temperature and time of heating respectively.

- The increase in iron grade, from 38 % Fe to 54.5 % Fe, has been found to be influenced positively by heating temperature and time of heating, suggesting that increasing both factors in view of material characteristics may yield better results.

- Three–dimensional diffusion models, particularly Jander and Ginstling–Brounshtein, are the reaction models representing the thermal decomposition kinetics of Hekimhan–Deveci siderite ore. Activation energies are E= 85.53 kJ/mol, E= 85.49 kJ/mol for models respectively. In the sense that activation energy corresponds to energy input requirement to the system, heat input requirement may be interpreted by activation energy values on kcal/ton of ore basis, E= $1.762*10^5$ kcal/ton and E= $1.761*10^5$ kcal/ton respectively.

- The results of the thesis study have proven effective in improving set of conditions implied for treatment of Hekimhan–Deveci siderite ore. Indicated optimum conditions, in literature, for treatment of Hekimhan–Deveci siderite ore were T= 800 °C for t= 15 minutes, which resulted in a final iron grade of Fe= 59% at most. Thus, thesis study has not only enhanced improvement of conditions, with an approximate final iron grade of Fe= 55%, but also provided it viable to characterize the final products in view of magnetic properties, giving way to alternate use of products such as direct feed material to smelter rather than being added in fixed proportions.

- Material characteristics of Hekimhan–Deveci siderite ore, such as crystal structure, porosity, should be analyzed broadly to draw reasonable explanations for differences in results with respect to microwave heating and kinetic model from literature. Analyzing both siderite samples with fine grains and coarse grains under same conditions may enhance sought explanations. Incidentally quantifying dielectric properties of the material may provide reasonings as for the relation between crystal structure and microwave heating, if any.

REFERENCES

Al-Harahsheh M., Kingman S.W., Microwave-Assisted Leaching–a Review, Hydrometallurgy (73) 2004, 189–203

Anonim, T.C. Başbakanlık Devlet Planlama Teşkilatı, "Sekizinci Beş Yıllık Kalkınma Planı", Madencilik Özel İhtisas Komisyonu, Metal Madenler Alt Komisyonu Demir Çalışma Grubu Raporu, (2001), Ankara

Atalay Ü., Uslu T., Arol A.I., Effect of Microwave Heating on Magnetic Separation of Pyrite, Colloids and Surfaces A: Physicochem. Eng. Aspects (225) 2003, 161–167

Atesok Gündüz, Dincer Hayrünnisa, Feasibility Studies for Calcination and Sintering of Hekimhan–Deveci Siderite Ores, 2000, I.T.U. Maden Fakültesi, Cevher ve Kömür Hazırlama Anabilim Dalı

Böhm A., Böhm B., Kogelbauer, Selective Magnetizing Flash Roasting of Carbonaceous Iron Ores – Mineral Products for Steel Production and Environmental Protection, International Mineral Processing Congress (IMPC), 2006, 2423–2428

Dhupe A.P., Gokarn A.N., Studies in the Thermal Decomposition of Natural Siderites in the Presence of Air, International Journal of Mineral Processing (28) 1990, 209–220

Frederichs T., von Dobeneck T., Bleil U., Dekkers M.J., Towards the Identification of Siderite, Rhodochrosite, and Vivianite in Sediments by their Low-Temperature Magnetic Properties, Physics and Chemistry of the Earth (28) 2003, 669–679

Gotor F.J., Macias M., Ortega A., Criado J.M., Comparative Study of the Kinetics of the Thermal Decomposition of Synthetic and Natural Siderite Samples, Phys Chem Minerals (27) 2000, 495–503

Güngör Alper, Grindability of Microwave-Heated Ores, MSc Thesis 1998, Middle East Technical University, Ankara

Huang J.H., Rowson N. A, Technical Note on Heating Characteristics and Decomposition of Pyrite and Marcasite in a Microwave Field, Minerals Engineering (14) 2001, 1113–1117

Hunt Christopher P., Moskowitz Bruce M., Banerjee Subir K., Magnetic Properties of Rocks and Minerals, Rock Physics and Phase Relations- A Handbook of Physical Constants, 1995, 189–203

Jackson K., Kingman S.W., Rowson N.A., Bradshaw S.M., Greenwood R., an Investigation into the Influence of Microwave Treatment on Mineral Ore Comminution, Powder Technology (146) 2004, 176–184

Jagtap S.B., Pande A.R., and Gokarn A.N., Kinetics of Thermal Decomposition of Siderite: Effect of Particle Size, International Journal of Mineral Processing (36) 1992, 113–124

Jones D.A.,. Lelyveld T.P, Mavrofidis S.D., Kingman S.W., Miles N.J., Microwave Heating Applications in Environmental Engineering—a Review, Resources, Conservation and Recycling (34) 2002, 75–90

Kingman S.W., Jackson K., Cumbane A., Bradshaw S.M., Rowson N.A., Greenwood R., Recent Developments in Microwave-Assisted Comminution, International Journal of Mineral Processing (74) 2004, 71–83

Kingman S.W., Rowson N.A., Microwave Treatment of Minerals-a Review, Minerals Engineering (11) 1998, 1081–1087

Lester E., Kingman S.W., the Effect of Microwave Pre-heating on Five Different Coals, Fuel (83) 2004, 1941–1947

Marland S., Han B., Rowson N.A., Merchant A.J., Microwave Embittlement and Desulphurization of Coal, Acta Montanistica Slovaca (3) 1998, 351–355

Meikap B.C., Purohit N.K, Mahadevan V., Effect of Microwave Pretreatment of Coal for Improvement of Rheological Characteristics of Coal–Water Slurries, Journal of Colloid and Interface Science (281) 2005, 225–235

Mookherji A., Mathur S.C., Magnetic Studies on Siderite ($FeCO_3$), Journal of the Physical Society of Japan (20) 1965, 1336–1339

Morar Roman, Iuga Alexandru, Cuglesan Ioan, Muntean Ovidiu, Dascalescu Lucian, Iron Ore Beneficiation Using Roll-Type High-Intensity Electric Field Separators, IEEE Transactions on Industry Applications (35) 1999, 218–224

Özbayoğlu G., Depci T., Improvement of Coal Grindability by Microwave Pretreatment, XXIII International Mineral Processing Congress 2006, 1177–1180

Pan Yongxin, Zhu Rixiang, Banerjee Subir K., Gill J., Williams Q., Rock Magnetic Properties related to Thermal Treatment of Siderite: Behavior and Interpretation, Journal of Geophysical Research (105) 2000, 783–794

Pan Yongxin, Zhu Rixiang, Low-Temperature Magnetic Behavior related to Thermal Alteration of Siderite, Geophysical Research Letters (29) 2002, 1–4

Teodorovich G. I., Authigenic Minerals in Sedimentary Rocks, USSR Academy of Sciences Press, 1961

Uslu T., Atalay U., Microwave Heating of Coal for Enhanced Magnetic Removal of Pyrite, Fuel Processing Technology (85) 2003, 21–29

Wang Yanmin, Forssberg Eric, Dry Comminution and Liberation with Microwave Assistance, Scandinavian Journal of Metallurgy (34) 2005, 57–63

Xia D. K., Pickles C. A., Microwave Caustic Leaching of Electric Arc Furnace Dust, Minerals Engineering (13) 2000, 79–94

Xiong Dahe, Liu Shuyi, Chen Jin, New Technology of Pulsating High Gradient Magnetic Separation, International Journal of Mineral Processing (54) 1998, 111–127

Yıldız Necati, Demir Raporu, TMMOB Maden Mühendisleri Odası, 2007 http://www.maden.org.tr, August 08, 2007

Znamenackova I., Mockovciakova A., Lovas M., Jakabsky S., Briancin J., Modification of Magnetic Properties of Siderite Ore by Microwave Energy, Separation and Purification Technology (43) 2005, 169–174

APPENDIX A

XRD ANALYSES & QUALITY CARDS OF MINERALS

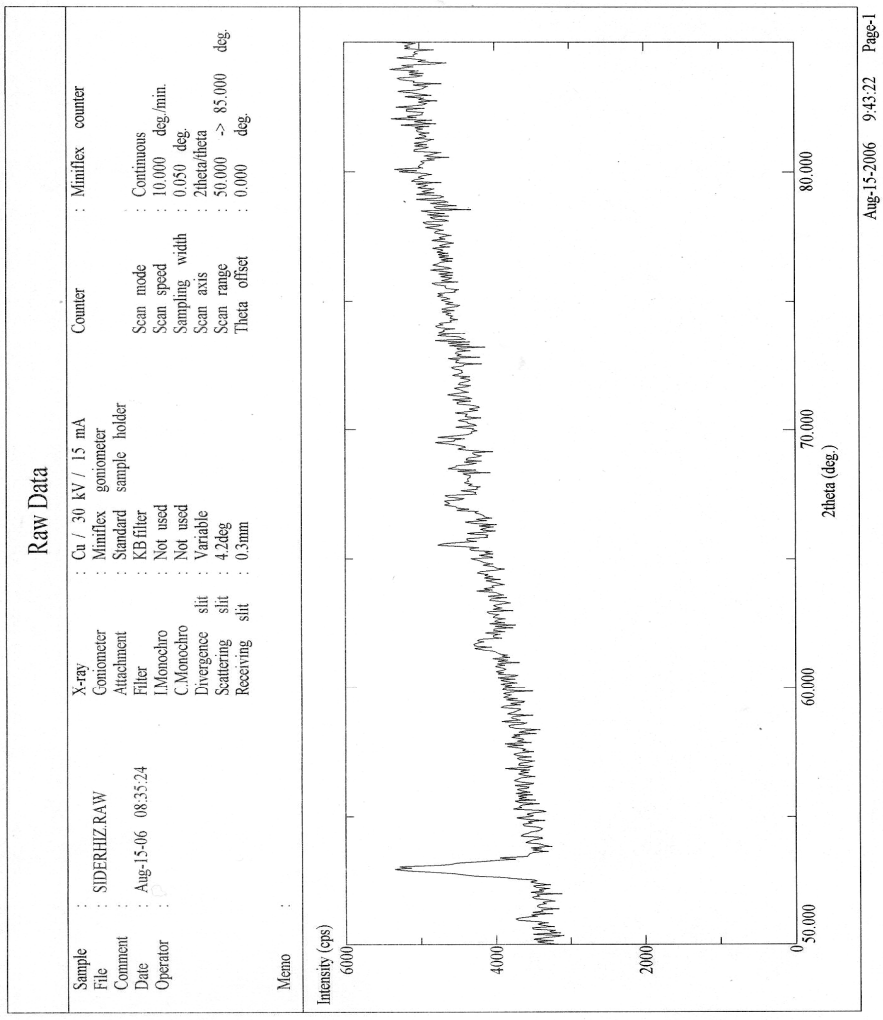

Fig.A.1– XRD Analysis of Run of Mine Sample *(1)*

Peak Search

Sample :
Comment :
Method : 2nd differential

File : SIDERHIZ.RAW
Memo :
Typical width : 0.150 deg.

Date : Aug-15-06 08:35:24
Min. height : 500.00 cps

Operator :

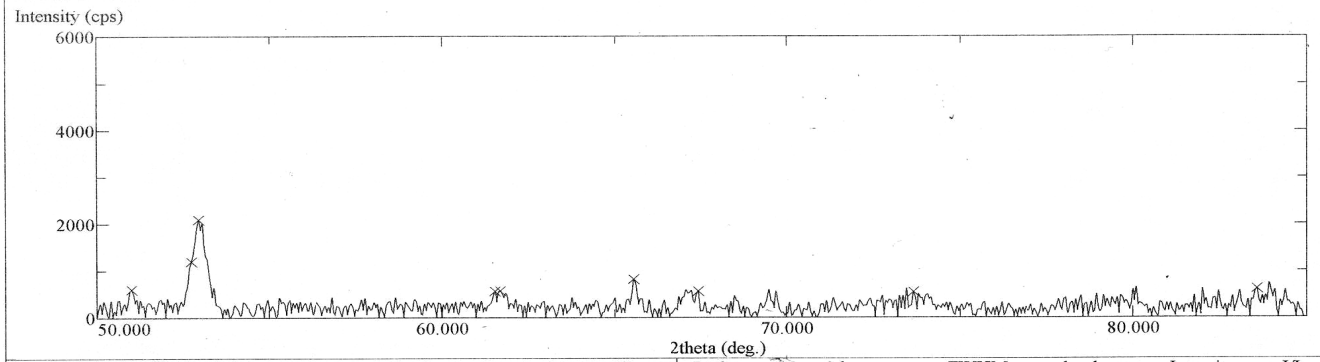

Peak no.	2theta	FWHM	d-value	Intensity	I/Io
1	51.000	0.176	1.7892	597	29
2	52.750	0.118	1.7339	1192	58
3	52.950	0.118	1.7278	2088	100
4	61.550	0.118	1.5054	561	27
5	61.700	0.176	1.5021	569	28
6	65.550	0.176	1.4229	809	39
7	67.450	0.118	1.3873	558	27
8	73.650	0.118	1.2851	537	26
9	83.600	0.118	1.1556	604	29

Peak no.	2theta	FWHM	d-value	Intensity	I/Io

Aug-15-2006 9:43:22 Page-2

Fig.A.2– XRD Analysis of Run of Mine Sample *(2)*

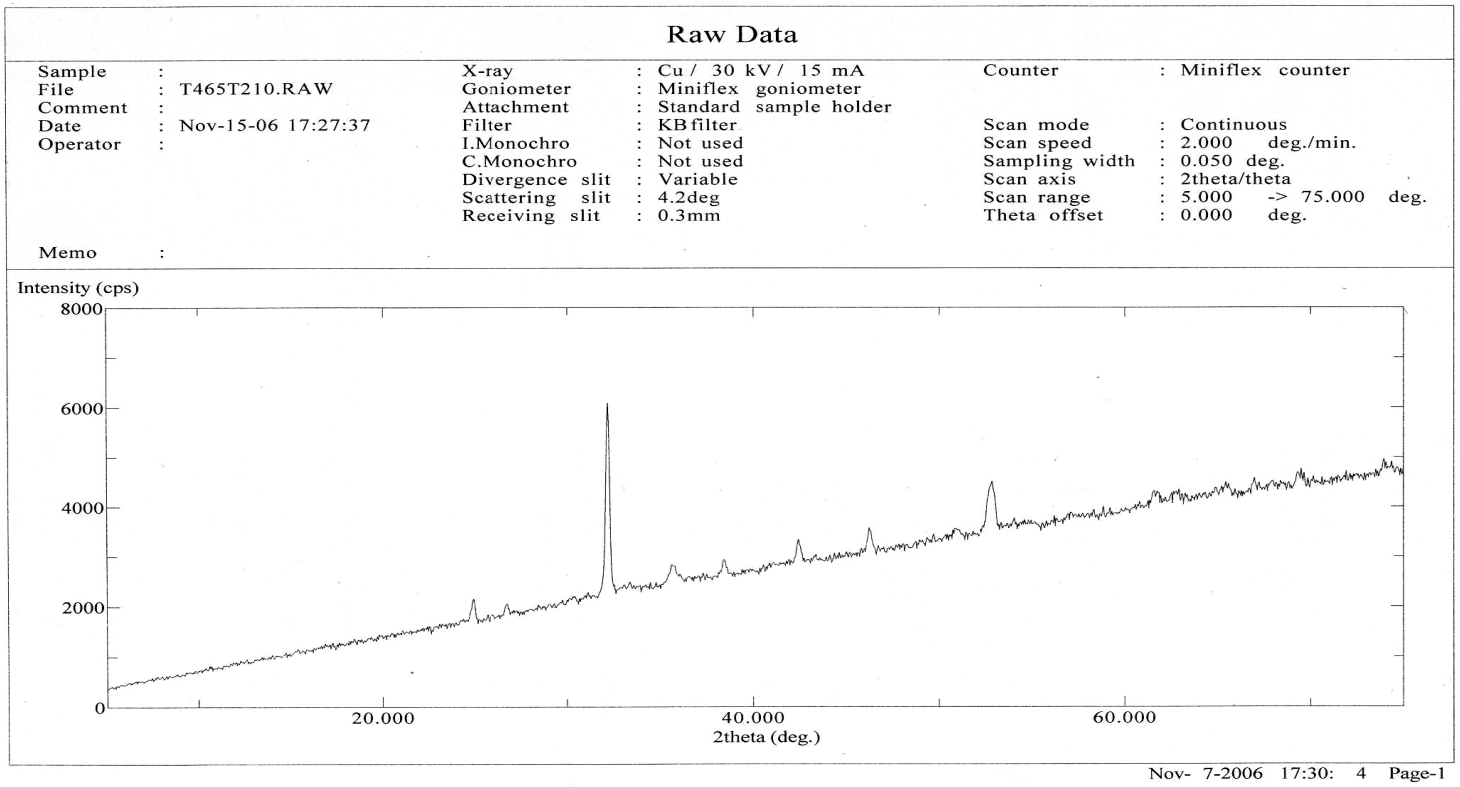

Fig.A.3– XRD Analysis of Samples heated at T= 465 ºC *(1)*

Peak Search

Sample :
Comment :
method : 2nd differential
File : T465T210.RAW Date : Nov-15-06 17:27:37 Operator :
Memo :
Typical width : 0.090 deg. Min. height : 200.00 cps

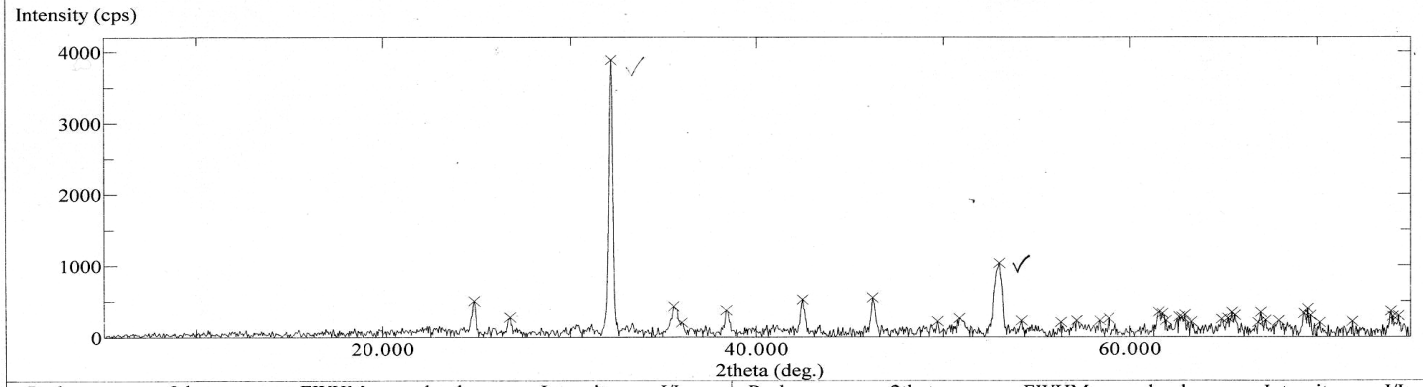

Peak no.	2theta	FWHM	d-value	Intensity	I/Io	Peak no.	2theta	FWHM	d-value	Intensity	I/Io
1	24.900	0.176	3.5728	504	13	16	58.850	0.059	1.5678	263	7
2	26.800	0.059	3.3237	281	8	17	61.550	0.176	1.5054	344	9
3	32.150	0.235	2.7818	3881	100	18	61.750	0.059	1.5010	328	9
4	35.600	0.176	2.5197	429	12	19	61.950	0.059	1.4966	231	6
5	36.050	0.118	2.4893	206	6	20	62.650	0.059	1.4816	283	8
6	38.400	0.235	2.3421	374	10	21	62.800	0.118	1.4784	280	8
7	42.450	0.176	2.1276	522	14	22	62.950	0.059	1.4752	310	8
8	46.250	0.059	1.9612	548	15	23	63.300	0.118	1.4679	213	6
9	49.700	*****	1.8329	219	6	24	64.900	0.118	1.4355	251	7
10	50.850	0.176	1.7941	262	7	25	65.250	0.059	1.4287	263	7
11	52.950	0.059	1.7278	1033	27	26	65.450	0.059	1.4248	345	9
12	54.150	0.059	1.6923	230	6	27	65.600	0.059	1.4219	306	8
13	56.250	0.059	1.6340	209	6	28	66.850	0.059	1.3983	203	6
14	57.100	0.176	1.6117	230	6	29	67.000	0.059	1.3955	347	9
15	58.350	0.118	1.5801	230	6	30	67.250	0.118	1.3910	236	7

Nov- 7-2006 17:29: 1 Page-1

Fig.A.4– XRD Analysis of Samples heated at T= 465 ºC *(2)*

Peak Search

Sample : File : T465T210.RAW Date : Nov-15-06 17:27:37 Operator :
Comment : Memo :
method : 2nd differential Typical width : 0.090 deg. Min. height : 200.00 cps

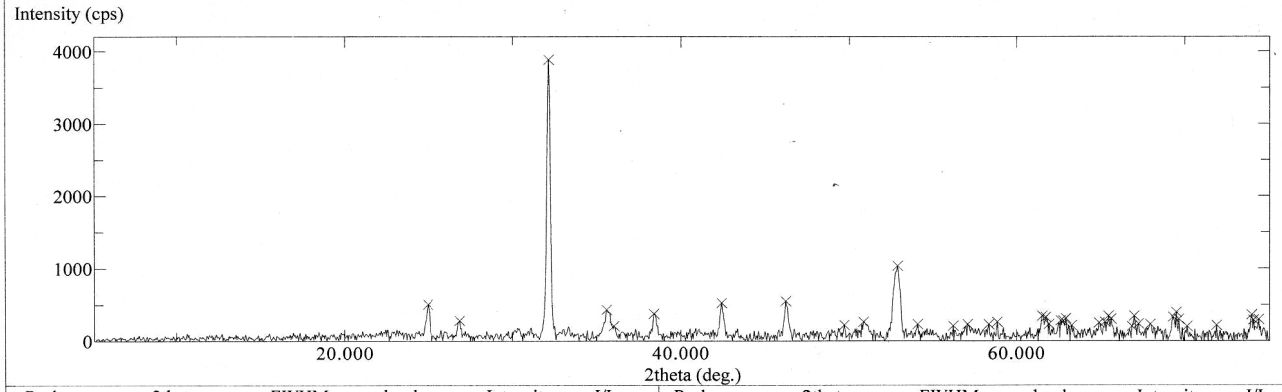

Peak no.	2theta	FWHM	d-value	Intensity	I/Io	Peak no.	2theta	FWHM	d-value	Intensity	I/Io
31	67.950	0.118	1.3783	231	6						
32	69.300	0.118	1.3547	332	9						
33	69.500	0.059	1.3513	396	11						
34	69.650	0.059	1.3488	301	8						
35	70.150	0.059	1.3404	201	6						
36	71.900	0.059	1.3120	217	6						
37	73.950	0.118	1.2806	361	10						
38	74.050	0.059	1.2791	288	8						
39	74.350	0.059	1.2747	298	8						

Nov- 7-2006 17:29: 1 Page-2

Fig.A.5– XRD Analysis of Samples heated at T= 465 ºC *(3)*

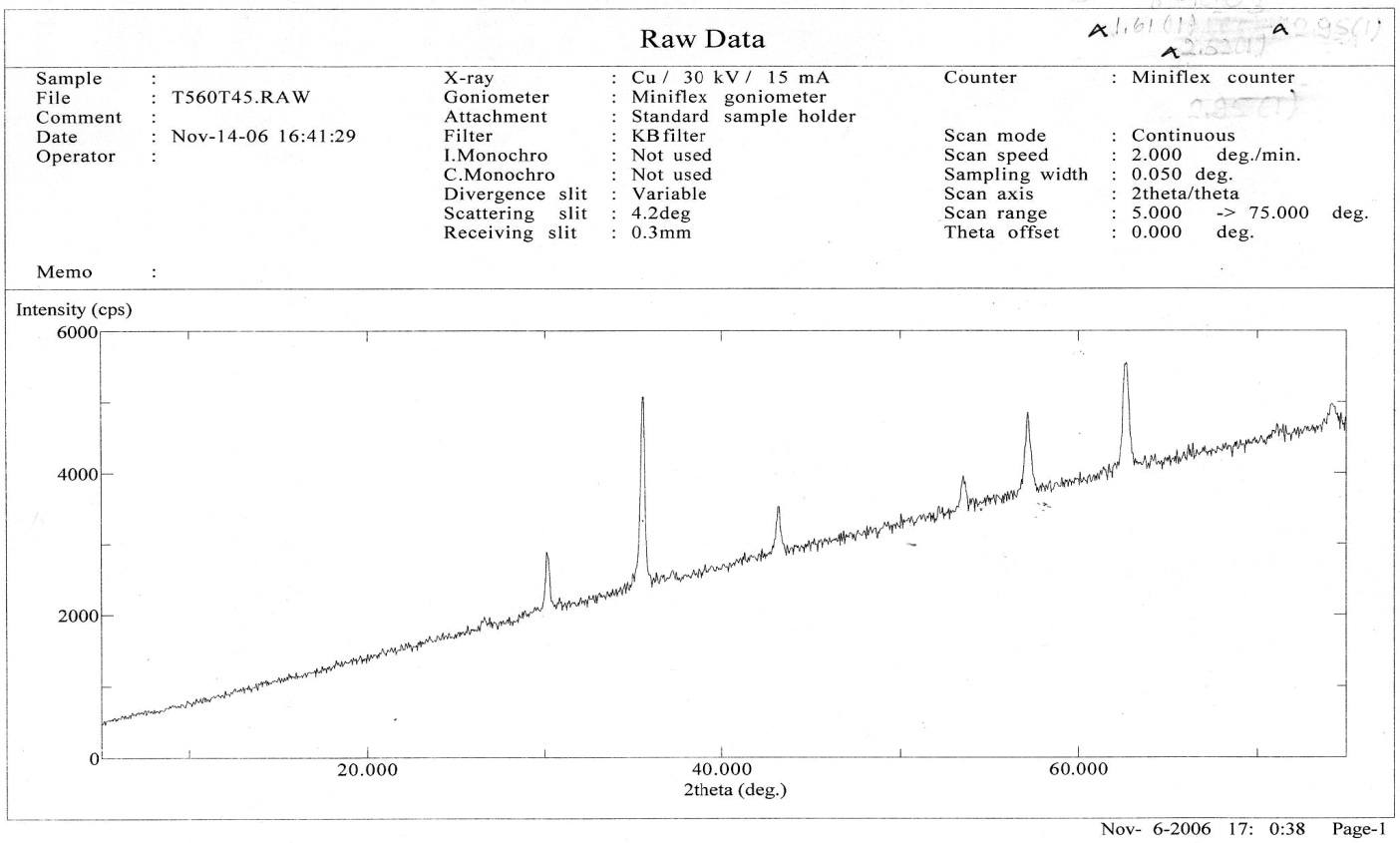

Fig.A.6– XRD Analysis of Samples heated at T= 560 ℃ *(1)*

Peak Search

Sample :
Comment :
method : 2nd differential
File : T560T45.RAW
Memo :
Typical width : 0.090 deg.
Date : Nov-14-06 16:41:29
Min. height : 150.00 cps
Operator :

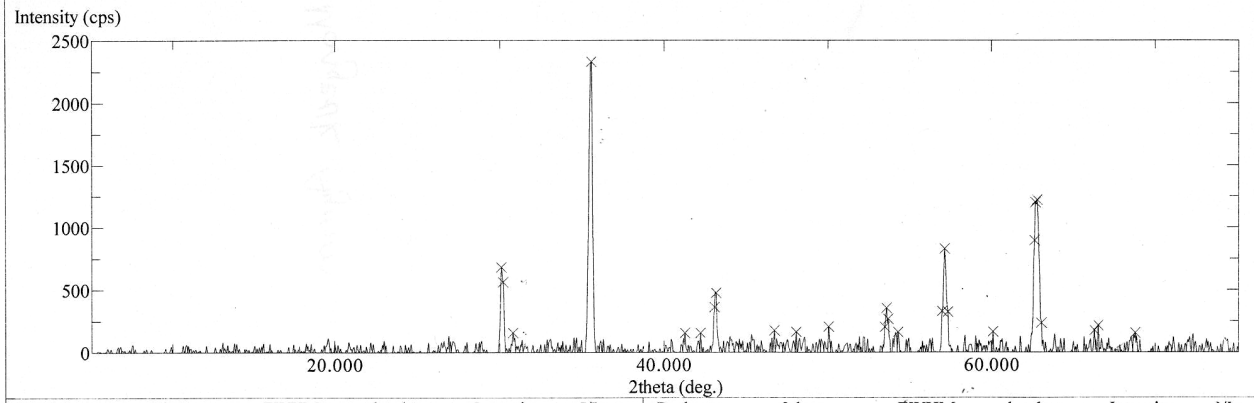

Peak no.	2theta	FWHM	d-value	Intensity	I/Io	Peak no.	2theta	FWHM	d-value	Intensity	I/Io
1	30.100	0.059	2.9664	682	30	16	56.950	0.059	1.6156	328	15
2	30.200	0.118	2.9568	562	25	17	57.100	0.176	1.6117	827	36
3	30.800	0.059	2.9005	155	7	18	57.300	0.059	1.6065	323	14
4	35.550	0.235	2.5231	2331	100	19	60.100	0.059	1.5382	164	8
5	41.300	0.059	2.1841	154	7	20	62.600	0.059	1.4826	894	39
6	42.250	0.059	2.1372	155	7	21	62.650	0.059	1.4816	1199	52
7	43.100	0.059	2.0970	361	16	22	62.750	0.235	1.4794	1220	53
8	43.200	0.118	2.0924	475	21	23	63.000	0.059	1.4742	234	11
9	46.800	0.059	1.9395	174	8	24	66.200	0.059	1.4105	175	8
10	48.100	0.059	1.8900	164	8	25	66.450	0.059	1.4058	214	10
11	50.050	0.118	1.8209	205	9	26	68.750	0.059	1.3642	155	7
12	53.450	0.059	1.7128	202	9						
13	53.550	0.059	1.7098	354	16						
14	53.650	0.059	1.7069	267	12						
15	54.250	0.118	1.6894	161	7						

Nov- 6-2006 17: 2: 2 Page-1

Fig.A.7– XRD Analysis of Samples heated at T= 560 ℃ *(2)*

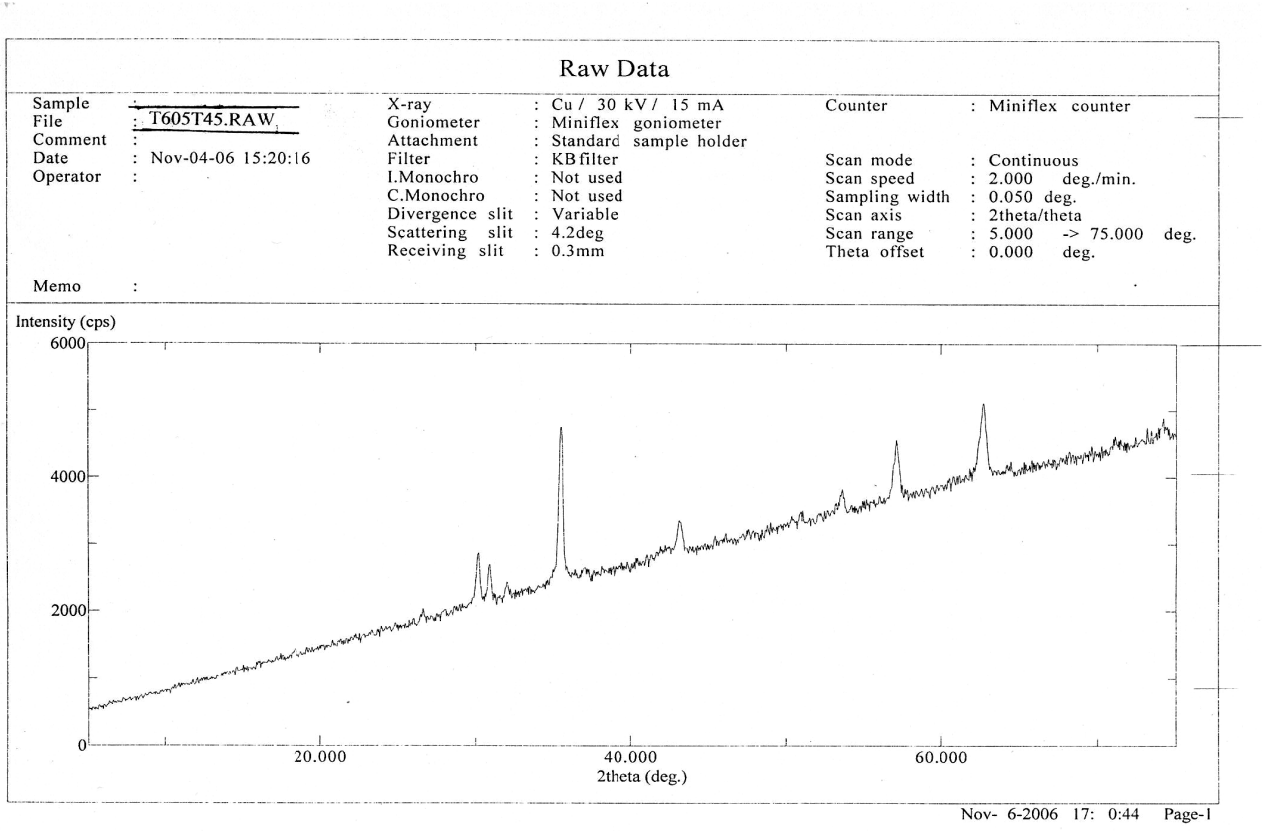

Fig.A.8– XRD Analysis of Samples heated at T= 605 ºC *(1)*

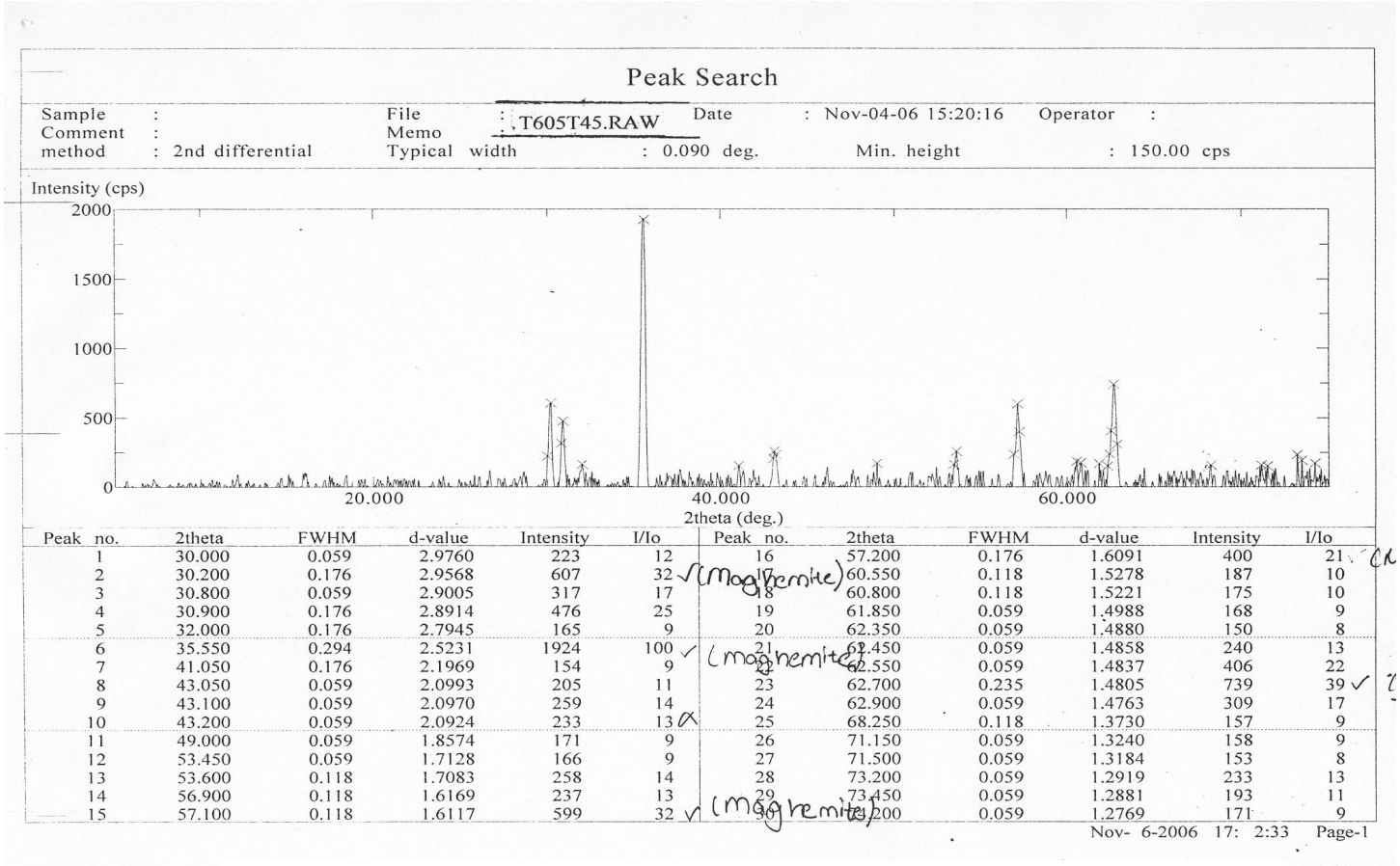

Peak no.	2theta	FWHM	d-value	Intensity	I/Io	Peak no.	2theta	FWHM	d-value	Intensity	I/Io
1	30.000	0.059	2.9760	223	12	16	57.200	0.176	1.6091	400	21
2	30.200	0.176	2.9568	607	32	17	60.550	0.118	1.5278	187	10
3	30.800	0.059	2.9005	317	17	18	60.800	0.118	1.5221	175	10
4	30.900	0.176	2.8914	476	25	19	61.850	0.059	1.4988	168	9
5	32.000	0.176	2.7945	165	9	20	62.350	0.059	1.4880	150	8
6	35.550	0.294	2.5231	1924	100	21	62.450	0.059	1.4858	240	13
7	41.050	0.176	2.1969	154	9	22	62.550	0.059	1.4837	406	22
8	43.050	0.059	2.0993	205	11	23	62.700	0.235	1.4805	739	39
9	43.100	0.059	2.0970	259	14	24	62.900	0.059	1.4763	309	17
10	43.200	0.059	2.0924	233	13	25	68.250	0.118	1.3730	157	9
11	49.000	0.059	1.8574	171	9	26	71.150	0.059	1.3240	158	9
12	53.450	0.059	1.7128	166	9	27	71.500	0.059	1.3184	153	8
13	53.600	0.118	1.7083	258	14	28	73.200	0.059	1.2919	233	13
14	56.900	0.118	1.6169	237	13	29	73.450	0.059	1.2881	193	11
15	57.100	0.118	1.6117	599	32	30	73.700	0.059	1.2769	171	9

Nov- 6-2006 17: 2:33 Page-1

Fig.A.9– XRD Analysis of Samples heated at T= 605 ºC *(2)*

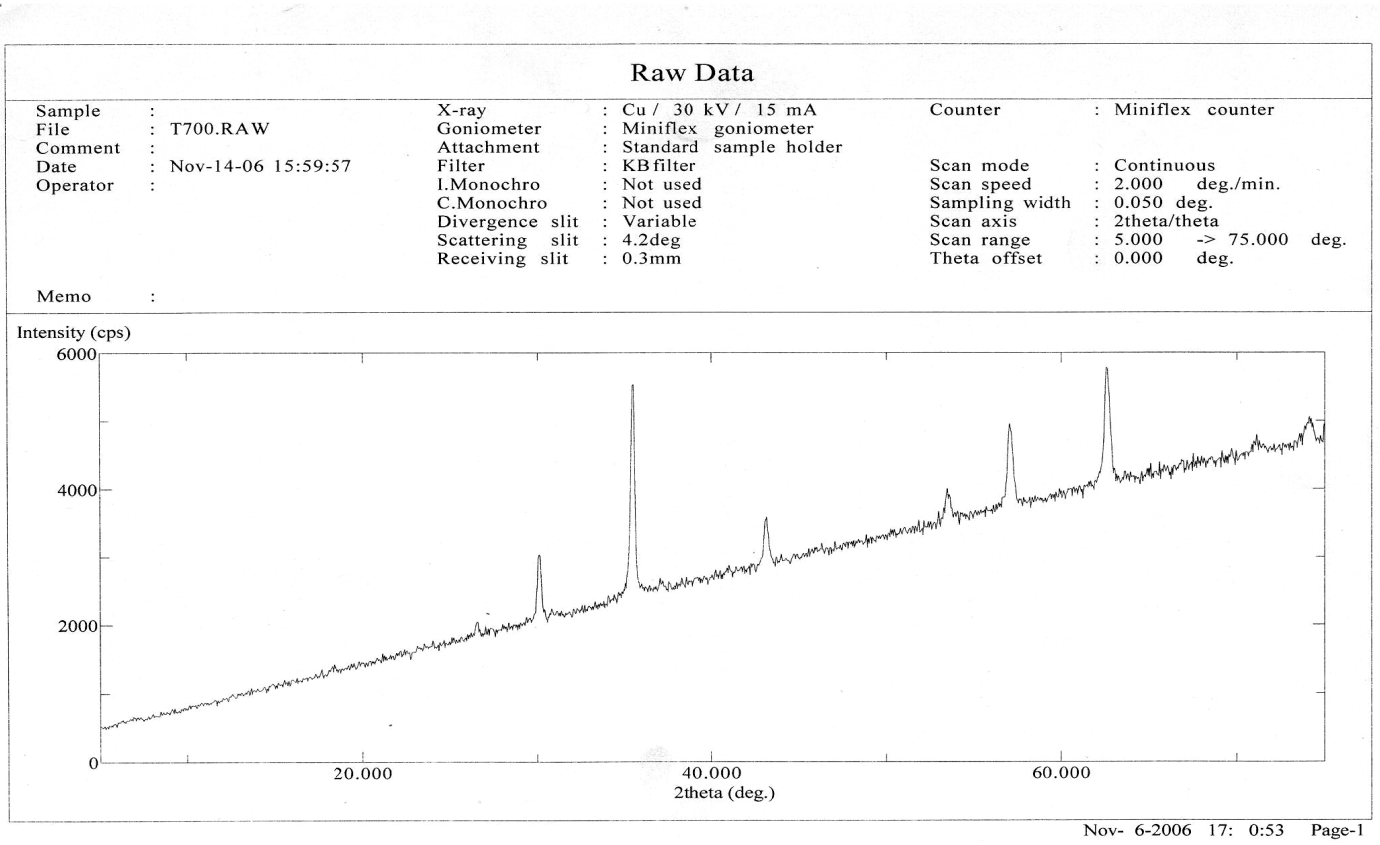

Fig.A.10– XRD Analysis of Samples heated at T= 700 ºC *(1)*

Peak Search

Sample :
Comment :
method : 2nd differential

File : T700.RAW
Memo :
Typical width : 0.090 deg.

Date : Nov-14-06 15:59:57
Min. height : 150.00 cps

Operator :

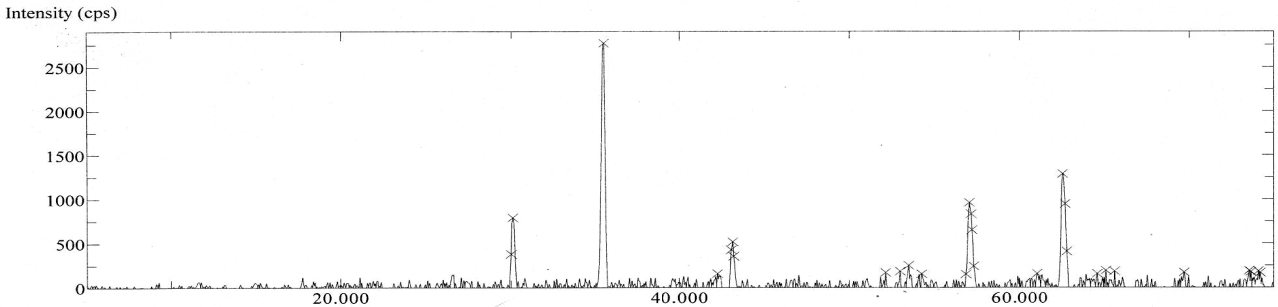

Peak no.	2theta	FWHM	d-value	Intensity	I/Io	Peak no.	2theta	FWHM	d-value	Intensity	I/Io
1	30.000	0.059	2.9760	379	14	16	57.250	0.059	1.6078	243	9
2	30.100	0.176	2.9664	790	29	17	61.050	0.176	1.5165	156	6
3	35.500	0.235	2.5266	2766	100	18	62.600	0.235	1.4826	1284	47 ✓
4	42.250	0.059	2.1372	157	6	19	62.750	0.059	1.4794	945	35 ✓
5	43.050	0.118	2.0993	427	16	20	62.850	0.059	1.4773	408	15
6	43.150	0.059	2.0947	517	19	21	64.650	0.118	1.4405	155	6
7	43.200	0.059	2.0924	354	13	22	65.150	0.059	1.4306	192	7
8	52.150	0.059	1.7524	169	7	23	65.650	0.059	1.4209	184	7
9	53.000	0.059	1.7263	183	7	24	69.700	0.118	1.3479	172	7
10	53.500	0.059	1.7113	251	10	25	73.550	0.059	1.2866	189	7
11	54.250	0.059	1.6894	152	6	26	73.650	0.059	1.2851	177	7
12	56.800	0.059	1.6195	152	6	27	74.100	0.059	1.2784	185	7
13	57.000	0.118	1.6143	960	35	28	74.200	0.059	1.2769	166	6
14	57.100	0.059	1.6117	832	31						
15	57.150	0.059	1.6104	652	24						

Nov- 6-2006 17: 3:26 Page-1

Fig.A.11– XRD Analysis of Samples heated at T= 700 °C *(2)*

Table A.1– XRD Quality Card of Siderite

Card No. : 29-0696 Quality : *

File Name :Inorganic
Formula :Fe C O3
Name :Siderite
Elements :Fe C O
System :Hexagonal
a:4.694 b:4.694 c:15.386
alpha:90.000 beta:90.000 gamma:120.000
Lambda:1.54050 Target:Cu

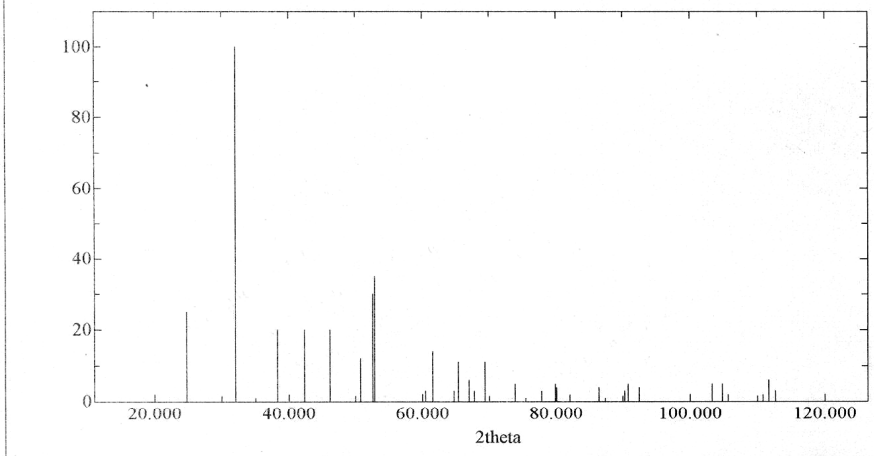

No.	2theta	d-value	Intensity	h	k	l	No.	2theta	d-value	Intensity	h	k	l
1	24.758	3.593	25	0	1	2	26	90.776	1.082	5	1	3	4
2	31.993	2.795	100	1	0	4	27	92.409	1.067	4	2	2	6
3	34.964	2.564	1	0	0	6	28	103.251	0.983	5	4	0	4
4	38.334	2.346	20	1	1	0	29	104.767	0.972	5	3	1	8
5	42.316	2.134	20	1	1	3	30	105.664	0.967	2	2	0	14
6	46.156	1.965	20	2	0	2	31	110.791	0.936	2	1	0	16
7	50.767	1.797	12	0	2	4	32	111.670	0.931	6	3	2	1
8	52.608	1.738	30	0	1	8	33	112.643	0.926	3	2	3	2
9	52.827	1.732	35	1	1	6							
10	60.494	1.529	3	2	1	1							
11	61.508	1.506	14	1	2	2							
12	64.724	1.439	3	1	0	10							
13	65.356	1.427	11	2	1	4							
14	66.926	1.397	6	2	0	8							
15	67.756	1.382	3	1	1	9							
16	69.296	1.355	11	3	0	0							
17	73.837	1.282	5	0	0	12							
18	75.418	1.259	1	2	1	7							
19	77.776	1.227	3	0	2	10							
20	79.848	1.200	5	1	2	8							
21	80.048	1.198	4	3	0	6							
22	82.030	1.174	2	2	2	0							
23	86.381	1.125	4	1	1	12							
24	87.349	1.115	1	3	1	2							
25	90.221	1.087	3	2	1	10							

Aug-17-2006 14:18:54 Page-1

Table A.2– XRD Quality Card of Magnesite

Card No. : 86-2345 Quality : C

File Name :Inorganic
Formula :Mg (C O3)
Name :Magnesite
Elements :Mg C O
System :Hexagonal
a:4.639 b:4.639 c:15.065
alpha:90.000 beta:90.000 gamma:120.000
Lambda:1.54050 Target:Cu

Relative intensity

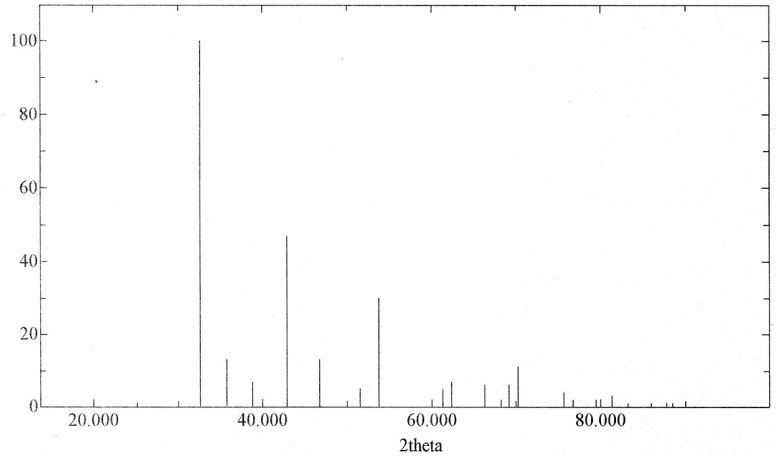

No.	2theta	d-value	Intensity	h	k	l	No.	2theta	d-value	Intensity	h	k	l
1	25.100	3.545	1	0	1	2							
2	32.560	2.748	100 ✓	1	0	4							
3	35.729	2.511	13	0	0	6							
4	38.790	2.319	7	1	1	0							
5	42.912	2.106	47 ✓	1	1	3							
6	46.763	1.941	13	2	0	2							
7	51.517	1.772	5	0	2	4							
8	53.755	1.704	30 ✓	1	1	6							
9	53.755	1.704	30 ✓	0	1	8							
10	61.304	1.511	5	2	1	1							
11	62.324	1.489	7	1	2	2							
12	66.314	1.408	6	2	1	4							
13	68.202	1.374	2	2	0	8							
14	69.147	1.357	6	1	1	9							
15	70.224	1.339	11	3	0	0							
16	75.692	1.255	4	0	0	12							
17	76.750	1.241	2	2	1	7							
18	79.449	1.205	2	0	2	10							
19	81.328	1.182	3	1	2	8							
20	81.328	1.182	3	3	0	6							
21	83.235	1.160	1	2	2	0							
22	85.942	1.130	1	2	2	3							
23	87.761	1.111	1	1	3	1							
24	88.477	1.104	1	1	1	12							

Aug-17-2006 14:33: 4 Page-1

Table A.3– XRD Quality Card of Ankerite

Card No. : 84-2067 Quality : C

File Name :Inorganic
Formula :Ca Mg0.27 Fe0.73 (C O3)2
Name :Ankerite
Elements :Ca Mg Fe C O
System :Hexagonal
a:4.831 b:4.831 c:16.166
alpha:90.000 beta:90.000 gamma:120.000
Lambda:1.54050 Target:Cu

Relative intensity

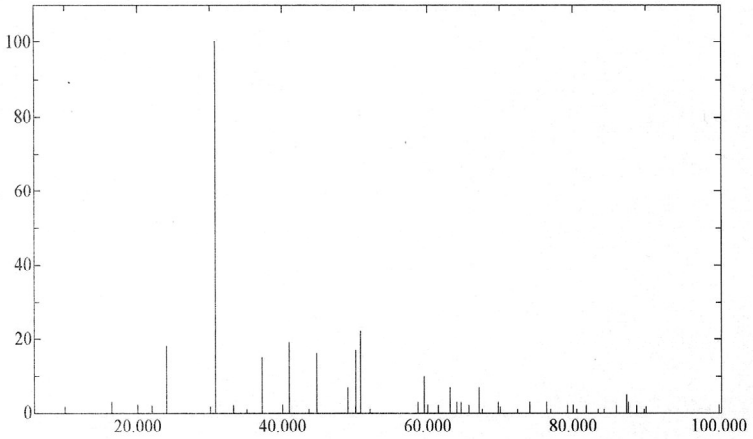

No.	2theta	d-value	Intensity	h	k	l	No.	2theta	d-value	Intensity	h	k	l
1	16.436	5.389	3	0	0	3	26	72.359	1.305	1	1	2	-7
2	21.924	4.050	2	1	0	1	27	74.047	1.279	3	0	2	10
3	23.928	3.716	18	0	1	2	28	76.411	1.245	3	2	1	-8
4	30.731	2.907	100 ✓	1	0	4	29	76.909	1.239	1	0	3	6
5	33.222	2.694	2	0	0	6	30	79.245	1.208	2	2	2	0
6	35.044	2.558	1	0	1	5	31	80.507	1.192	1	1	0	13
7	37.189	2.416	15	1	1	0	32	81.786	1.177	2	1	1	-12
8	40.906	2.204	19 ✓	1	1	-3	33	83.438	1.157	1	3	1	-1
9	43.587	2.075	1	0	2	1	34	84.223	1.149	1	1	3	-2
10	44.708	2.025	16	2	0	2	35	85.900	1.130	2	1	2	-10
11	48.988	1.858	7	0	2	4	36	87.354	1.115	5	1	3	4
12	50.085	1.820	17	0	1	8	37	87.573	1.113	3	0	1	14
13	50.713	1.799	22 ✓	1	1	-6	38	88.673	1.102	2	2	2	-6
14	52.022	1.756	1	2	0	5	39	89.696	1.092	1	3	1	5
15	58.602	1.574	3	2	1	1							
16	59.512	1.552	10	2	1	-2							
17	59.512	1.552	10	0	2	7							
18	61.432	1.508	2	1	0	10							
19	63.072	1.473	7	1	2	-4							
20	64.005	1.453	3	2	0	8							
21	64.602	1.441	3	1	1	-9							
22	65.669	1.421	2	2	1	-5							
23	67.048	1.395	7	3	0	0							
24	67.489	1.387	1	0	1	11							
25	69.744	1.347	3	0	0	12							

Aug-17-2006 14:39:17 Page-1

Table A.4– XRD Quality Card of Dolomite

Card No. : 75-1758 Quality : C

File Name :Inorganic
Formula :Ca Mg(C O3)2
Name :Dolomite
Elements :Ca Mg C O
System :Hexagonal
a:4.808 b:4.808 c:16.022
alpha:90.000 beta:90.000 gamma:120.000
Lambda:1.54050 Target:Cu

Relative intensity

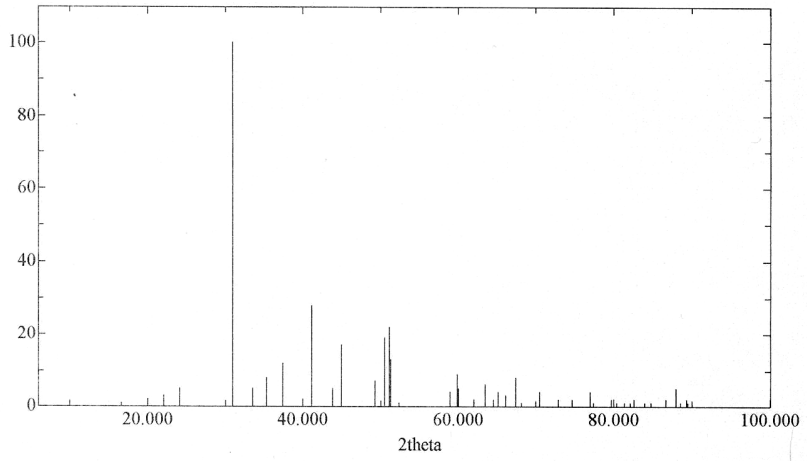

No.	2theta	d-value	Intensity	h	k	l	No.	2theta	d-value	Intensity	h	k	l
1	16.585	5.341	1	0	0	3	26	69.974	1.343	1	3	0	3
2	22.037	4.030	3	1	0	1	27	70.465	1.335	4	0	0	12
3	24.067	3.695	5	0	1	2	28	72.877	1.297	2	1	2	-7
4	30.951	2.887	100	1	0	4	29	74.692	1.270	2	0	2	10
5	33.530	2.670	5	0	0	6	30	76.991	1.237	4	2	1	-8
6	35.313	2.539	8	0	1	5	31	77.429	1.232	1	0	3	6
7	37.375	2.404	12	1	1	0	32	79.704	1.202	2	2	2	0
8	41.142	2.192	28	1	1	-3	33	80.390	1.193	1	2	0	11
9	43.811	2.065	5	0	2	1	34	81.351	1.182	1	1	0	13
10	44.947	2.015	17	2	0	2	35	82.118	1.173	1	2	2	-3
11	49.286	1.847	7	0	2	4	36	82.584	1.167	2	1	1	-12
12	50.526	1.805	19	0	1	8	37	83.934	1.152	1	1	3	1
13	51.077	1.787	22	1	1	-6	38	84.732	1.143	1	1	3	-2
14	51.274	1.780	13	0	0	9	39	86.635	1.123	2	1	2	-10
15	52.361	1.746	1	2	0	5	40	87.917	1.110	5	3	1	-4
16	58.915	1.566	4	1	2	-1	41	88.534	1.104	1	0	1	14
17	59.839	1.544	9	2	1	-2	42	89.293	1.096	2	2	2	-6
18	60.016	1.540	5	0	2	7	43	89.447	1.095	1	0	3	9
19	62.009	1.495	2	1	0	10							
20	63.451	1.465	6	1	2	-4							
21	64.506	1.443	2	2	0	8							
22	65.148	1.431	4	1	1	-9							
23	66.086	1.413	3	2	1	-5							
24	67.415	1.388	8	3	0	0							
25	68.145	1.375	1	0	1	11							

Aug-17-2006 13:34:25 Page-1

Table A.5– XRD Quality Card of Magnetite

Card No. : 72-2303 Quality : C

File Name :Inorganic
Formula :Fe3 O4
Name :Magnetite
Elements :Fe O
System :Cubic
a:8.400 b:8.400 c:8.400
alpha:90.000 beta:90.000 gamma:90.000
Lambda:1.54050 Target:Cu

Relative intensity

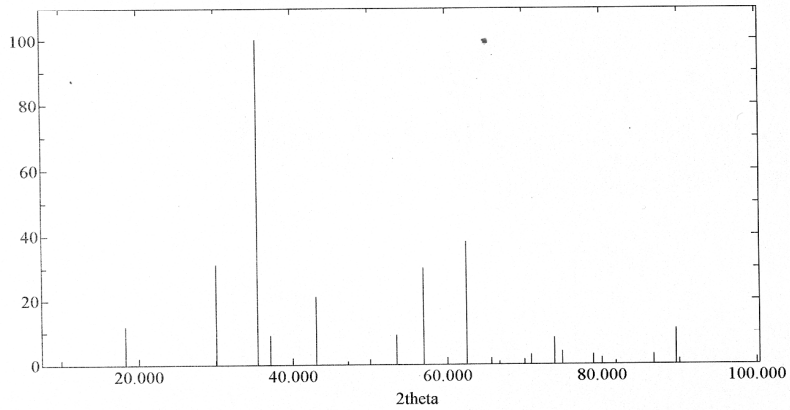

No.	2theta	d-value	Intensity	h	k	l	No.	2theta	d-value	Intensity	h	k	l
1	18.277	4.850	12	1	1	1							
2	30.064	2.970	31	2	2	0							
3	35.411	2.533	100	3	1	1							
4	37.041	2.425	9	2	2	2							
5	43.035	2.100	21	4	0	0							
6	47.118	1.927	1	3	3	1							
7	53.387	1.715	9	4	2	2							
8	56.910	1.617	30	5	1	1							
9	62.492	1.485	38	4	4	0							
10	65.706	1.420	2	5	3	1							
11	66.759	1.400	1	4	4	2							
12	70.892	1.328	3	6	2	0							
13	73.925	1.281	8	5	3	3							
14	74.925	1.266	4	6	2	2							
15	78.883	1.212	3	4	4	4							
16	81.815	1.176	1	5	5	1							
17	86.659	1.122	3	6	4	2							
18	89.551	1.094	11	7	3	1							

Aug-17-2006 14:38:59 Page-1

Table A.6– XRD Quality Card of Hematite

Card No. : 76-1821 Quality : C

File Name :Inorganic
Formula :Fe2 O3
Name :
Elements :Fe O
System :Hexagonal
a:5.560 b:5.560 c:22.550
alpha:90.000 beta:90.000 gamma:120.000
Lambda:1.54050 Target:Cu

Relative intensity

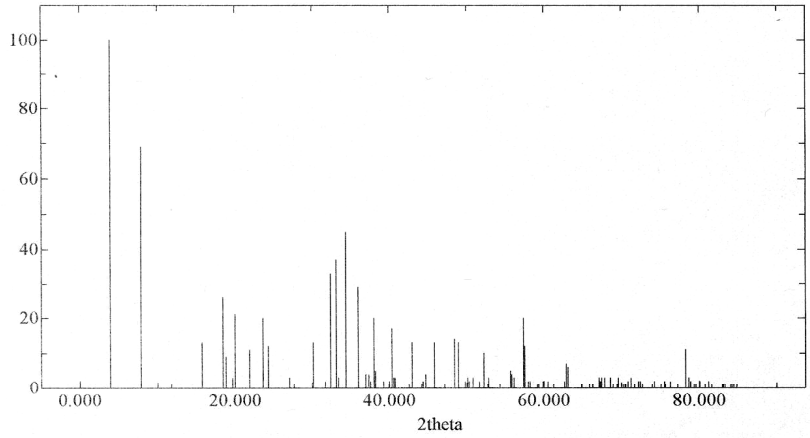

No.	2theta	d-value	Intensity	h	k	l	No.	2theta	d-value	Intensity	h	k	l
1	3.915	22.550	100	0	0	1	26	39.260	2.293	2	2	0	3
2	7.834	11.275	69	0	0	2	27	39.946	2.255	1	0	0	10
3	11.763	7.517	1	0	0	3	28	40.318	2.235	17	1	1	-6
4	15.706	5.637	13	0	0	4	29	40.552	2.223	3	0	1	9
5	18.410	4.815	26	1	0	0	30	40.716	2.214	3	0	2	4
6	18.829	4.709	9	1	0	1	31	42.528	2.124	1	2	0	5
7	19.667	4.510	3	0	0	5	32	42.935	2.105	13	1	1	-7
8	20.034	4.428	21	0	1	2	33	44.139	2.050	1	0	0	11
9	21.902	4.055	11	0	1	3	34	44.318	2.042	2	1	0	10
10	23.653	3.758	20	0	0	6	35	44.660	2.027	4	0	2	6
11	24.288	3.661	12	1	0	4	36	45.803	1.979	13	1	1	-8
12	27.066	3.292	3	0	1	5	37	47.082	1.928	1	0	2	7
13	27.667	3.221	1	0	0	7	38	48.396	1.879	14	0	0	12
14	30.138	2.963	13	1	0	6	39	48.894	1.861	13	1	1	-9
15	31.717	2.819	2	0	0	8	40	49.763	1.831	2	2	0	8
16	32.421	2.759	33	1	1	-1	41	50.077	1.820	3	1	2	0
17	33.162	2.699	37	1	1	-2	42	50.251	1.814	2	2	1	1
18	33.438	2.677	3	1	0	7	43	50.771	1.797	3	2	1	-2
19	34.364	2.607	45	1	1	3	44	51.629	1.769	2	1	2	3
20	35.989	2.493	29	1	1	-4	45	52.185	1.751	10	1	1	10
21	36.919	2.433	4	0	1	8	46	52.185	1.751	10	1	0	12
22	37.318	2.408	4	2	0	0	47	52.679	1.736	1	2	0	9
23	37.537	2.394	2	0	2	1	48	52.679	1.736	1	0	0	13
24	37.989	2.367	20	1	1	-5	49	52.813	1.732	3	1	2	-4
25	38.191	2.354	5	2	0	2	50	54.309	1.688	1	2	1	-5

Aug-17-2006 13:12:40 Page-1

Table A.7– XRD Quality Card of Iron

Card No. : 87-0721 Quality : C

File Name :Inorganic
Formula :Fe
Name :Iron
Elements :Fe
System :Cubic
a:2.866 b:2.866 c:2.866
Alpha:90.000 Beta:90.000 Gamma:90.000
Lambda:1.54050 Target:Cu

Relative intensity

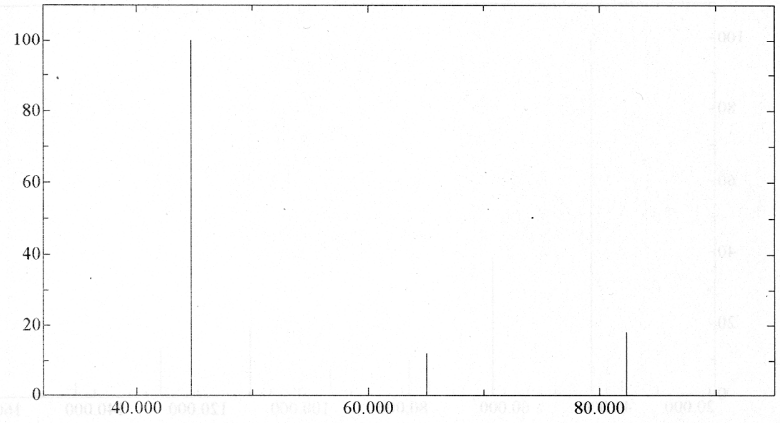

No.	2Theta	d-Value	Intensity	h	k	l	No.	2Theta	d-Value	Intensity	h	k	l
1	44.673	2.027	100	1	1	0							
2	65.023	1.433	12	2	0	0							
3	82.335	1.170	18	2	1	1							

Aug-15-2006 13:38:45 Page-1

Table A.8– XRD Quality Card of Quartz

Card No. : 47-0718 Quality : O

File Name :Inorganic
Formula :Si O2
Name :Silicon Oxide
Elements :Si O
System :Unknown
a:0.000 b:0.000 c:0.000
alpha:0.000 beta:0.000 gamma:0.000
Lambda:1.54050 Target:Cu

Relative intensity

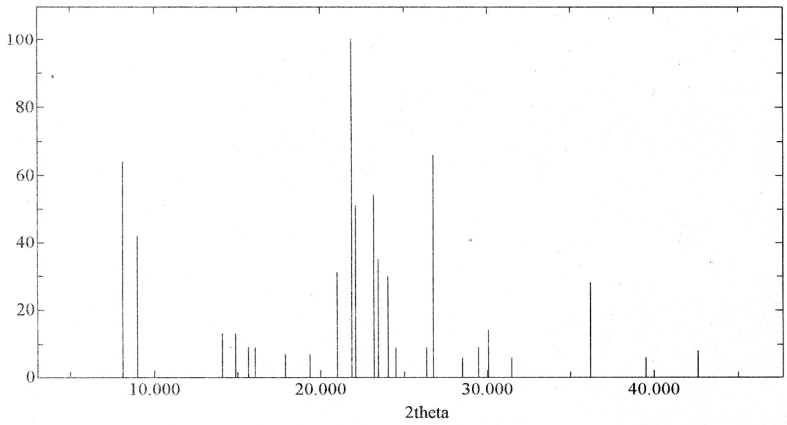

No.	2theta	d-value	Intensity	h	k	l	No.	2theta	d-value	Intensity	h	k	l
1	8.104	10.900	64 ✓	0	0	0							
2	8.988	9.830	42	0	0	0							
3	14.090	6.280	13	0	0	0							
4	14.876	5.950	13	0	0	0							
5	15.643	5.660	9	0	0	0							
6	16.042	5.520	9	0	0	0							
7	17.868	4.960	7	0	0	0							
8	19.364	4.580	7	0	0	0							
9	20.983	4.230	31	0	0	0							
10	21.873	4.060	100 ✓	0	0	0							
11	22.093	4.020	51	0	0	0							
12	23.204	3.830	54	0	0	0							
13	23.452	3.790	35	0	0	0							
14	24.031	3.700	30	0	0	0							
15	24.501	3.630	9	0	0	0							
16	26.345	3.380	9	0	0	0							
17	26.748	3.330	66 ✓	0	0	0							
18	28.492	3.130	6	0	0	0							
19	29.453	3.030	9	0	0	0							
20	30.062	2.970	14	0	0	0							
21	31.473	2.840	6	0	0	0							
22	36.189	2.480	28	0	0	0							
23	39.489	2.280	6	0	0	0							
24	42.609	2.120	8	0	0	0							

Aug-17-2006 13:25:14 Page-1

APPENDIX B

DSC ANALYSIS OF RUN OF MINE ORE

Orta Doğu Teknik Üniversitesi
Merkezi Laboratuvar, AR-GE Eğitim ve Ölçme Merkezi, 06531 Ankara
Tel : 0 312 210 64 21 Fax : 0 312 210 64 25
http://www.merkezilab.metu.edu.tr

ANALİZ SONUÇ RAPORU

Evrak Kayıt No: 1427	**Tarih :** 26 / 3 / 2007
Talep Eden: Dilek Alkaç	**Kurum:** ODTÜ

Sayın İlgili,
Laboratuvarımız tarafından yapılan analizler sonucunda numune/numunelerinizde aşağıda belirtilen sonuçlar elde edilmiştir.
Analiz sonuçları yalnızca aşağıda belirtilen numune/numuneler için geçerlidir.

ANALİZ SONUÇLARI

DSC sonucu ektedir.

Ekler: 1 Sayfa DSC sonucu.

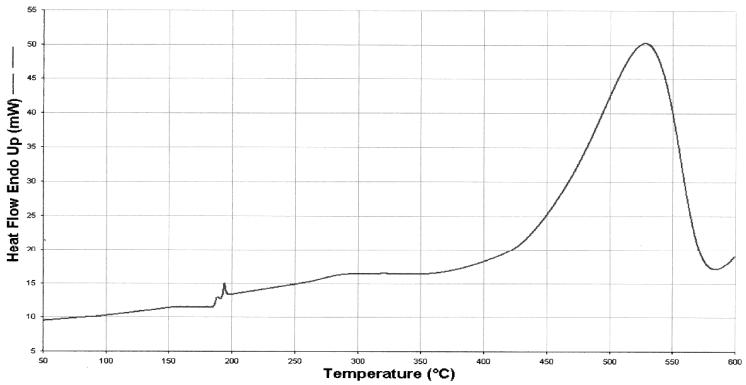

Fig.B.1– DSC Analysis of R.O.M. Ore

APPENDIX C

ANALYSIS FOR DETERMINATION OF TOTAL IRON IN SIDERITE ($FeCO_3$) SAMPLES

Determination of iron percentage in samples of siderite has been carried out; analysis has been done on -0.4 g- subsamples.

In experiments, subsamples prepared according to the standards, ***E877/ASTM; TS 495***, have been used. Combination of methods referred by Standard procedures in total iron determination has been applied **[E1028/ASTM; TS 1455].**

Briefly, the method is based on decomposition of the samples in certain chemicals followed by titration with Potassium Dichromate. The steps of the analysis consisted of addition of hydrochloric acid (HCl), tin chloride ($SnCl_2$) solution, hydrofluoric acid (HF).

500 ml flasks are used for treatment of samples. Heating of the solution follows the preparation with HCl, $SnCl_2$, and HF with standard amounts **[E246/ASTM**; **TS 1455].** 5 ml of *Potassium Permangate* ($KMnO_4$) solution is added with subsequent heating for 10 minutes, without boiling. Addition of other chemicals is performed, i.e. *mercury chloride ($HgCl_2$)* solution.

Dilution is made with 200 ml of distilled water; then the solution is treated with acid mixture [sulphuric acid (H_2SO_4); phosphoric acid (H_3PO_4); distilled water], boric acid (H_3BO_3) solution and sodium diphenylamine sulphonate solution (SDAS) as indicator. Finally, the solution is titrated with *Potassium Dichromate* ($K_2Cr_2O_7$) solution till the color of it turns from green to purple

The determination of percentage of iron (Fe %) is made using the following formula for computations;

$$Fe\% = \frac{V(ml) \times 0{,}5585}{mass\ of\ sample\,(g)} \quad (C.1) \quad ;$$

V= volume of $K_2Cr_2O_7$ solution used in titration (ml)

In contrast to the standards, a volume of 3 ml of SDAS has been used in analyses.